

**JAERI - M**  
**91-127**

EXPERIMENTAL DATA REPORT FOR TEST JM-I

[ SERIES OF REACTIVITY INITIATED ACCIDENT TEST  
IN NSRR WITH FUEL ROD PRE-IRRADIATED IN JMTR ]

August 1991

Kiyomi ISHIJIMA, Sadamitsu TANZAWA, Toyoshi FUKETA  
Kozo HOMMA and Toshio FUJISHIRO

JAERI-Mレポートは、日本原子力研究所が不定期に公刊している研究報告書です。  
入手の問合わせは、日本原子力研究所技術情報部情報資料課（〒319-11茨城県那珂郡東海村）あて、お申しこしてください。なお、このほかに財団法人原子力弘済会資料センター（〒319-11 茨城県那珂郡東海村日本原子力研究所内）で複写による実費頒布をおこなっております。

JAERI-M reports are issued irregularly.

Inquiries about availability of the reports should be addressed to Information Division, Department of Technical Information, Japan Atomic Energy Research Institute, Tokai-mura, Naka-gun, Ibaraki-ken 319-11, Japan.

Experimental Data Report for Test JM-1  
[ Series of Reactivity Initiated Accident Test  
in NSRR with Fuel Rod Pre-irradiated in JMTR ]

Kiyomi ISHIJIMA, Sadamitsu TANZAWA, Toyoshi FUKETA  
Kozo HOMMA and Toshio FUJISHIRO

Department of Fuel Safety Research  
Tokai Research Establishment  
Japan Atomic Energy Research Institute  
Tokai-mura, Naka-gun, Ibaraki-ken

(Received July 10, 1991)

This report presents experimental data for Test JM-1 which is the first pre-irradiated fuel rod test performed in Nuclear Safety Research Reactor (NSRR) in July, 1989. A fuel rod used in this test is a short-sized PWR (14 × 14) type one pre-irradiated in Japan Materials Testing Reactor (JMTR) up to a fuel burnup of approximately 20,000 MWd/t.

Pulse irradiation of the rod was performed under stagnant water cooling conditions of atmospheric pressure and ambient temperature using a newly developed double container type experimental capsule. Energy deposited in the rod by the pulse irradiation was estimated to be less than 126 cal/g·UO<sub>2</sub> (95 cal/g·UO<sub>2</sub> in terms of peak fuel enthalpy) by chemical FP analyses. No fuel failure was observed.

This report contains test design and conduct, fuel burnup measurements, transient behavior of the rod during pulse irradiation and results of post-pulse irradiation examination.

Keywords: NSRR, PIA, JMTR Pre-irradiated, Reactor Fuel, Pulse, PIE  
Transient

---

Note: This work has been done in co-operation with Department of JMTR Project, Department of Research Reactor, Department of Chemistry and NSRR Operation Division, Department of Fuel Safety Research.

実験 JM-1 に関する実験データレポート

〔 NSRR における JMTR 前照射燃料 〕  
〔 を用いた反応度事故模擬実験シリーズ 〕

日本原子力研究所東海研究所燃料安全工学部

石島 清見・丹沢 貞光・更田 豊志

本間 功三・藤城俊夫

(1991 年 7 月 10 日受理)

本報告書は、1989 年 7 月に NSRR において実施された、第 1 回目の照射済燃料実験である JM-1 実験により得られた実験データを取りまとめたものである。実験に使用した燃料は、PWR (14 × 14) 型の短尺燃料であり、材料試験炉 JMTR において約 20,000 MWd/t の燃焼度まで予備照射を受けたものである。

燃料のパルス照射は、新しく開発した二重容器型の実験カプセルを用い、大気圧・室温の静止水冷却条件下で行った。パルス照射による燃料の発熱量は、FP の化学分析により、126 cal/g・UO<sub>2</sub> (ピーク燃料エンタルピーでいえば 95 cal/g・UO<sub>2</sub>) 以下と評価された。本実験では、燃料の破損は生じなかった。

本報告書には、実験条件と実験方法、燃料燃焼度の測定結果、パルス照射時の燃料の過渡挙動及びパルス照射後行われた試験検査の結果が含まれている。

---

本研究は、大洗研究所材料試験炉部、東海研究所研究炉部、化学部及び燃料安全工学部 NSRR 管理室の協力のもとに実施されたものである。

東海研究所：〒319-11 茨城県那珂郡東海村白方字白根2-4

## Contents

1. Introduction .....	1
2. NSRR Design and Capabilities .....	3
3. Test Design and Conduct .....	4
3.1 Test Fuel Rod Design .....	4
3.2 Pre-irradiation of Test Fuel Rod in JMTR .....	4
3.2.1 Pre-irradiation of Test Fuel Rod .....	4
3.2.2 Results of Post-irradiation Examination .....	6
3.3 Experimental Capsule Design .....	11
3.4 Instrumentation .....	11
3.5 Test Conduct .....	12
4. Fuel Burnup Measurements .....	12
4.1 Evaluation of Long-term Burnup due to Pre-irradiation in JMTR .....	13
4.2 Evaluation of Short-term Burnup due to Pulse Irradiation in NSRR .....	14
5. Transient Behavior of Test Fuel Rod during Pulse Irradiation .....	15
6. Results of Post-pulse Irradiation Examination .....	16
6.1 Nondestructive Tests .....	16
6.2 Destructive Tests .....	19
7. Discussion .....	20
8. Conclusions .....	22
Acknowledgements .....	23
References .....	23

## 目 次

1. はじめに .....	1
2. NSRR の概要と実験能力 .....	3
3. 実験物の設計と実験方法 .....	4
3.1 試験燃料の設計 .....	4
3.2 JMTR における試験燃料の予備照射 .....	4
3.2.1 試験燃料の予備照射 .....	4
3.2.2 照射後試験の結果 .....	6
3.3 実験カプセルの設計 .....	11
3.4 実験計装 .....	11
3.5 実験の実施手順 .....	12
4. 燃料の燃焼度測定 .....	12
4.1 JMTR での予備照射による長期燃焼の評価 .....	13
4.2 NSRR でのパルス照射による短期燃焼の評価 .....	14
5. パルス照射中の試験燃料の過渡挙動 .....	15
6. パルス照射後検査の結果 .....	16
6.1 非破壊検査 .....	16
6.2 破壊検査 .....	19
7. 考 察 .....	20
8. 結 論 .....	22
謝 辞 .....	23
参考文献 .....	23

## 1. Introduction

In Nuclear Safety Research Reactor (NSRR) which is the only pulsing reactor in Japan and is operated by Japan Atomic Energy Research Institute (JAERI), extensive experimental studies on the reactor fuel failure behavior under simulated Reactivity Initiated Accident (RIA) conditions have been continued since the start of the test program in 1975. The number of fuel irradiation tests performed so far reached approximately 950 runs and accumulated experimental data were used as the fundamental data base of the safety evaluation guideline for reactivity initiated events in light water cooled nuclear power plants established by the nuclear safety commission on January 19th, 1984<sup>(1)</sup>

All of the experimental data used to establish the guideline were, however, limited to those derived from the tests with fresh fuels as the test samples because of the limitation of experimental facilities on the handling of highly radioactive materials. In times past, the tests with pre-irradiated fuels were conducted in SPERT and PBF projects<sup>(2,3)</sup> at Idaho National Engineering Laboratory in the United States of America. The number of the tests performed in these projects was, however, limited to 13 runs in all and, seems to be insufficient for completely clarifying the influences of fuel burnup on fuel behavior under RIA conditions. The present Japanese safety evaluation guideline, therefore, introduces the peak fuel enthalpy of 85 cal/g-UO<sub>2</sub> which was adopted from the SPERT data as a provisional failure threshold of pre-irradiated fuel under RIA conditions and, says that this value should be modified based on NSRR experiments in the future. Recent trend of nuclear fuel development includes the extension of fuel burnup. This brings another subject in the nuclear safety study.

According to the above requirements, new NSRR experimental program with pre-irradiated fuel as the test sample was started in July, 1989 after the completion of necessary modifications of the experimental facilities. The objectives of this program are;

- ① to understand the basic behavior of pre-irradiated fuel under RIA conditions,
- ② to determine the failure thresholds of pre-irradiated fuels with respect to amount of fuel burnups, initial rod power and fuel design parameters,

- ③ to clarify the failure modes and the failure mechanisms of pre-irradiated fuels and,
- ④ to clarify the consequences of the failure of pre-irradiated fuels.

Pre-irradiated test fuels are prepared by the following two ways;

- ① refabrication of 4 m long fuel rods pre-irradiated in commercial PWRs and BWRs into short segments and,
- ② pre-irradiation of short-sized test fuels with similar design to the present NSRR standard test fuel (14×14 PWR type fuel) in Japan Materials Testing Reactor (JMTR) owned and operated by JAERI.

Fuels already procured from commercial power reactors include;

- ① BWR fuel from Tsuruga Reactor 1 of Japan Atomic Power Co.  
fuel burnup : 22,000 MWd/t (assembly average)  
initial enrichment : 2.8 %
- ② PWR fuel from Mihama Reactor 2 of Kansai Electric Power Co.  
fuel burnup : 32,000 MWd/t (assembly average)  
initial enrichment : 2.6 %
- ③ PWR fuel from Genkai Reactor 1 of Kyushu Electric Power Co.  
fuel burnup : 35,000 MWd/t (assembly average)  
initial enrichment : 3.4 %

Refabrication of these fuel rods into short segments is performed at reactor fuel examination division, JAERI.

Pre-irradiation of the test fuels in JMTR started in March, 1982 and presently irradiation of 29 capsules (containing 87 test fuels) has completed or been progressing. These test fuels will accumulate fuel burnups ranging from 10,000 to 36,000 MWd/t. Among these, some fuels have higher initial enrichment (20 %) or different rod design (e.g. gap width).

The first pre-irradiated fuel test in NSRR was performed with the test fuel pre-irradiated in JMTR up to a burnup of approximately 20,000 MWd/t and this report presents its test design and conduct, results of burnup measurements, transient behavior of the fuel during pulse irradiation and results of post-pulse irradiation examination.



## 2. NSRR Design and Capabilities

NSRR is a modified TRIGA-ACPR (Annular Core Pulse Reactor). It was built for studying reactor fuel behavior under RIA conditions and went to the initial criticality in May, 1975. As shown in Fig. 1, the reactor core is mounted on the bottom of 3.6 m wide, 4.5 m long and 9 m deep open pool and cooled by natural circulation of pool water.

At the center of NSRR core, there exists large experimental cavity whose inner diameter is 22 cm where the test fuel rods contained in a capsule or a loop are subjected to a power burst. Access to the experimental cavity is provided either by the vertical loading tube or the offset loading tube. The vertical one is used for a long-sized experiment such as a loop and the offset one is selected for a short-sized capsule type experiment. Due to the offset location, no radiation shielding plug is required in the offset loading tube. This allows easy insertion and removal of the capsule into/from the experimental cavity. As a matter of fact, more than one hundred tests have been done per year using short-sized capsules containing fresh fuels.

The operational core configuration is shown in Fig. 2. The reactor core contains 149 driver fuel rods, 2 safety rods, 8 regulating rods and 3 transient rods. The driver fuel rod consists of 3 blocks of U-ZrH<sub>1.6</sub> and graphite end reflectors clad with stainless steel thin tube. The safety and the regulating rods consist of natural B<sub>4</sub>C blocks clad with stainless steel and fuel-follower and, are moved by electric drive mechanisms. The transient rod consists of enriched B<sub>4</sub>C blocks clad with aluminum alloy thin tube and air-follower and, is fired off by pneumatic drive mechanism.

The operation modes and their reactor power characteristics are listed in Table 1. Steady state operation of up to 300 kW is controlled by slow movement of the regulating rods. Natural pulse operation is realized by quick withdrawal of 3 transient rods at the same time under zero power condition. The maximum reactivity insertion of 3.43 % $\Delta k/k$  (\$4.7) is allowed to produce peak reactor power of up to 23,000 MW and burst energy of up to 130 MWs. This type of pulsing operation can simulate an RIA event from nearly zero power. Shaped pulse operation is a prolonged power transient from a few seconds to a few minutes of up to 10 MW produced by fast movement of the regulating rods and is used to

study fuel behavior under abnormal power transient such as ATWS. Combined pulse operation is a combined power transient of a shaped pulse and a natural pulse operations produced by fast movement of the regulating rods and quick withdrawal of the transient rods. Reactivity insertion by the transient rods in this mode is limited to  $\$4$ . Combined pulse operation is mainly used to study fuel behavior under an RIA from rated power. The maximum allowable burst energy in a shaped or combined pulse operation is 110 MWs and slightly lower than that of a natural pulse operation.

Table 2 summarizes the major characteristics of NSRR.

### 3. Test Design and Conduct

This chapter describes the test design and the conduct for the 1st pre-irradiated fuel test in NSRR (Test JM-1).

#### 3.1 Test fuel rod design

Figure 3 illustrates the design of the test fuel rod. The test rod contains 10  $\text{UO}_2$  pellets initially enriched to 10 % in  $^{235}\text{U}$  which compose the main part of fuel stack of 100 mm in height. At the both ends of it, a natural and a 5 %-enriched  $\text{UO}_2$  pellets are located to avoid undesirable axial power peaking at the both ends of 10 %-enriched fuel stack during pre-irradiation and pulse irradiation. On the top of fuel stack, an alumina pellet for thermal insulation and an iron core for the stack elongation measurement are placed. These items are clad with zircaloy-4 thin tube (outer diameter is 10.72 mm and wall thickness is 0.62mm). Inside of the rod is filled with pure helium of approximately 0.1 MPa. The initial radial gap width is 0.095 mm.

#### 3.2 Pre-irradiation of test fuel rod in JMTR

##### 3.2.1 Pre-irradiation of test fuel rod

Pre-irradiation of the test fuel rod used in Test JM-1 was performed in JMTR. JMTR in Oarai Research Establishment, JAERI is a reactor with the highest neutron flux in Japan for testing materials and operated at 50 MW for irradiation tests of reactor materials and fuels to meet the needs of JAERI itself as well as from outside and, post-irradiation

study fuel behavior under abnormal power transient such as ATWS. Combined pulse operation is a combined power transient of a shaped pulse and a natural pulse operations produced by fast movement of the regulating rods and quick withdrawal of the transient rods. Reactivity insertion by the transient rods in this mode is limited to  $\$4$ . Combined pulse operation is mainly used to study fuel behavior under an RIA from rated power. The maximum allowable burst energy in a shaped or combined pulse operation is 110 MWs and slightly lower than that of a natural pulse operation.

Table 2 summarizes the major characteristics of NSRR.

### 3. Test Design and Conduct

This chapter describes the test design and the conduct for the 1st pre-irradiated fuel test in NSRR (Test JM-1).

#### 3.1 Test fuel rod design

Figure 3 illustrates the design of the test fuel rod. The test rod contains 10  $\text{UO}_2$  pellets initially enriched to 10 % in  $^{235}\text{U}$  which compose the main part of fuel stack of 100 mm in height. At the both ends of it, a natural and a 5 %-enriched  $\text{UO}_2$  pellets are located to avoid undesirable axial power peaking at the both ends of 10 %-enriched fuel stack during pre-irradiation and pulse irradiation. On the top of fuel stack, an alumina pellet for thermal insulation and an iron core for the stack elongation measurement are placed. These items are clad with zircaloy-4 thin tube (outer diameter is 10.72 mm and wall thickness is 0.62mm). Inside of the rod is filled with pure helium of approximately 0.1 MPa. The initial radial gap width is 0.095 mm.

#### 3.2 Pre-irradiation of test fuel rod in JMTR

##### 3.2.1 Pre-irradiation of test fuel rod

Pre-irradiation of the test fuel rod used in Test JM-1 was performed in JMTR. JMTR in Oarai Research Establishment, JAERI is a reactor with the highest neutron flux in Japan for testing materials and operated at 50 MW for irradiation tests of reactor materials and fuels to meet the needs of JAERI itself as well as from outside and, post-irradiation

examinations are carried out at the hot laboratory attached to JMTR.

## (1) Irradiation capsule

Capsule used for the pre-irradiation of the test fuel rods in JMTR is illustrated in Fig. 4. The capsule is made of aluminum alloy and contains 3 test fuel rods in a vertical array. Heat generated by the test fuel rods during the pre-irradiation is removed using heat transfer medium of aluminum alloy closely fitted to the rods. The capsule is filled with pure helium of atmospheric pressure.

Figure 5 shows the core configuration of JMTR at the operation cycle No. 78 containing the capsules for this research. Those are capsules 81F-3A and 81F-4A and, were located in the aluminum reflector region far apart from the fuel region. This was intended to avoid excessive increase of cladding temperature of the test fuel rod during the pre-irradiation due to the poor heat removal capability of the capsule.

The capsule 81F-3A contained NJB07, 08 and 09 rods and, the capsule 81F-4A contained NJB10, 11 and 12 rods. The usage of these test rods is as follows:

### Capsule 81F-3A

Rod NJB07 (upper position) : used for Test JM-1  
 Rod NJB08 (middle position): used for Test JM-2  
 Rod NJB09 (lower position) : used for Test JM-3

### Capsule 81F-4A

Rod NJB10 (upper position) : used for Test JM-4  
 Rod NJB11 (middle position): used for Test JM-5  
 Rod NJB12 (lower position) : used for destructive test (reference rod)

## (2) Irradiation history

Irradiation histories of the capsules 81F-3A and 4A are shown in Fig. 6. The pre-irradiation of these capsules in JMTR started at the operation cycle No. 58 (March 13, 1982) and completed at the operation cycle No. 81 (April 17, 1988). During this period, accumulated irradiation time reached 11,412 hours (in 50 MW equivalent time).

Expected fuel burnup is 20,000 MWd/t. The estimated maximum fuel burnups for the capsules 81F-3A and 4A were 20,316 and 19,314 MWd/t, respectively. The maximum linear heat rates during the pre-irradiation for the capsules 81F-3A and 4A were also estimated to be 390 and 361 W/cm, respectively. These estimations were made by neutronic calculation for axial peak power location.

### (3) Fast neutron fluence

Each capsule was provided with iron wires to measure fast neutron fluences ( $>1$  MeV) for the cladding tubes using  $^{54}\text{Fe}$  (n,p)  $^{54}\text{Mn}$  reaction. Figures 7 and 8 give the results of fast neutron fluence measurements including the locations of the test fuel rods for the capsules 81F-3A and 4A, respectively. These results reflect the axial power distribution of JMTR core. The measured maximum fast neutron fluences for the capsules 81F-3A and 4A were  $2.15 \times 10^{20}$  and  $2.55 \times 10^{20}$  n/cm<sup>2</sup>, respectively.

### 3.2.2 Results of post-irradiation examination

After the completion of the pre-irradiation, nondestructive tests were performed for all of the test fuel rods contained in the capsules. Destructive tests were, however, performed only for NJB12 rod contained in the capsule 81F-4A.

#### (1) Nondestructive test

Nondestructive tests performed for the test rods include visual observation and photography, X-ray radiography,  $\gamma$ -ray scanning and spectrum measurement, dimensional measurement and eddy current measurement. Here we summarize the results of nondestructive tests for NJB07 rod used in Test JM-1 and NJB12 rod supplied to destructive tests without pulse irradiation.

For both test fuel rods, no abnormality was observed through visual observations and X-ray radiographies except the slight discolorations of the cladding surfaces in the active fuel regions. These discolorations are probably due to oxidation by the residual air in the capsules in spite of the substitution process of air by helium.

Photographs 1 and 2 include the appearances of the test fuel rods

NJB07 and NJB12 after the completion of the pre-irradiation, respectively.

$\gamma$ -ray scanings of the test fuel rods were performed by selecting the following  $\gamma$ -rays:

gross  $\gamma$ -rays : energy range from 40 to 1642 keV  
 $\gamma$ -rays from  $^{95}\text{Zr}$ - $^{95}\text{Nb}$  : energy range from 719 to 770 keV  
 $\gamma$ -rays from  $^{137}\text{Cs}$  : energy range from 657 to 667 keV.

In each case, the scanning speed was 10 mm/min. Measured axial distributions of the  $\gamma$ -ray intensity for the above three different  $\gamma$ -rays had almost the same behavior. Here, therefore, we give the results for gross  $\gamma$ -rays only in Fig. 9. The figure includes the results for NJB07 rod located in upper position in the capsule (a) and for NJB12 rod located in lower position (b). These distributions clearly reflect the axial power distribution of JMTR core as in the case of fast neutron fluence measurements and the presence of pellets with lower enrichments at the both ends of 10 %-enriched fuel stack and, also show the positions of pellet-pellet boundaries. There exists no abnormal part.

$\gamma$ -ray spectrum measurement of each test fuel rod was performed at 84.5 mm from the bottom (10 %-enriched fuel stack region) approximately 8 months after the completion of the pre-irradiation. Data accumulations were continued for 2000 s. Results for NJB07 and NJB12 rods were almost the same and, therefore, that for NJB07 rod only is given in Fig. 10. Detected major radioactive isotopes are  $^{95}\text{Zr}$ ,  $^{95}\text{Nb}$ ,  $^{103}\text{Ru}$ ,  $^{106}\text{Rh}$ ,  $^{134}\text{Cs}$ ,  $^{137}\text{Cs}$ ,  $^{144}\text{Ce}$ ,  $^{144}\text{Pr}$  and  $^{154}\text{Eu}$ . Radioactive isotopes with relatively short half-lives such as  $^{140}\text{La}$  and  $^{140}\text{Ba}$  were not detected.

Dimensional measurements of the test fuel rods were performed using laser scanning micrometer. Measured items were outer diameters in  $0^\circ$  and  $90^\circ$  directions along axial direction (axial profile) and total length of rod. Accuracies of the measurements are  $\pm 0.005$  mm for diameter and  $\pm 0.05$  mm for length. For NJB07 rod, cross-sectional profile was also measured at 79 mm from the bottom. Figures 11 and 12 give the axial profiles of NJB07 and NJB12 rods, respectively. Axial profile of NJB07 rod in  $0^\circ$  direction (Fig. 11) only has a few small peaks due to deposits on the cladding surface. Outer diameters and total lengths for both rods measured before pre-irradiation were approximately 10.73 mm and 220.3 mm.

respectively. On the other hand, outer diameters and total lengths for both rods measured after pre-irradiation were approximately 10.73~10.74 mm and 220.3~220.4 mm, respectively. If we consider the accuracies of the measurements, these results suggests that there was no severe pellet-clad mechanical interaction during pre-irradiation. Figure 13 presents the result of cross-sectional profile measurement for NJB07 rod. From the figure, only slight ovality toward 0° direction is recognized.

Figures 14 and 15 give the representative results of eddy current measurements at phase angle 40° for NJB07 and NJB12 rods, respectively, together with those for reference tube with standard defects. Scanning speed was 20 mm/s in any case. Detected major signals (B, C, D in Fig. 14 and A in Fig. 15) were identified as those due to small deposits on the cladding tube surfaces. Other signals (A in Fig. 14 and B in Fig. 15) are presently estimated to be due to small ridge formations and are under the detailed investigation in the hot laboratory attached to JMTR. These results show that no significant defect of the cladding tube was formed during the pre-irradiation of the both test fuel rods.

## (2) Destructive test

Major destructive tests performed for NJB12 rod to obtain reference data for NJB07 rod which was used in Test JM-1 are collection of FP gas (rod puncture test), measurement of fuel pellet density, micro  $\gamma$ -ray scanning, and metallography including X-ray microprobe analysis and observation of inner surface of cladding tube.

Plenum of the test fuel rod was punctured by FP gas collection device and, free volume in the rod, amount of released gases and internal rod pressure were measured. Volume ratios of the released gases and abundances of isotopes were also measured using mass spectrograph. Measured free volume and released gases were  $2.1 \times 10^{-6} \text{ m}^3$  and  $2.02 \times 10^{-6} \text{ m}^3$  in STP, respectively. This means internal rod pressure of 0.106 MPa at 25 °C. The rod was initially filled with helium of atmospheric pressure (approximately 0.1 MPa). Therefore, FP gas release into free volume during the pre-irradiation was very small and estimated to be about 0.2 %. Measured volume ratios of the released gases and abundances of isotopes were as follows;

(Volume ratios of the released gases)

He : 96.11 %      Kr : 0.70 %      Xe : 3.19 %

(Abundances of isotopes)

$^{83}\text{Kr}$ : 13.59 %	$^{131}\text{Xe}$ : 11.06 %
$^{84}\text{Kr}$ : 28.68 %	$^{132}\text{Xe}$ : 18.33 %
$^{85}\text{Kr}$ : 5.61 %	$^{134}\text{Xe}$ : 31.03 %
$^{86}\text{Kr}$ : 52.12 %	$^{136}\text{Xe}$ : 39.58 %

These results also suggest small FP release during the pre-irradiation.

Density of the fuel pellet was measured by weighing a piece of pellet in the substitution liquid (meta-xylene) with a balance under atmospheric pressure. Two samples were taken from 10 %-enriched fuel stack and measured densities for each sample were 95.07 %TD. This result means that there was no density change of pellet during the pre-irradiation.

Micro  $\gamma$ -ray scannings of fuel pellet were performed for one sample taken from 10 %-enriched fuel stack along two radial directions. Gross  $\gamma$ -ray (energy range : 40 ~ 2000 keV) and  $\gamma$ -ray from  $^{137}\text{Cs}$  (energy range : 656 ~ 667 keV) were selected for the measurements. Scanning speed was 5 mm/min in each measurement. Figure 16 presents the result of the measurement for one direction. As shown in the figure, the distributions of the  $\gamma$ -ray intensities for both gross  $\gamma$ -ray and  $\gamma$ -ray from  $^{137}\text{Cs}$  are governed by the fission density distribution and have concave shapes.  $\gamma$ -ray spectrum measurement was also attempted at the center of the fuel pellet and the detected nuclides were essentially the same as those detected in the  $\gamma$ -ray spectrum measurement of the test fuel rod performed during non-destructive test stage.

Two samples of the radial sections from the maximum (139 mm from the bottom of the rod) and average (90 mm from the bottom) power positions and one sample of longitudinal section from the minimum power position (40~50 mm from the bottom) were used for metallography. Etchings of the samples were performed using the following methods.

Etching liquid for pellet	$\text{H}_2\text{SO}_4$ : $\text{H}_2\text{O}_2$ = 1 : 8
Etching method for pellet	Dip method (90 s)
Etching liquid for cladding	$\text{HNO}_3$ : $\text{H}_2\text{O}_2$ : HF = 43 : 43 : 4
Etching method for cladding	Swab method (10 s)



Photograph 3 gives the macroscopic view of 5 magnifications of the cross-sectional sample taken from the top pellet of 10 %-enriched fuel stack (this pellet had the maximum linear heat rate during the pre-irradiation) after etching treatment. Some large cracks of the pellet which are typical to the burnup fuels are shown in the photography. It seems that relatively large pores are rather uniformly distributed, however, density of small ones is larger in the peripheral region. Microscopic photographs of the same sample of 400 magnifications were performed at the central, middle and peripheral positions and, the results are given in Photos. 4, 5 and 6. From these photographs, the average grain sizes in central, middle and position were estimated to be approximately 11, 12 and 9  $\mu\text{m}$ , respectively. Only slight growth of the grain is recognized at the inner part of the pellet.

Photographs 7 and 8 show the microscopic view of 200 magnifications of the inside and the outside of the cladding tube which belongs to the same sample. It seems that there are no significant change in microscopic structure and no significant oxidation due to the pre-irradiation.

Examples of the precipitation of hydride in the cladding tube are shown in Photos. 9 for the cross-sectional sample taken from the top pellet of 10 %-enriched fuel stack and 10 for the longitudinal sample taken from the bottom pellet where the linear heat rate was minimum. From these photographs, it can be concluded that the precipitation of hydride is rather significant in the region of low linear heat rate but, still very small.

X-ray microprobe analyses were performed for a few samples. Photograph 11 shows the secondary electron image of 3000 magnifications for the inner surface of the cladding tube which clads a pellet in the central part of 10 %-enriched fuel stack. Many small particles stick to the surface. Photographs 12 and 13 gives the results of surface analyses by wave length dispersion method performed at the same place to identify materials and, show the presence of uranium and zirconium, respectively. These results indicate that the main material stuck to the inner surface is  $\text{UO}_2$  powder. Point analyses by energy dispersion method were also performed at the several positions in the same sample to detect other materials. However, no special material other than uranium was detected. This means that there was no significant release of FPs to the gap during the pre-irradiation.

Secondary electron images of 1000 magnifications for the peripheral, middle and central positions of the fuel sample taken from the central part of 10 %-enriched fuel stack are shown in Photos. 14, 15 and 16, respectively. There is no indication of the formation of onset FP gas bubble in any position.

Photograph 17 shows the appearance of the inner surface of the cladding tube which was used in the X-ray microprobe analyses. The marks of the fuel pellet edges and some stuck materials can be recognized. However, no defect such as a crack is identified.

### 3.3 Experimental capsule design

The experimental capsule used in Test JM-1 is a newly developed double-container type one (type X-1 atmospheric pressure capsule) for pre-irradiated fuel test. Schematic configuration of this capsule is given in Fig. 17. Outer capsule is a sealed container of 130 mm in inner diameter and 1,250 mm in height. Inner capsule is a sealed pressure vessel of 72 mm in inner diameter and 680 mm in height. In the design work of the capsule, the easiness of assembling and disassembling jobs by remote handling was the major concern as well as structural strength. Type X-1 capsule was specially designed for the test with the test fuel rod pre-irradiated in JMTR and can be used in the test where energy deposition in a rod is less than 250 cal/g·UO<sub>2</sub>. The capsule contains an instrumented test fuel rod, is filled with water of ambient temperature and atmospheric pressure, and is subjected to a pulse irradiation in NSRR.

### 3.4 Instrumentation

Figure 18 illustrates the instrumentation used in Test JM-1. The test fuel rod was equipped with 6 thermocouples (Pt/Pt-13%Rh, 0.2 mm  $\phi$ ) to measure cladding surface temperature. T/C#1(T/C#4), T/C#2(T/C#5) and T/C#3(T/C#6) were located at the centers of No.9, No.6 and No.3 pellets (from the top of 10 %-enriched fuel stack), respectively. The inner capsule was instrumented with 2 thermocouples (CA) to measure coolant (stagnant water) temperature near the center and the top of the test rod. The reactor power and its integrated value during the power burst were monitored using two micro fission chambers located in the periphery of the reactor core to correlate with the transient fuel rod behavior.

### 3.5 Test conduct

Figure 19 shows the outline of general procedure used in the pre-irradiated fuel rod test in NSRR. Test fuel rods pre-irradiated in JMTR or refabricated from the rods pre-irradiated in commercial power reactor are transported to NSRR. In NSRR, the test fuel rod is instrumented using remotely controlled device in a small hot cell and assembled into a experimental capsule using automatic assembling device in a hot cave. Using capsule loading device, the assembled capsule is transported from the cave to the inlet of off-set loading tube, inserted into the experimental cavity and irradiated by a pulse operation of NSRR. Using the same device, the irradiated capsule is removed from the core and returned to the hot cave. Only the outer capsule is disassembled there after the confirmation of the shields in the capsule. The inner capsule containing the test fuel rod is transported from NSRR to a hot laboratory. In the hot laboratory, the inner capsule is disassembled to remove the test fuel rod and the detailed examination of the rod is performed. Small sample taken from the rod is transferred to the chemical analysis center to evaluate the base burnup due to the pre-irradiation in JMTR and the energy deposition due to the pulse irradiation in NSRR for the test rod.

Pulse irradiation in Test JM-1 was performed at 14:32:00, July 20, 1989. Inserted reactivity was  $\$2.55$ . The initial coolant temperature was 25.8 °C.

### 4. Fuel Burnup Measurements

The long-term burnup (base burnup) due to the pre-irradiation in JMTR and the short-term burnup (energy deposition) due to pulse irradiation in NSRR were evaluated by the chemical FP analyses of the sample taken from the test fuel rod NJB07 after the completion of the pulse irradiation.

After resin injection, a slice of the test rod of approximately 2 mm thick was cut off at the center of the second pellet position from the top of 10 %-enriched fuel stack. This slice was boiled and dissolved in 8 Mol-nitric acid solution for 5 hours. After dilution of the solution with pure water and 4 Mol-nitric acid solution to 1/1000, the sample of 5 ml containing 1.422 mg of  $\text{UO}_2$  was taken for chemical analysis.

### 3.5 Test conduct

Figure 19 shows the outline of general procedure used in the pre-irradiated fuel rod test in NSRR. Test fuel rods pre-irradiated in JMTR or refabricated from the rods pre-irradiated in commercial power reactor are transported to NSRR. In NSRR, the test fuel rod is instrumented using remotely controlled device in a small hot cell and assembled into a experimental capsule using automatic assembling device in a hot cave. Using capsule loading device, the assembled capsule is transported from the cave to the inlet of off-set loading tube, inserted into the experimental cavity and irradiated by a pulse operation of NSRR. Using the same device, the irradiated capsule is removed from the core and returned to the hot cave. Only the outer capsule is disassembled there after the confirmation of the shields in the capsule. The inner capsule containing the test fuel rod is transported from NSRR to a hot laboratory. In the hot laboratory, the inner capsule is disassembled to remove the test fuel rod and the detailed examination of the rod is performed. Small sample taken from the rod is transferred to the chemical analysis center to evaluate the base burnup due to the pre-irradiation in JMTR and the energy deposition due to the pulse irradiation in NSRR for the test rod.

Pulse irradiation in Test JM-1 was performed at 14:32:00, July 20, 1989. Inserted reactivity was \$2.55. The initial coolant temperature was 25.8 °C.

### 4. Fuel Burnup Measurements

The long-term burnup (base burnup) due to the pre-irradiation in JMTR and the short-term burnup (energy deposition) due to pulse irradiation in NSRR were evaluated by the chemical FP analyses of the sample taken from the test fuel rod NJB07 after the completion of the pulse irradiation.

After resin injection, a slice of the test rod of approximately 2 mm thick was cut off at the center of the second pellet position from the top of 10 %-enriched fuel stack. This slice was boiled and dissolved in 8 Mol-nitric acid solution for 5 hours. After dilution of the solution with pure water and 4 Mol-nitric acid solution to 1/1000, the sample of 5 ml containing 1.422 mg of  $UO_2$  was taken for chemical analysis.

## 4.1 Evaluation of long-term burnup due to pre-irradiation in JMTR

Burnup measurement was performed by determining the fractional amounts of isotopes of neodymium, uranium and plutonium using the isotopic dilution method. For this purpose, traceable amounts of  $^{150}\text{Nd}$ ,  $^{233}\text{U}$  and  $^{242}\text{Pu}$  were added to the sample. Traceable amount of  $^{133}\text{Ba}$  was also added for the evaluation of short-term burnup which will be mentioned later.

The first stage of the chemical analysis was the separation of uranium, plutonium, neptunium, zirconium and FPs with anion exchange method in hydrochloric acid system. Isotopic fractions of the separated uranium and plutonium were measured with mass spectrograph as follows:

Uranium
 $4.7866 \times 10^{17}$  Atoms/g·soln

 $^{234}\text{U}$  : 0.063 Atom.%

 $^{235}\text{U}$  : 7.847 Atom.%

 $^{236}\text{U}$  : 0.442 Atom.%

 $^{238}\text{U}$  : 91.648 Atom.%

 $\text{Pu/U}$  :  $1.764 \times 10^{-3}$ 
Plutonium
 $8.4435 \times 10^{14}$  Atoms/g·soln

 $^{238}\text{Pu}$  : 0.121 Atom.%

 $^{239}\text{Pu}$  : 90.223 Atom.%

 $^{240}\text{Pu}$  : 8.395 Atom.%

 $^{241}\text{Pu}$  : 1.200 Atom.%

 $^{242}\text{Pu}$  : 0.062 Atom.%

From this result, fuel burnup was estimated to be 2.102 %FIMA.

The second step of the chemical analysis was the separation of neodymium, americium, curium, a group of barium and europium and a group of cesium, strontium and yttrium with anion exchange method in methanol-nitric acid system. Isotopic fraction of the separated neodymium was measured with mass spectrograph as follows:

 $^{142}\text{Nd}$  : 0.129 Atom.%

 $^{143}\text{Nd}$  : 26.945 Atom.%

 $^{144}\text{Nd}$  : 27.458 Atom.%

 $^{145}\text{Nd}$  : 18.948 Atom.%

 $^{146}\text{Nd}$  : 14.914 Atom.%

 $^{148}\text{Nd}$  : 8.305 Atom.%

 $^{150}\text{Nd}$  : 3.301 Atom.%

 $^{148}\text{Nd}$  :  $1.7030 \times 10^{14}$  Atoms/g·soln

From this result, fuel burnup of 2.077 %FIMA was estimated.

These results well agree with each other and give the fuel burnup of approximately 20,100 MWd/t as a result of the pre-irradiation in JMTR. Additional burnup due to the pulse irradiation in NSRR is negligibly small compared with that due to the pre-irradiation.

## 4.2 Evaluation of short-term burnup due to pulse irradiation in NSRR

Evaluation of the short-term burnup, that is, energy deposition due to the pulse irradiation in NSRR includes severe difficulty because of the presence of large amount of  $\gamma$ -ray emitting fission products due to the pre-irradiation.

To select the appropriate nuclide from FPs for the measurement of energy deposition in the test fuel rod, FP inventory in a rod containing 10 10%-enriched UO<sub>2</sub> pellets pre-irradiated in JMTR up to a fuel burnup of 20,000 MWd/t and that for a fresh rod were estimated using ORIGEN-2 code at 2 years after the completion of the pre-irradiation and at 60 days after a pulse irradiation in NSRR, respectively. The results for the interesting FPs are as follows;

FP	Half life	2 years after pre-irradiation (Bq)	60 days after pulse irradiation (Bq)
<sup>137</sup> Cs	30 years	$1.6 \times 10^{11}$	$2.4 \times 10^5$
<sup>95</sup> Zr	64 days	$7.0 \times 10^8$	$1.6 \times 10^7$
<sup>95</sup> Nb	35 days	$1.7 \times 10^9$	$1.4 \times 10^7$
<sup>140</sup> Ba	13 days	< 1	$7.0 \times 10^6$
<sup>140</sup> La	40 hours	< 1	$7.8 \times 10^6$

As shown in the above table, <sup>140</sup>Ba and <sup>140</sup>La have relatively good properties. As described later, however, separation of photo-peaks of <sup>140</sup>Ba and <sup>140</sup>La among the others by the direct  $\gamma$ -ray spectrum measurement of a rod after a pulse irradiation is almost impossible. Therefore, a chemical separation process of these nuclides is essential to estimate an energy deposition. By considering easiness of the chemical separation, <sup>140</sup>Ba was selected as the target isotope.

From the group of barium and europium obtained from the second step of the chemical analysis for the evaluation of the long-term burnup, barium was separated with cation exchange method in nitric acid system. Chemical yield of barium through these processes was estimated to be 69 % by the measurement of <sup>133</sup>Ba activity.

Figure 20 shows an example of the  $\gamma$ -ray spectrum measurement for the processed solution. The photo-peak of  $^{133}\text{Ba}$  at 356 keV and that of  $^{140}\text{Ba}$  at 537.3 keV can be identified. After the detailed measurements, the number of fissions in the fuel (sampled 10 %-enriched  $\text{UO}_2$ ) due to the pulse irradiation in NSRR and the corresponding energy deposition was estimated to be  $1.92 \times 10^{13}$  and 126 cal/g- $\text{UO}_2$ , respectively.

## 5. Transient Behavior of Test Fuel Rod during Pulse Irradiation

In this chapter, transient data on the reactor power, the cladding surface temperature and the coolant temperature measured during the pulse irradiation are presented.

### (1) Reactor power

The reactor power and the integrated reactor power measured by two micro fission chambers in Test JM-1 are shown in Figs. 21 and 22, respectively. The maximum reactor power reached approximately 4,000 MW. The half width at half maximum was about 9 ms. The minimum reactor period was estimated to be 2.68 ms. The integrated reactor power reached 45.2MWs at its maximum.

### (2) Cladding surface temperature

One of the thermocouples for the cladding surface temperature measurement (T/C#6: upper position) was failed during the preparation stage of the test. The other thermocouples survived the pulse irradiation. Figs. 23, 24 and 25 give the measured transient histories of the cladding surface temperatures at the lower, center and upper locations, respectively. The maximum cladding surface temperature of approximately 140 °C was attained at one of the thermocouples located in the center position. In test JM-1, as shown in these figures, no DNB (departure from nucleate boiling) occurred on the cladding surface.

### (3) Coolant temperature

Figure 26 presents the measured transient histories of the coolant temperatures near the fuel center and the top of the test rod, respectively. The coolant temperature measured by the thermocouple near the fuel center increases rapidly just after the initiation of the pulse ir-

Figure 20 shows an example of the  $\gamma$ -ray spectrum measurement for the processed solution. The photo-peak of  $^{133}\text{Ba}$  at 356 keV and that of  $^{140}\text{Ba}$  at 537.3 keV can be identified. After the detailed measurements, the number of fissions in the fuel (sampled 10 %-enriched  $\text{UO}_2$ ) due to the pulse irradiation in NSRR and the corresponding energy deposition was estimated to be  $1.92 \times 10^{13}$  and 126 cal/g $\cdot\text{UO}_2$ , respectively.

## 5. Transient Behavior of Test Fuel Rod during Pulse Irradiation

In this chapter, transient data on the reactor power, the cladding surface temperature and the coolant temperature measured during the pulse irradiation are presented.

### (1) Reactor power

The reactor power and the integrated reactor power measured by two micro fission chambers in Test JM-1 are shown in Figs. 21 and 22, respectively. The maximum reactor power reached approximately 4,000 MW. The half width at half maximum was about 9 ms. The minimum reactor period was estimated to be 2.68 ms. The integrated reactor power reached 45.2MWs at its maximum.

### (2) Cladding surface temperature

One of the thermocouples for the cladding surface temperature measurement (T/C#6: upper position) was failed during the preparation stage of the test. The other thermocouples survived the pulse irradiation. Figs. 23, 24 and 25 give the measured transient histories of the cladding surface temperatures at the lower, center and upper locations, respectively. The maximum cladding surface temperature of approximately 140 °C was attained at one of the thermocouples located in the center position. In test JM-1, as shown in these figures, no DNB (departure from nucleate boiling) occurred on the cladding surface.

### (3) Coolant temperature

Figure 26 presents the measured transient histories of the coolant temperatures near the fuel center and the top of the test rod, respectively. The coolant temperature measured by the thermocouple near the fuel center increases rapidly just after the initiation of the pulse ir-



radiation, shows violent oscillation reflecting nucleate boiling on the cladding surface, and reaches about 70 °C at its maximum. The thermocouple near the top of the test fuel rod shows the delayed increase and rather mild oscillation of the coolant temperature. The maximum temperature of approximately 40 °C was attained. The initial coolant temperature in Test JM-1 was about 26 °C.

## 6. Results of Post-pulse Irradiation Examination

After the pulse irradiation, the inner capsule containing the test rod NJB07 was transported to the hot laboratory and there, the nondestructive tests including visual observation and photography, X-ray radiography, dimensional measurement, eddy current measurement,  $\gamma$ -ray scanning and  $\gamma$ -ray spectrum measurement and the destructive tests including metallography and X-ray microprobe analysis were performed.

### 6.1 Nondestructive tests

#### (1) Visual observation and photography

Before disassembling, the inner capsule containing the test fuel was visually inspected to check the soundness and then photographed. As shown in Photo. 18, no abnormality was identified. After disassembling the capsule, the test fuel rod supported by the holder was visually examined and then photographed (Photo. 19). Through this observation, no abnormality was identified, again.

After removing the holder, the test fuel rod was carefully observed to check the presence of any abnormality and then photographed. Photograph 20 gives the appearances of the rod in two directions. Only slight discoloration of the cladding surface along the active fuel region was recognized. As described in the section 3.2.2, this discoloration may be caused by the slight oxidation of the cladding surface during the pre-irradiation. Additional oxidation of the cladding surface by the pulse irradiation can be neglected because of the measured low cladding temperatures (the measured maximum temperature was approximately 140 °C in Test JM-1).

radiation, shows violent oscillation reflecting nucleate boiling on the cladding surface, and reaches about 70 °C at its maximum. The thermocouple near the top of the test fuel rod shows the delayed increase and rather mild oscillation of the coolant temperature. The maximum temperature of approximately 40 °C was attained. The initial coolant temperature in Test JM-1 was about 26 °C.

## 6. Results of Post-pulse Irradiation Examination

After the pulse irradiation, the inner capsule containing the test rod NJB07 was transported to the hot laboratory and there, the nondestructive tests including visual observation and photography, X-ray radiography, dimensional measurement, eddy current measurement,  $\gamma$ -ray scanning and  $\gamma$ -ray spectrum measurement and the destructive tests including metallography and X-ray microprobe analysis were performed.

### 6.1 Nondestructive tests

#### (1) Visual observation and photography

Before disassembling, the inner capsule containing the test fuel was visually inspected to check the soundness and then photographed. As shown in Photo. 18, no abnormality was identified. After disassembling the capsule, the test fuel rod supported by the holder was visually examined and then photographed (Photo. 19). Through this observation, no abnormality was identified, again.

After removing the holder, the test fuel rod was carefully observed to check the presence of any abnormality and then photographed. Photograph 20 gives the appearances of the rod in two directions. Only slight discoloration of the cladding surface along the active fuel region was recognized. As described in the section 3.2.2, this discoloration may be caused by the slight oxidation of the cladding surface during the pre-irradiation. Additional oxidation of the cladding surface by the pulse irradiation can be neglected because of the measured low cladding temperatures (the measured maximum temperature was approximately 140 °C in Test JM-1).

## (2) X-ray radiography

Before disassembling, the inner capsule containing the test fuel rod was radiographed with X-ray to check the integrity of the rod. In this step of the radiography, no breakdown of the rod was confirmed. After disassembling the capsule and removing the test fuel rod from the holder, the rod was radiographed with X-ray in two directions. Photograph 21 shows the result of the radiography. In some places, pellet-pellet boundaries can be identified. No other finding such as a crack of the fuel pellet could not be obtained.

## (3) Dimensional measurement

Outer diameter, bending and total length of the test fuel rod were measured using a laser scanning micrometer. Accuracies of the measurements are  $\pm 0.005$  mm for diameter and  $\pm 0.05$  mm for bending and length. The total lengths of the test fuel rod measured in  $0^\circ$  and  $90^\circ$  directions were 220.24 and 220.23 mm, respectively. These rod lengths are slightly shorter than that (220.39 mm) measured after the completion of the pre-irradiation. This is probably due to the generation of the slight bending of the test rod. Figure 27 gives the measured rod bendings in  $0^\circ$  and  $90^\circ$  directions. The maximum bending was approximately 0.03 mm and very small.

The axial profiles of the rod measured in  $0^\circ$  and  $90^\circ$  directions are shown in Fig. 28. They are very smooth except some peaks due to deposits on the cladding tube and suggest that significant PCMI did not occur in this test. Measured diameter approximately ranged from 10.74 to 10.75 mm

## (4) Eddy current measurement

Figure 29 gives the result of eddy current measurement at phase angle  $30^\circ$  for NJB07 rod. Test frequency was 400 kHz and scanning speed was 30 mm/s. The positions of the significant signals except signal ④ almost correspond to those detected before pulse irradiation (see Fig.14). Signals ① ~ ④ may be due to the small white deposits on the cladding surface and signal ⑤ due to small ridge-shaped deformation.

(5)  $\gamma$ -ray scanning and  $\gamma$ -ray spectrum measurement

$\gamma$ -ray scanings of the test fuel rods were performed by selecting the following  $\gamma$ -rays:

gross  $\gamma$ -rays : energy range from 40 to 2342 keV  
 $\gamma$ -rays from  $^{137}\text{Cs}$  : energy range from 656 to 666 keV.

In each case, the scanning speed was 5 mm/min. Measured axial distributions of the  $\gamma$ -ray intensities for the above  $\gamma$ -rays are shown in Fig. 30. These distributions have almost the same shape as those measured before pulse irradiation (see Fig. 9). It may be, however, noted that  $\gamma$ -ray intensities from  $^{137}\text{Cs}$  in 5%-enriched  $\text{UO}_2$  pellets at the both ends of 10%-enriched fuel stack tend to increase at the lower temperature sides.

$\gamma$ -ray spectrum measurements of the test fuel rod were performed at 5 locations near the center of 10%-enriched fuel stack (distance between 2 measuring points was 2.5 mm). Data accumulations were continued for 10,000 s. The result is summarized as follows:

	Point A1 (lower)	Point A2	Point A3 (center)	Point A4	Point A5 (upper)
$^{144}\text{Ce}$ ( 133.53keV)	14.79	14.94	14.45	14.57	14.62
$^{144}\text{Pr}$ ( 696.49keV)	8.39	8.26	7.67	8.32	8.29
$^{103}\text{Ru}$ ( 497.08keV)	0.55	0.57	0.00	0.00	0.00
$^{106}\text{Rh}$ ( 621.87keV)	8.45	8.39	7.61	8.34	8.31
$^{125}\text{Sb}$ ( 427.95keV)	2.34	2.22	2.13	2.19	2.10
$^{134}\text{Cs}$ ( 604.74keV)	29.98	29.68	27.07	29.16	28.82
$^{137}\text{Cs}$ ( 661.65keV)	242.21	241.19	221.77	241.08	239.06
$^{95}\text{Zr}$ ( 756.72keV)	10.98	10.97	10.04	10.97	10.89
$^{95}\text{Nb}$ ( 765.79keV)	43.00	42.92	39.43	42.90	42.75
$^{154}\text{Eu}$ (1274.45keV)	0.47	0.47	0.44	0.47	0.47

(unit:cps)

$^{125}\text{Sb}$  is the only radioactive isotope newly detected in the measurement after the pulse irradiation.  $^{140}\text{La}$  and  $^{140}\text{Ba}$  were not detected, again. Figure 31 gives the representative  $\gamma$ -ray spectrum measured at point A1. Long-term measurement (300,000 s) was attempted at point A1 to detect  $^{140}\text{La}$  or  $^{140}\text{Ba}$  and failed to detect them.

## 6.2 Destructive tests

Two samples for metallography (a radial and a longitudinal samples) and one sample for X-ray microprobe analysis were taken from 10%-enriched fuel stack as shown in Fig. 32. The figure includes macroscopic photographs of 5 magnifications before etching for the above three samples.

### (1) Metallography

Etching was performed for fuel part only using the same method as that described in section 3.2.2.

Photograph 22 gives the macroscopic photograph of 5 magnifications and the microscopic photographs of 1000 magnifications at the central, middle and peripheral parts of the fuel after etching for the sample of radial section and, photograph 23 gives those for the sample of longitudinal sample. The following findings were obtained through this work.

- 1) Generation of large cracks in the fuel pellet subjected to a pulse irradiation was almost the same degree as that after the completion of pre-irradiation (see Photo. 3).
- 2) Many small cracks toward the surface of the pellet generated at the peripheral region. This is probably due to the very large temperature gradient at the peripheral region brought by the pulse irradiation.
- 3) Average grain sizes of the fuel estimated from these samples were approximately  $7\ \mu\text{m}$  and slightly smaller than those measured after the completion of pre-irradiation (approximately  $10\ \mu\text{m}$ ). Position dependency of the average grain size is very small.
- 4) Separation of the grain boundary was rather significant at the peripheral region.
- 5) Oxidation of the cladding inner and outer surfaces was very small (less than  $1\ \mu\text{m}$ ).

## (2) X-ray microprobe analysis

X-ray microprobe analysis was performed for one sample. Photograph 24 shows the secondary electron images of 100 and 1000 magnifications for the inner surface of the cladding tube. Only adhesive and small particles stuck to the surface can be seen. No defect was identified. The secondary electron images of 1000 and 3000 magnifications for the fuel surface at the central, middle and peripheral regions are given in Photo. 25. There is no indication of the formation of FP gas bubble in any location.

Point analysis by energy dispersion method was also performed at one point on the cladding inner surface and the result is given in Fig. 33. Presence of barium, cesium and tellurium was confirmed through this measurement. This means that there exists the release of FP gases into the gap region during the pulse irradiation.

## 7. Discussion

### (1) Pre-irradiation

The pre-irradiation of the test fuel rods in JMTR itself was favorably completed. There were, however, two problems. The first problem is the discoloration of the cladding surface by the pre-irradiation. This is probably due to oxidation by the residual air in the capsule in spite of the substitution process of air by helium at the assembling stage of the capsule. The destructive tests for the reference rod after the pre-irradiation and for NJB07 rod after the pulse irradiation showed that oxide thicknesses of the cladding outer surfaces for both rods were very small ( $\sim 1 \mu\text{m}$ ) and, therefore, the discoloration could be negligible for the assessment of the fuel behavior.

The second problem is the presence of the small deposits on the cladding surface which was confirmed by the dimensional and eddy current measurements of the test rod before and after the pulse irradiation. As a matter of course, this kind of deposit was not observed before the pre-irradiation. Therefore, these deposits were formed during the pre-irradiation in JMTR. The cause of this phenomenon is not known and now under investigation in the hot laboratory.

## (2) X-ray microprobe analysis

X-ray microprobe analysis was performed for one sample. Photograph 24 shows the secondary electron images of 100 and 1000 magnifications for the inner surface of the cladding tube. Only adhesive and small particles stuck to the surface can be seen. No defect was identified. The secondary electron images of 1000 and 3000 magnifications for the fuel surface at the central, middle and peripheral regions are given in Photo. 25. There is no indication of the formation of FP gas bubble in any location.

Point analysis by energy dispersion method was also performed at one point on the cladding inner surface and the result is given in Fig. 33. Presence of barium, cesium and tellurium was confirmed through this measurement. This means that there exists the release of FP gases into the gap region during the pulse irradiation.

## 7. Discussion

### (1) Pre-irradiation

The pre-irradiation of the test fuel rods in JMTR itself was favorably completed. There were, however, two problems. The first problem is the discoloration of the cladding surface by the pre-irradiation. This is probably due to oxidation by the residual air in the capsule in spite of the substitution process of air by helium at the assembling stage of the capsule. The destructive tests for the reference rod after the pre-irradiation and for NJB07 rod after the pulse irradiation showed that oxide thicknesses of the cladding outer surfaces for both rods were very small ( $\sim 1 \mu\text{m}$ ) and, therefore, the discoloration could be negligible for the assessment of the fuel behavior.

The second problem is the presence of the small deposits on the cladding surface which was confirmed by the dimensional and eddy current measurements of the test rod before and after the pulse irradiation. As a matter of course, this kind of deposit was not observed before the pre-irradiation. Therefore, these deposits were formed during the pre-irradiation in JMTR. The cause of this phenomenon is not known and now under investigation in the hot laboratory.

## (2) Transient behavior of the test fuel rod

Instrumentation of the test fuel rod (spot-weldings of the very thin thermocouples on the cladding surface), installation of the test rod into the holder with other instruments such as CA thermocouples and assembling them into the double-container type experimental capsule were performed in the hot cells using remotely controlled and partially computerized equipments. Such jobs were the first experience for us. Transient responses of the instrumentation used in Test JM-1 showed that the above procedures were successfully performed (only one of the thermocouples attached on the cladding surface failed before the pulse irradiation).

## (3) Post-irradiation examination

Puncture test performed for the reference rod after the completion of the pre-irradiation showed that FP gas release was very small. However, X-ray microprobe analysis of the cladding innersurface after the pulse irradiation showed the evidence of FP release clearly and, generation of many small radial cracks and separation of the grain boundaries observed at the peripheral region of the fuel pellet suggest the possibility of the significant release of gaseous FP during the pulse irradiation. Unfortunately, puncture test for the rod used in Test JM-1 was impossible at this moment due to the lack of the device and time. Estimation of the energy deposition by chemical analysis of FP ( $^{140}\text{Ba}$ ) requested quick transfer of the sample because of the short half-life of  $^{140}\text{Ba}$ . Presently, preparation for the puncture test was completed and all of the test rod with no cladding failure will be supplied to the puncture test to estimate the FP gas release due to a pulse irradiation.



## 8. Conclusions

The following major conclusions were derived through this study.

- (1) Effectivenesses of all of the test facilities and procedures for the pre-irradiated fuel test in NSRR were confirmed through the conduct of the first test, JM-1.
- (2) Pre-irradiation of the test fuel rods in JMTR was favorably completed. However, presence of the small white deposits on the cladding surface was found by the dimensional measurement and eddy current measurement of the test fuels after the completion of the pre-irradiation. Slight discoloration of the cladding surface was another finding. This is probably due to oxidation by the residual air in the irradiation capsule.
- (3) PCMI did not occur during the pre-irradiation and swelling of the fuel was not significant. Puncture test for the reference rod showed that FP gas release during the pre-irradiation was very small.
- (4) The test rod subjected to an energy deposition of  $126 \text{ cal/g} \cdot \text{UO}_2$  by the pulse irradiation in NSRR did not fail. This energy deposition exceeds the minimum energy of fuel failure observed in SPERT project with pre-irradiated rods. No DNB occurred in this test.
- (5) Newly observed phenomena by the examination of the test fuel rod after the pulse irradiation are generation of the many radial small cracks and slight separation of the grain boundaries at the peripheral region of the fuel pellet. No PCMI was identified through the examination.

## Acknowledgements

This work has been done in co-operation with Department of JMTR Project, Department of Research Reactor, Department of Chemistry and Department of Fuel Safety Research, JAERI. The authors wish to thank those people who are working with us in these departments for their excellent contributions to this study. The authors also gratefully acknowledge the collaborations in conducting the experiment and many useful discussions by their colleagues in Reactivity Accident Laboratory and NSRR Operation Division, JAERI.

## References

- (1) M. Ishikawa and S. Shiozawa, "A Study of Fuel Behavior Under Reactivity Initiated Accident Conditions - Review", J. Nucl. Mat., Vol. 95, Nos. 1&2, Nov. 1980, pp. 1-30
- (2) P. E. MacDonald, et. al., "Assessment of Light-Water-Reactor Fuel Damage During a Reactivity-Initiated Accident", Nuclear Safety, Vol. 21, No. 5, Sept.-Oct. 1980, pp. 582-602
- (3) T. G. Taxelius, et. al., "Annual Report SPERT Project October 1968-September 1969", IN-1370/TID-4500, June 1970, pp. 26-29

## Acknowledgements

This work has been done in co-operation with Department of JMTR Project, Department of Research Reactor, Department of Chemistry and Department of Fuel Safety Research, JAERI. The authors wish to thank those people who are working with us in these departments for their excellent contributions to this study. The authors also gratefully acknowledge the collaborations in conducting the experiment and many useful discussions by their colleagues in Reactivity Accident Laboratory and NSRR Operation Division, JAERI.

## References

- (1) M. Ishikawa and S. Shiozawa, "A Study of Fuel Behavior Under Reactivity Initiated Accident Conditions - Review", J. Nucl. Mat., Vol. 95, Nos. 1&2, Nov. 1980, pp. 1-30
- (2) P. E. MacDonald, et. al., "Assessment of Light-Water-Reactor Fuel Damage During a Reactivity-Initiated Accident", Nuclear Safety, Vol. 21, No. 5, Sept.-Oct. 1980, pp. 582-602
- (3) T. G. Taxelius, et. al., "Annual Report SPERT Project October 1968-September 1969", IN-1370/TID-4500, June 1970, pp. 26-29

Table 1 Operation modes of NSRR

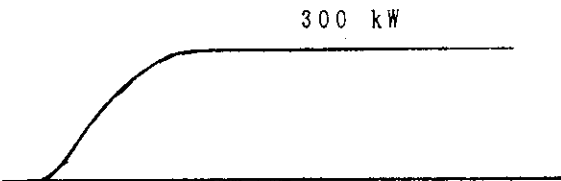
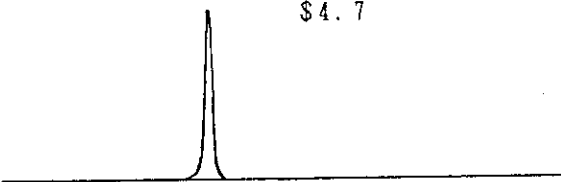
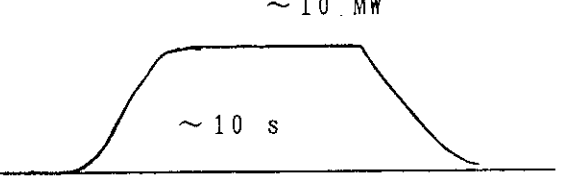
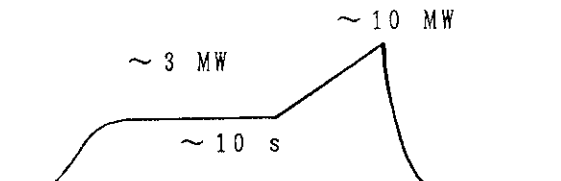
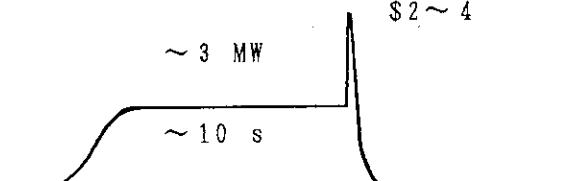
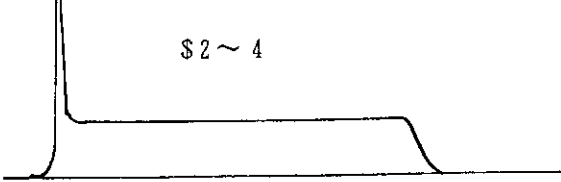
Operation mode	Reactor power characteristics	
Steady state operation	Steady state	 <p>300 kW</p>
Natural pulse operation	Pulse from zero power	 <p>4.7</p>
Shaped pulse operation	Power decrease from high power	 <p>~ 10 MW ~ 10 s</p>
	Power increase from high power	 <p>~ 3 MW ~ 10 s ~ 10 MW</p>
Combined pulse operation	Pulse from high power	 <p>~ 3 MW ~ 10 s 2 ~ 4</p>
	Pulse from zero power and high runout power	 <p>2 ~ 4</p>

Table 2 Major characteristics of NSRR

1. <u>Reactor type</u>	: Modified TRIGA-ACPR (Annular Core Pulse Reactor)
2. <u>Reactor pool</u>	: 3.6 m(wide) × 4.5 m(long) × 9 m(deep) open pool
3. <u>Driver fuel</u>	:
Fuel type	12 wt%U-ZrH <sub>1.6</sub>
Fuel enrichment	20 wt% in <sup>235</sup> U
Cladding material	Stainless steel
Fuel diameter	3.56 cm
Cladding diameter	3.76 cm (outer diameter)
Fuel stack length	38.1 cm
Number of fuel rods	157 (including 8 fuel-follower control rods)
Equivalent core dia.	
4. <u>Control rods</u>	:
Number	8 (including 2 safety rods)
Type	Fuel-follower type
Poison material	Natural B <sub>4</sub> C
Rod drive	Electric rack and pinion drive
5. <u>Transient rods</u>	:
Number	2 fast transient rods and 1 adjustable transient rod
Type	Air-followed type
Poison material	92% enriched B <sub>4</sub> C
Rod drive	Fast: Pneumatic drive Adjustable: Rack&pinion and pneumatic drives
6. <u>Core performance</u>	:
a) Steady state operation	
Max. reactor power	
b) Natural pulse operation	
Max. reactor power	2,3000 MW
Max. burst energy	130 MWs
Max. reactivity insertion	\$4.7
Min. period	1.17 ms (at \$4.67)
Min. pulse width	4.4 ms (at \$4.67)
c) Shaped pulse operation	
Max. reactor power	10 MW
Max. burst energy	110 MWs
d) Combined pulse operation	
Max. reactor power	23,000 MW by transient rods 10 MW by regulating rods
Max. burst energy	110 MWs
Max. reactivity insertion	\$4.0
7. <u>Experimental tube</u>	:
Inner diameter	22 cm

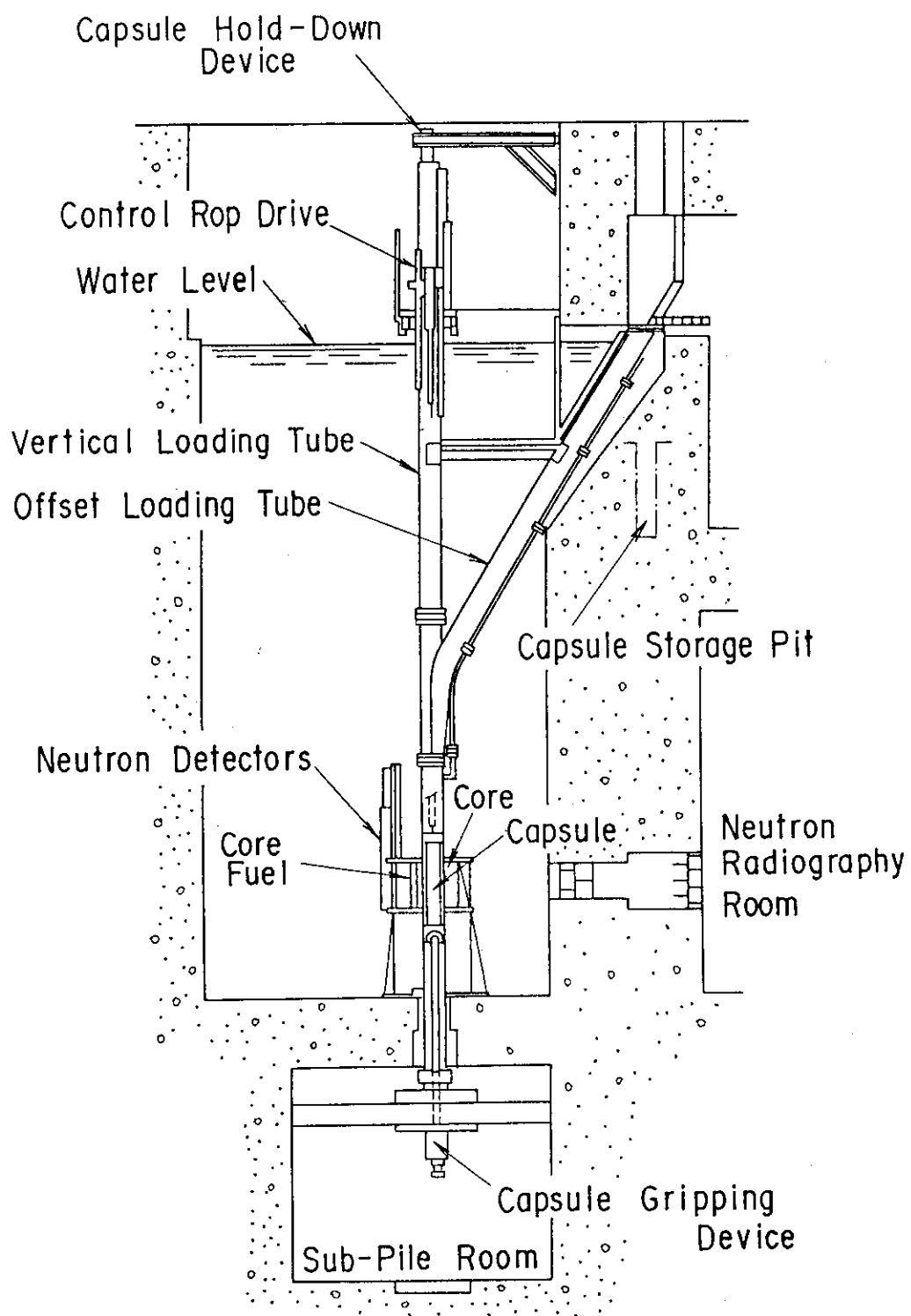


Fig. 1 Vertical cross-section of NSRR

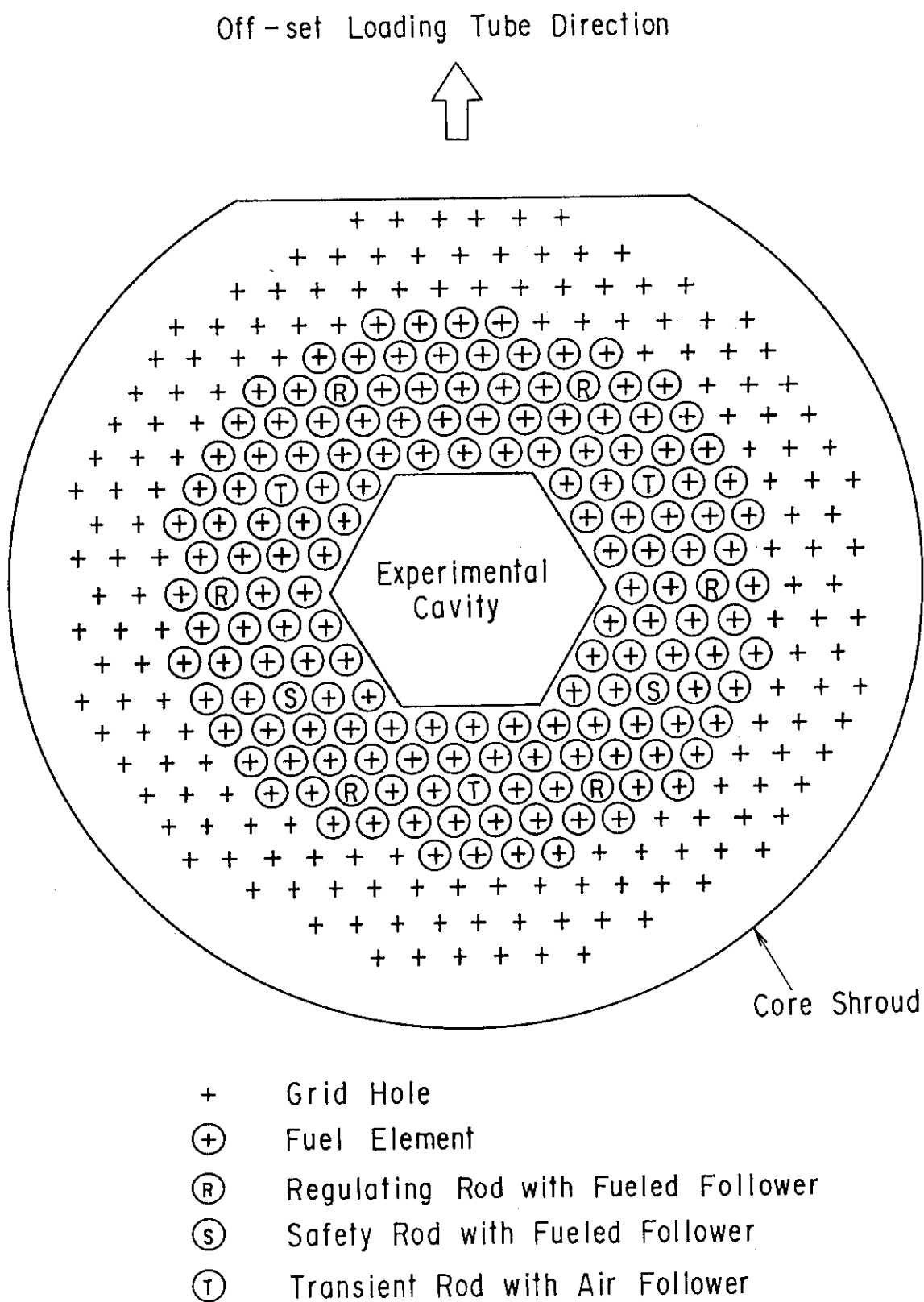
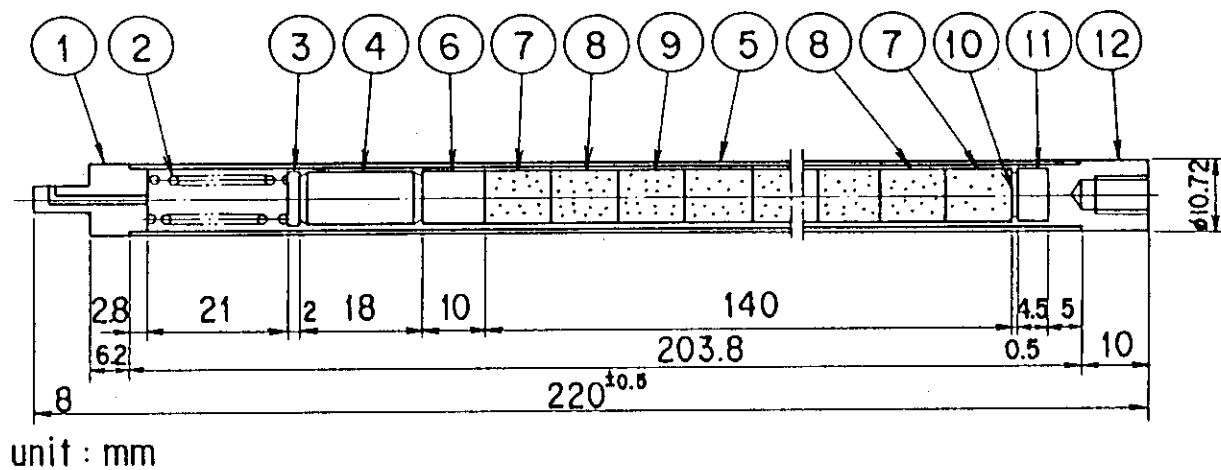


Fig. 2 Operational core configuration of NSRR



No.	Item	Material
1	Top end fitting	Zry-4
2	Spring	Inconel
3	Spring holder	SUS 304
4	Iron core	MEIF
5	Cladding tube	Zry-4
6	Alumina pellet	Al <sub>2</sub> O <sub>3</sub>
7	UO <sub>2</sub> pellet (Nat.)	UO <sub>2</sub>
8	UO <sub>2</sub> pellet ( 5% )	UO <sub>2</sub>
9	UO <sub>2</sub> pellet (10%)	UO <sub>2</sub>
10	Disk	SUS304
11	Spacer	SUS304
12	Bottom end fitting	Zry-4

Fig. 3 Design of test fuel rod



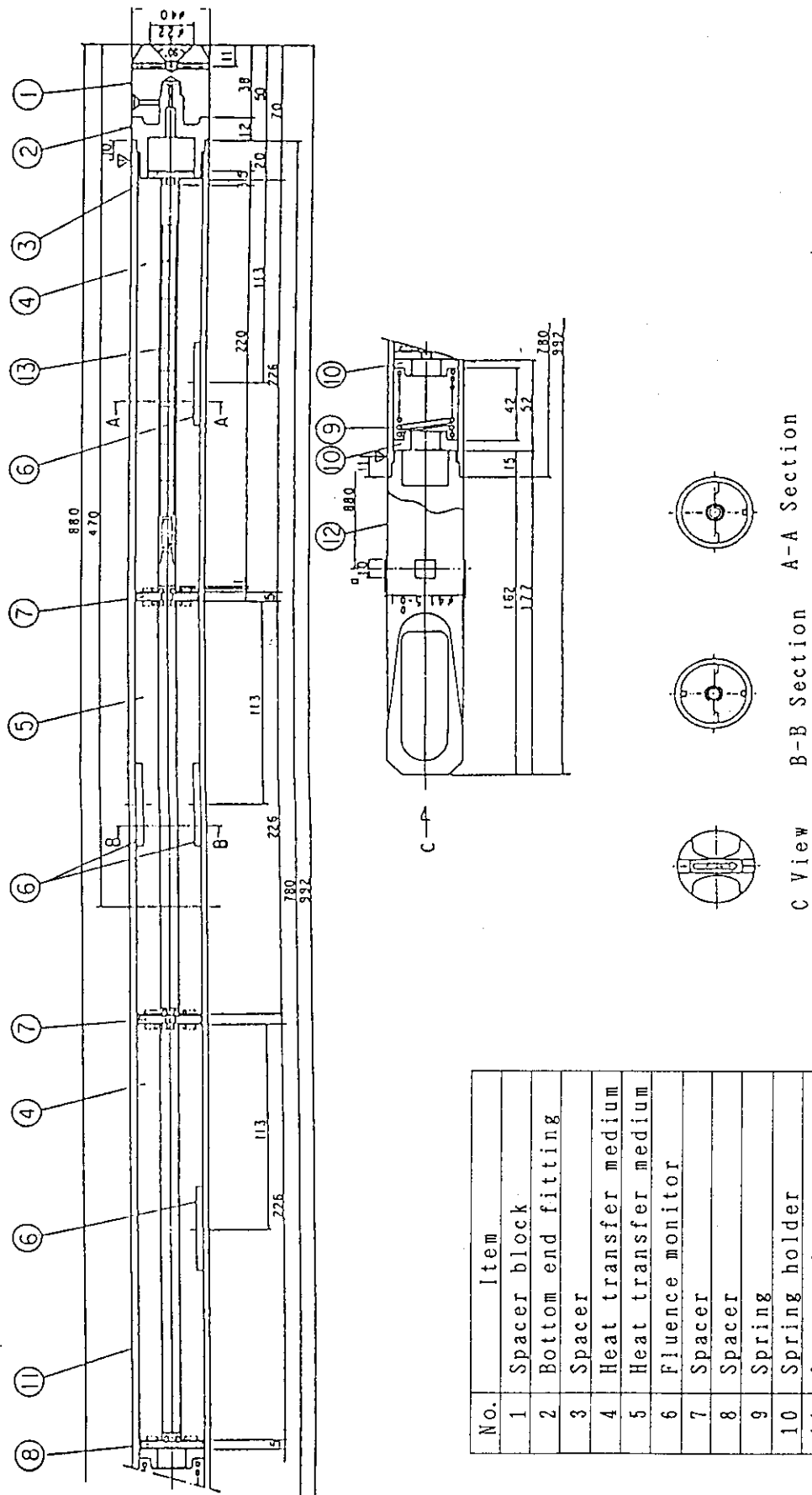


Fig. 4 Capsule for pre-irradiation of test fuel rod

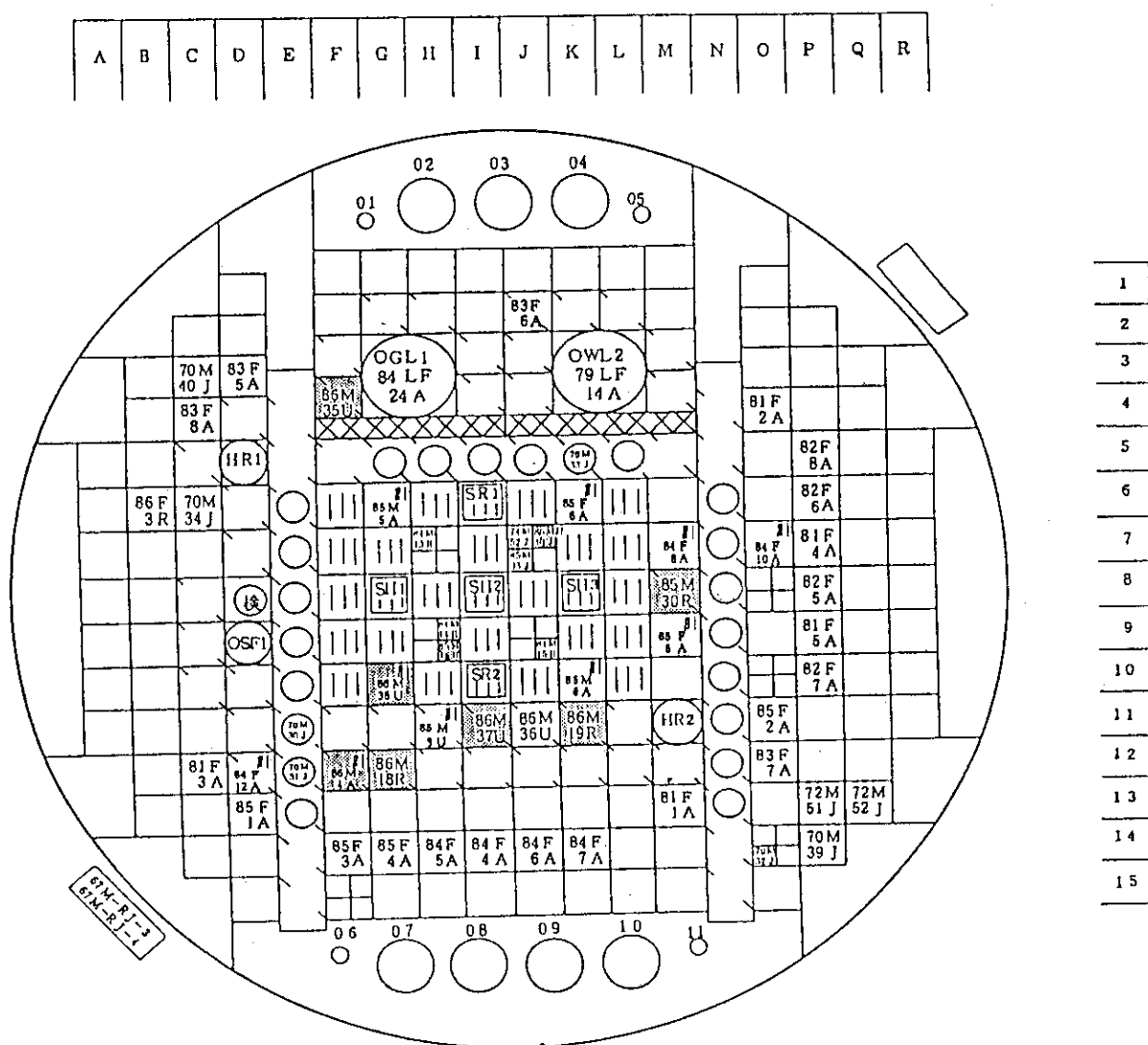


Fig. 5 Core configuration of JMTR at the operation cycle No.78

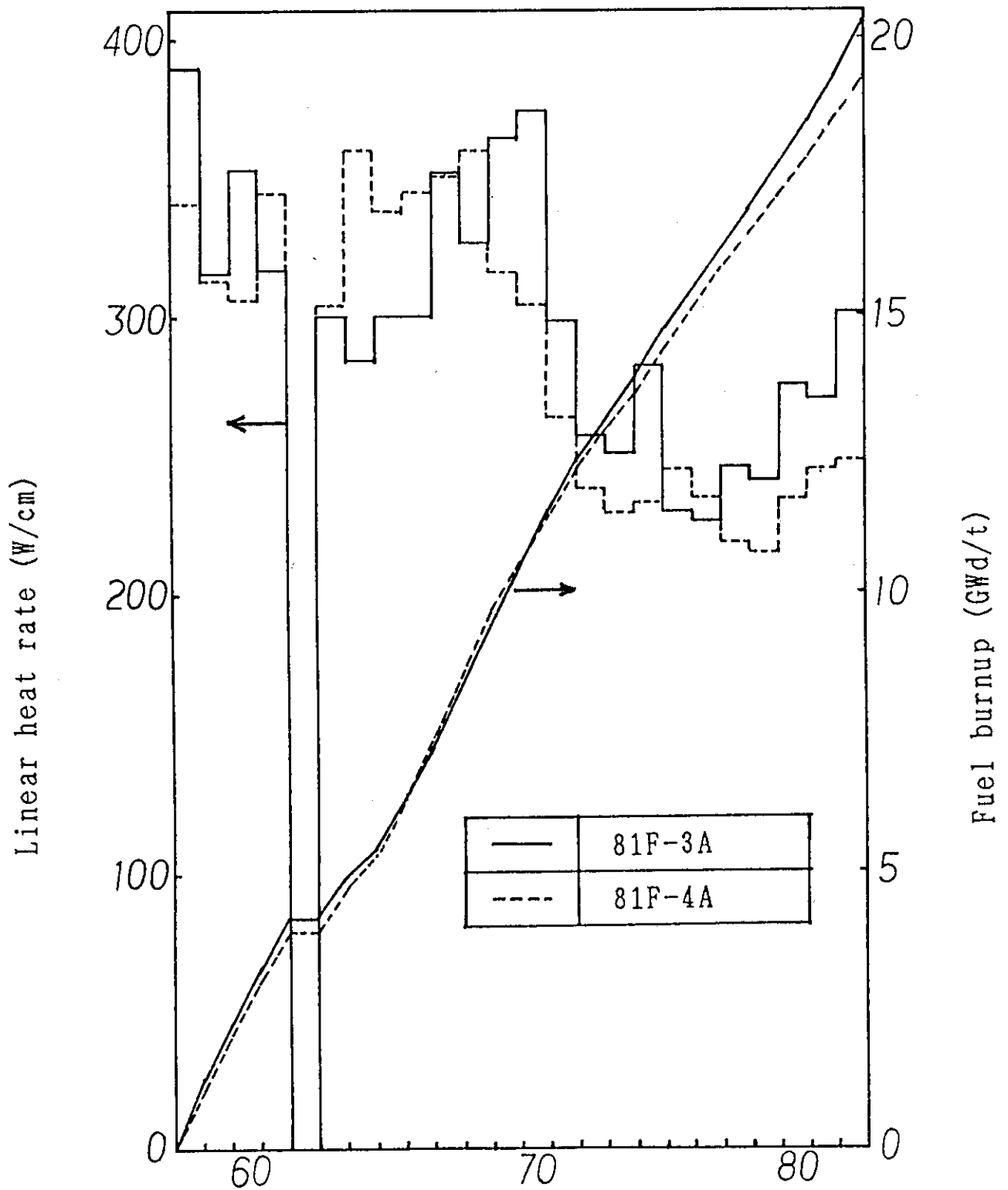


Fig. 6 Irradiation histories of the capsules 81F-3A and 4A.

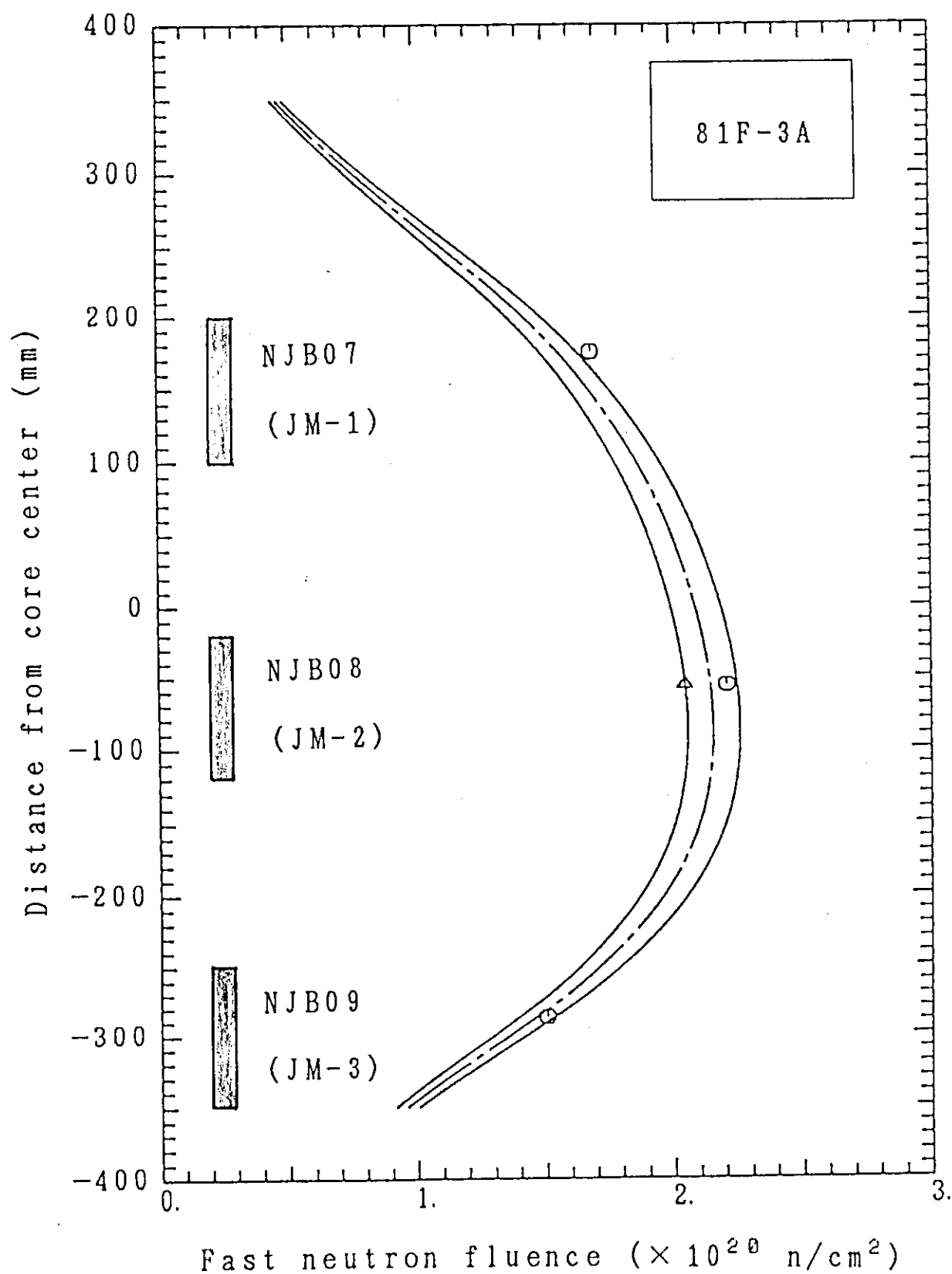


Fig. 7 Result of fast neutron fluence measurement for 81F-3A capsule

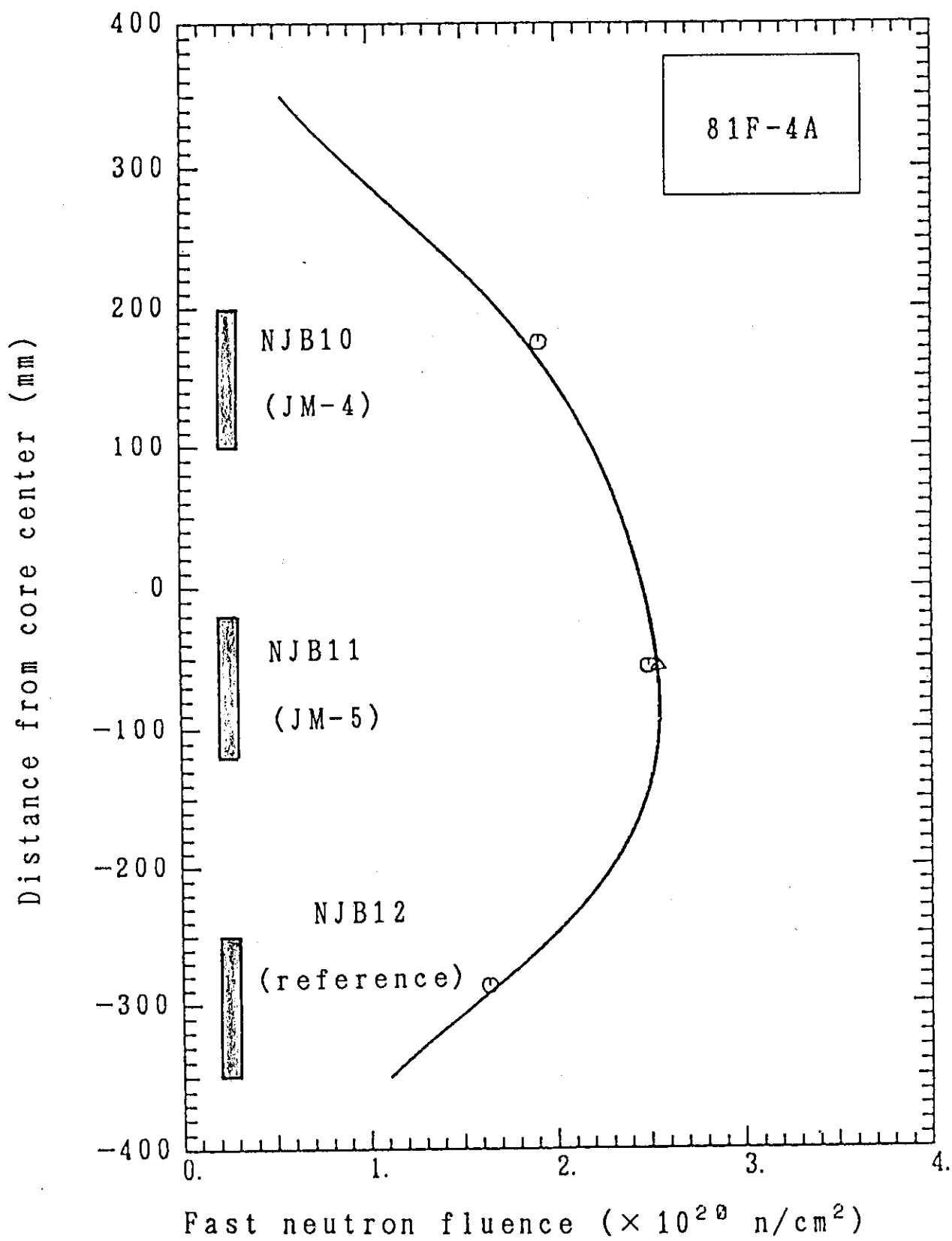


Fig. 8 Result of fast neutron fluence measurement for 81F-4A capsule

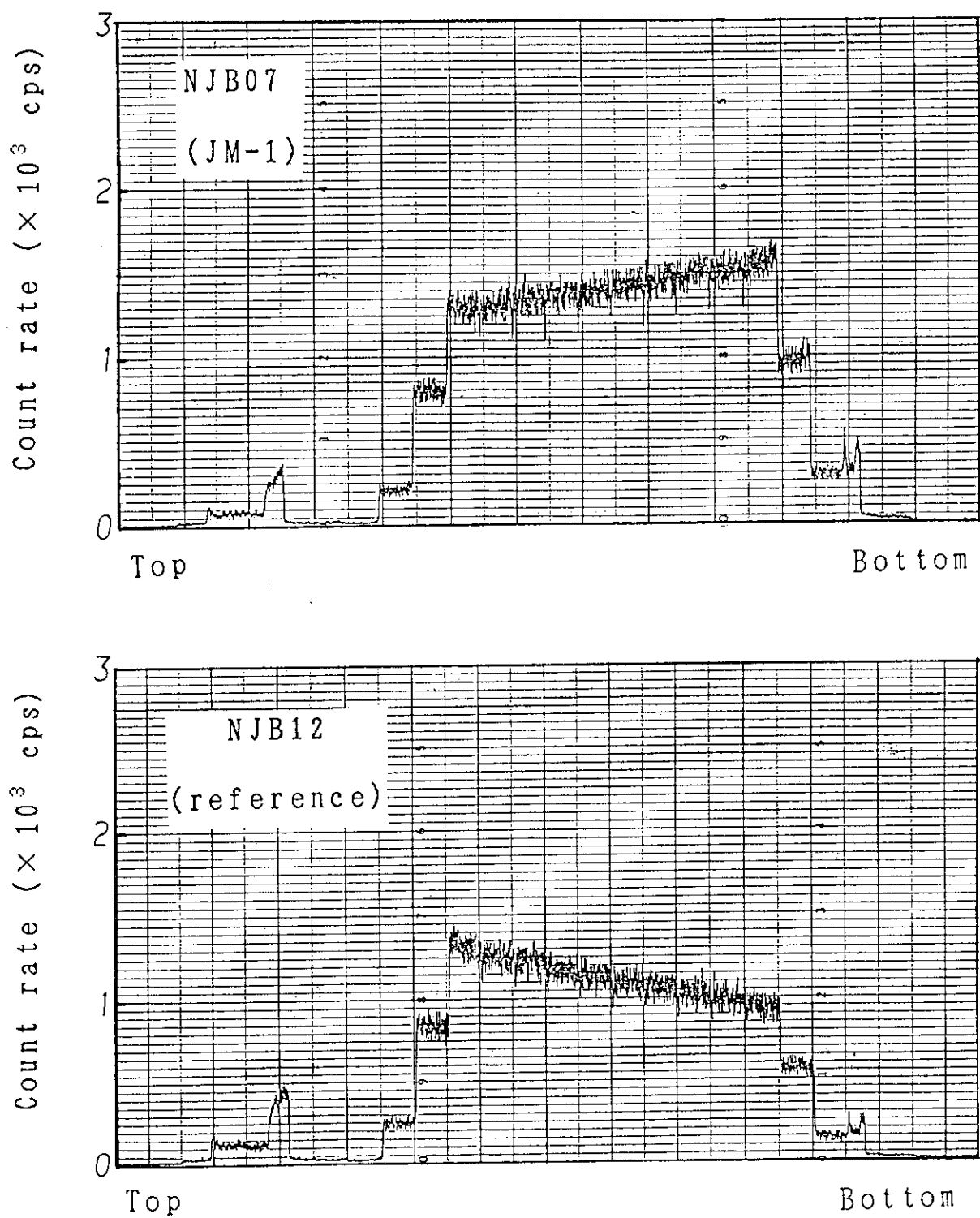


Fig. 9 Result of gross  $\gamma$ -ray scanning for NJB07 and NJB12 rods after the completion of the pre-irradiation

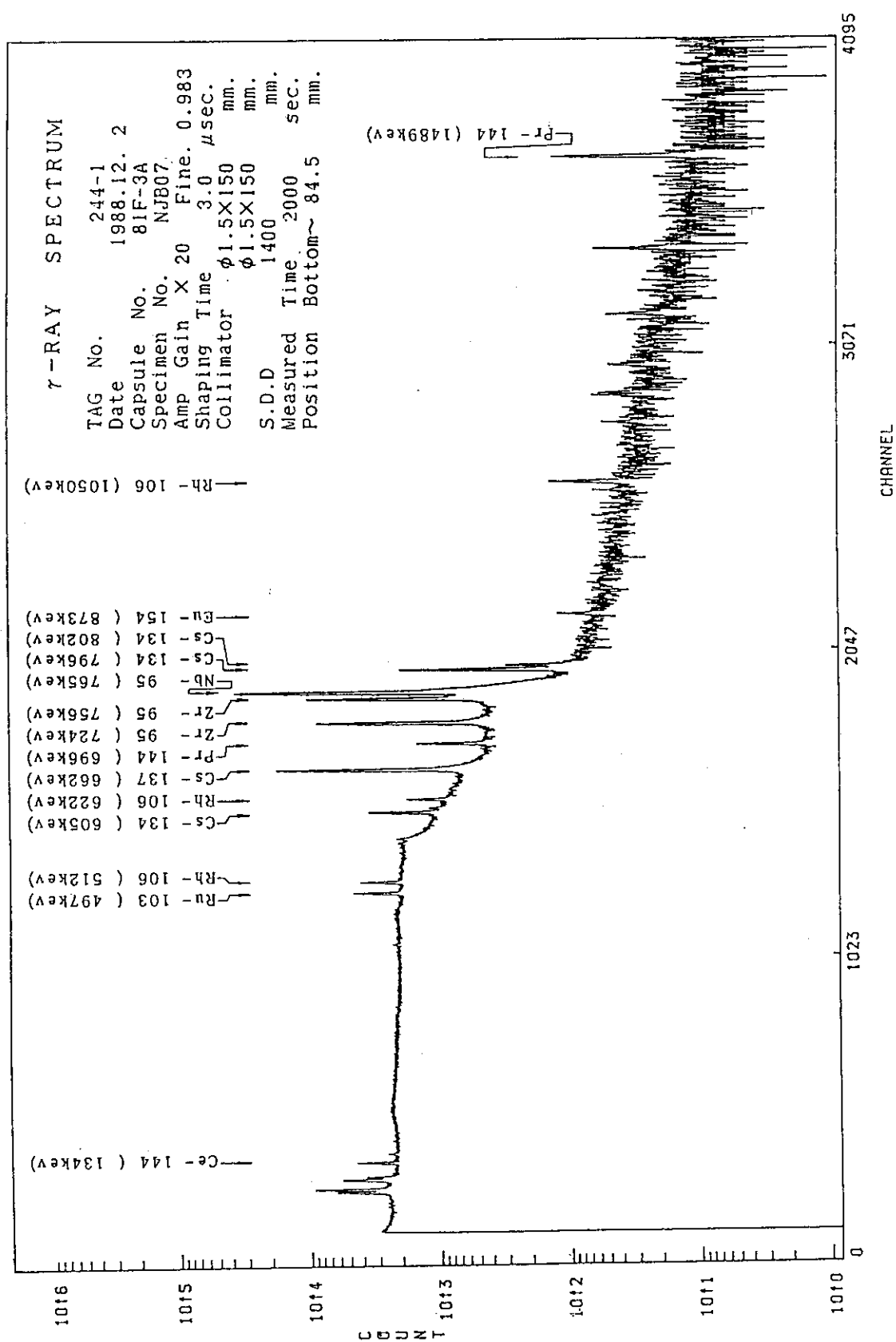


Fig. 10 Result of γ-ray spectrum measurement for NJB07 rod  
after the completion of the pre-irradiation

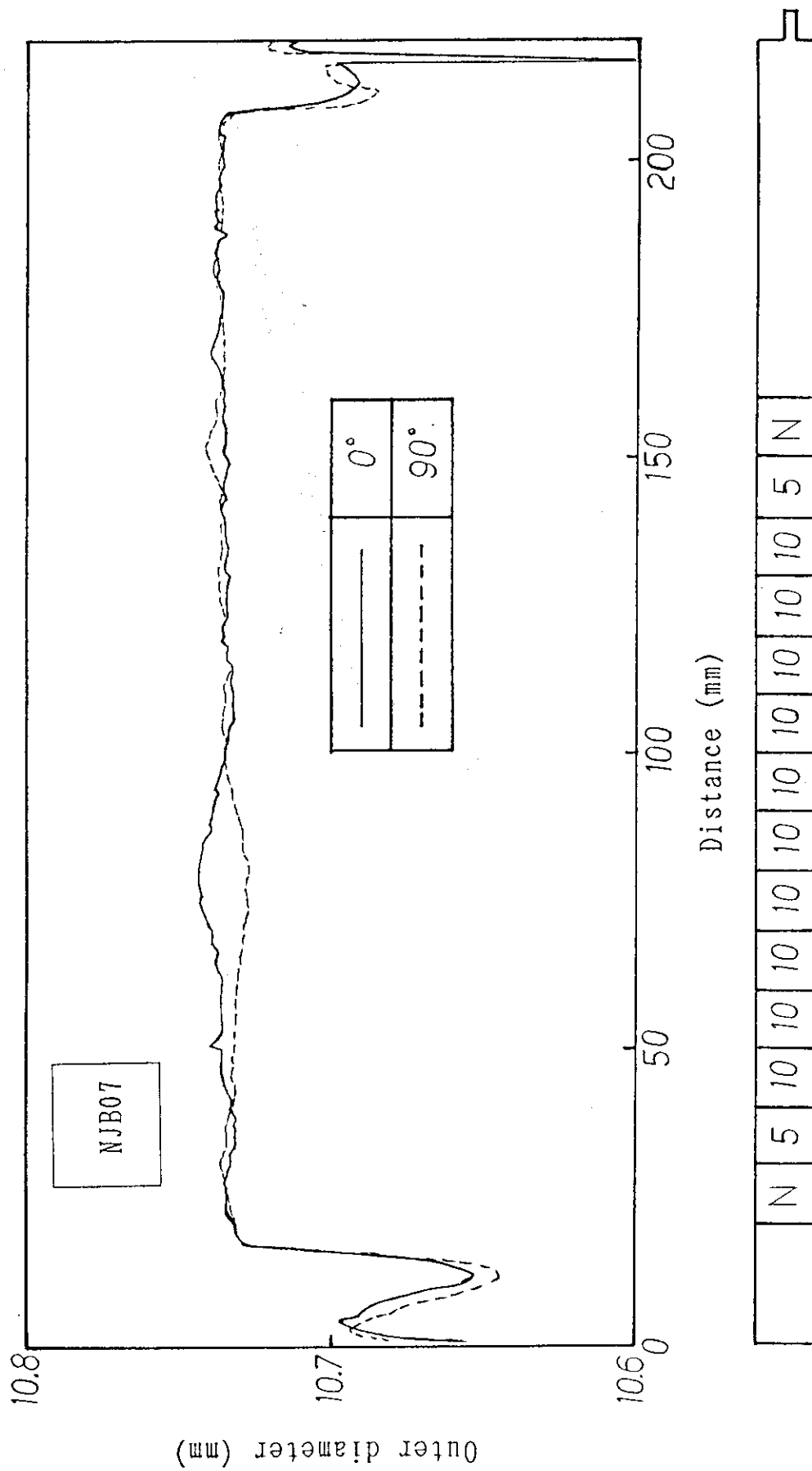


Fig. 11 Axial profile of NJB07 rod measured after the completion of the pre-irradiation



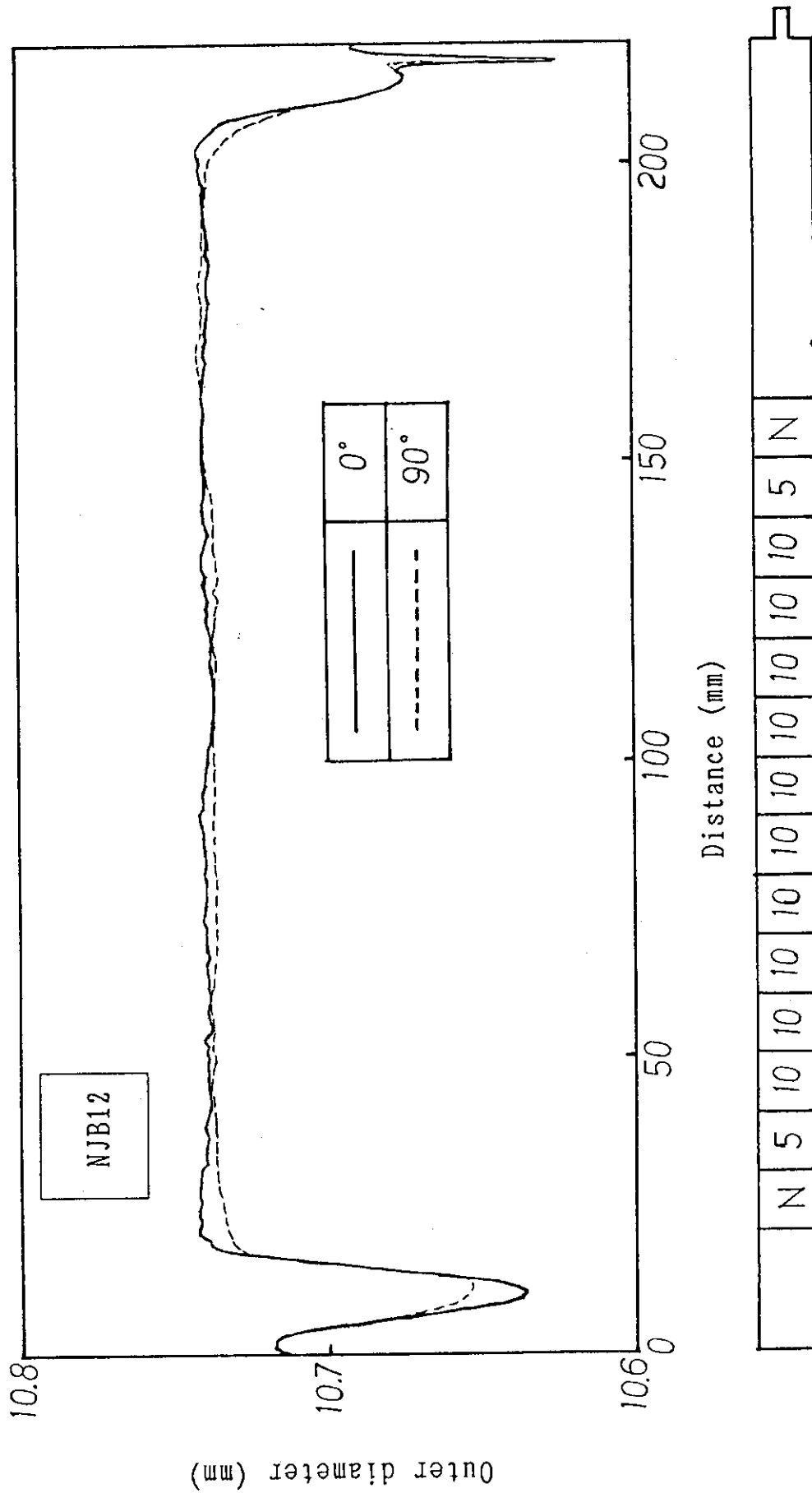
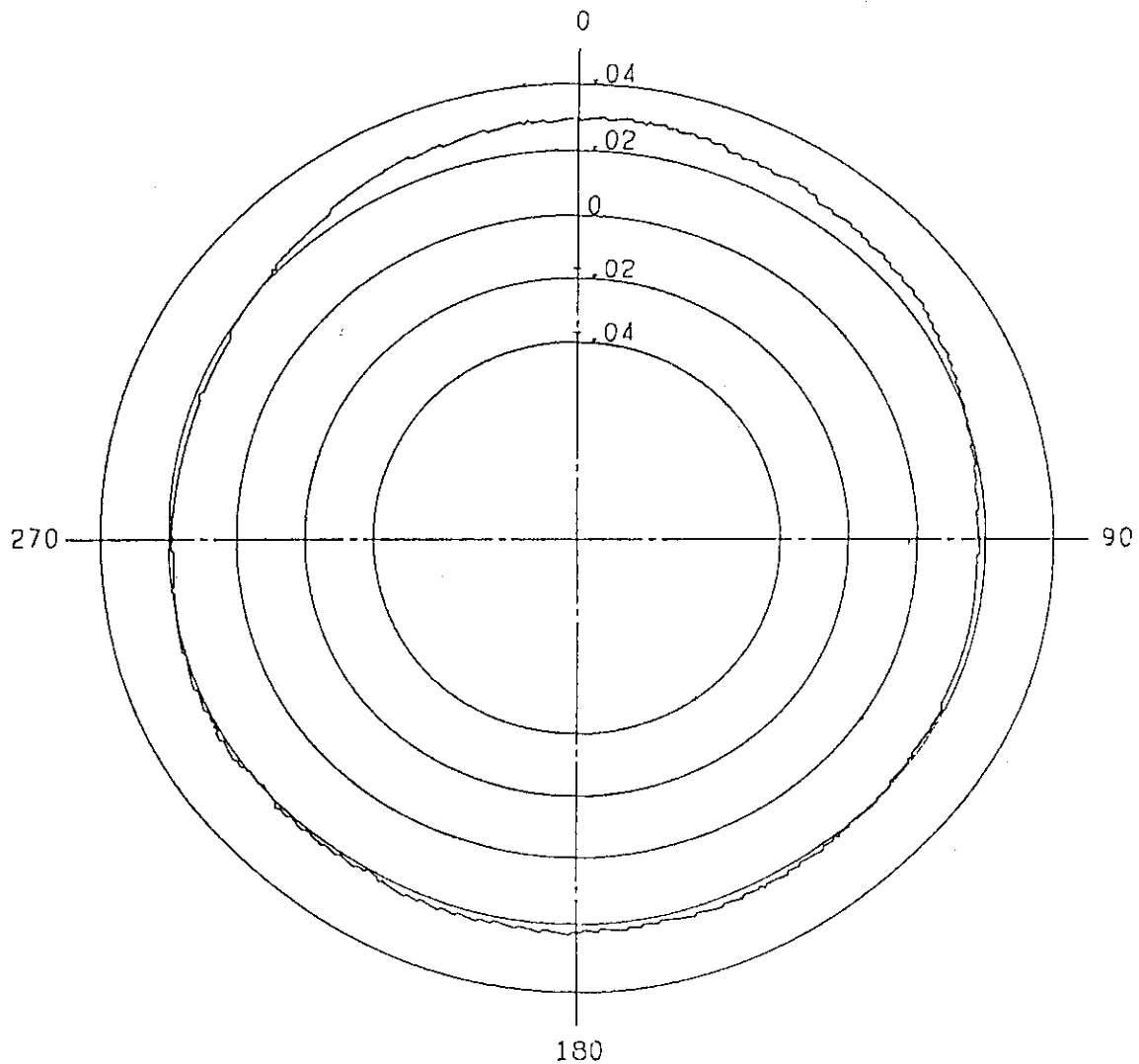


Fig. 12 Axial profile of NJB12 rod measured after the completion of the pre-irradiation

\*\*\*\*\* 81F-3A Cross-Section Profile \*\*\*\*\*

NO.NJB07

ADDRESS 79 (MM)



Sheet No.1

Fig. 13 Cross-sectional profile of NJB07 rod measured after the completion of the pre-irradiation

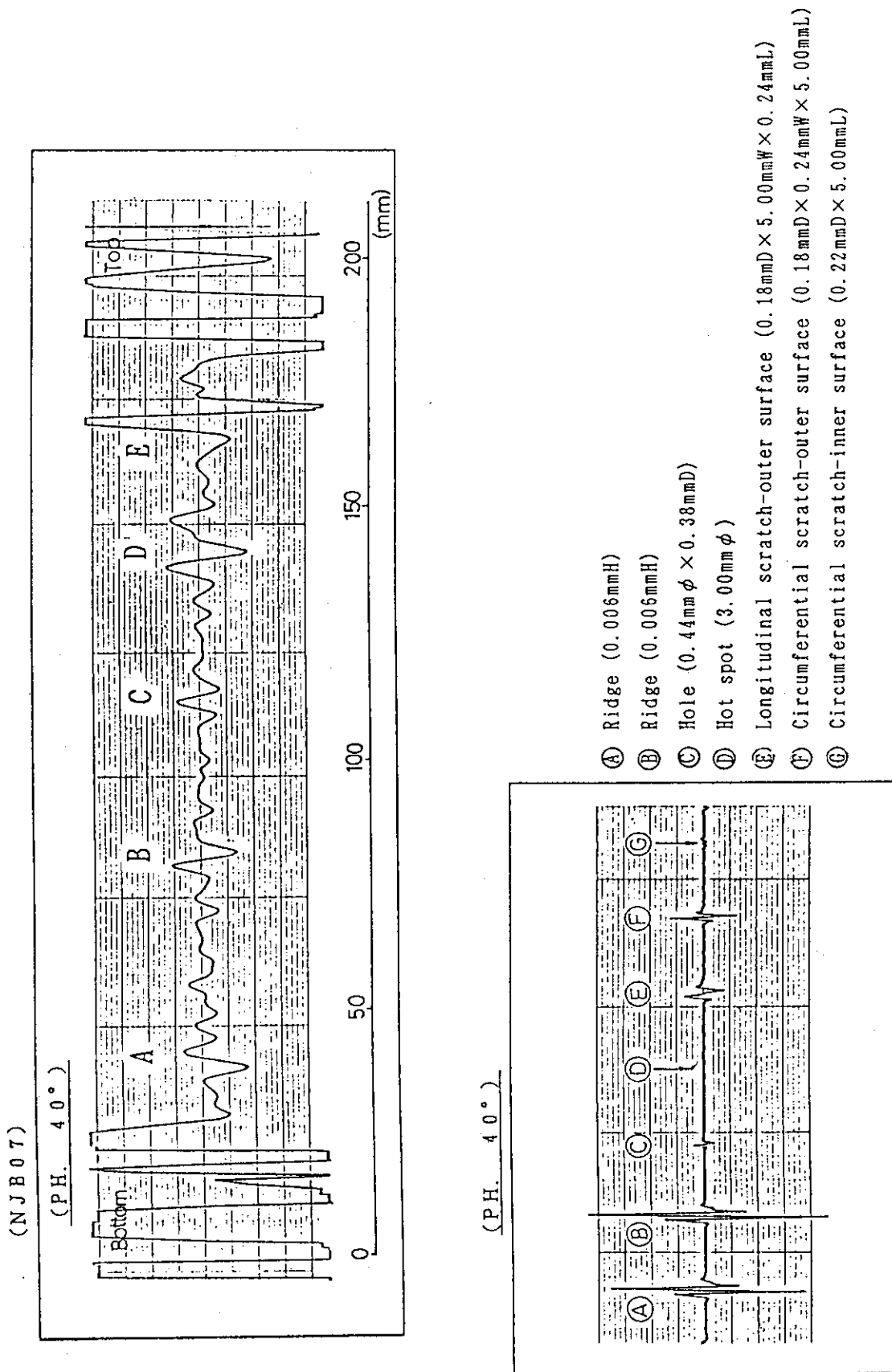


Fig. 14 Result of eddy current measurement for NJB07 rod after the completion of the pre-irradiation

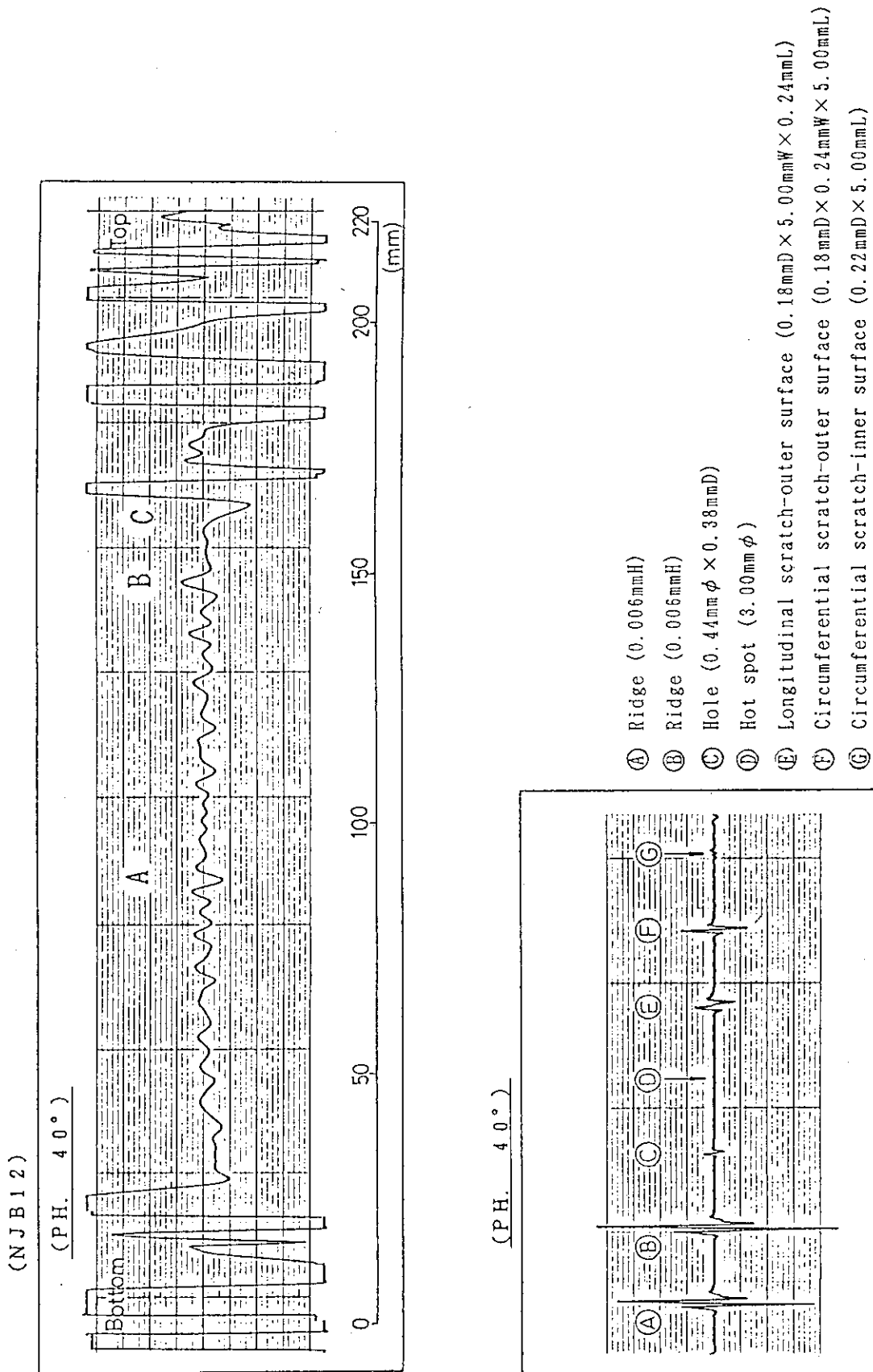


Fig. 15 Result of eddy current measurement for NJB12 rod after the completion of the pre-irradiation

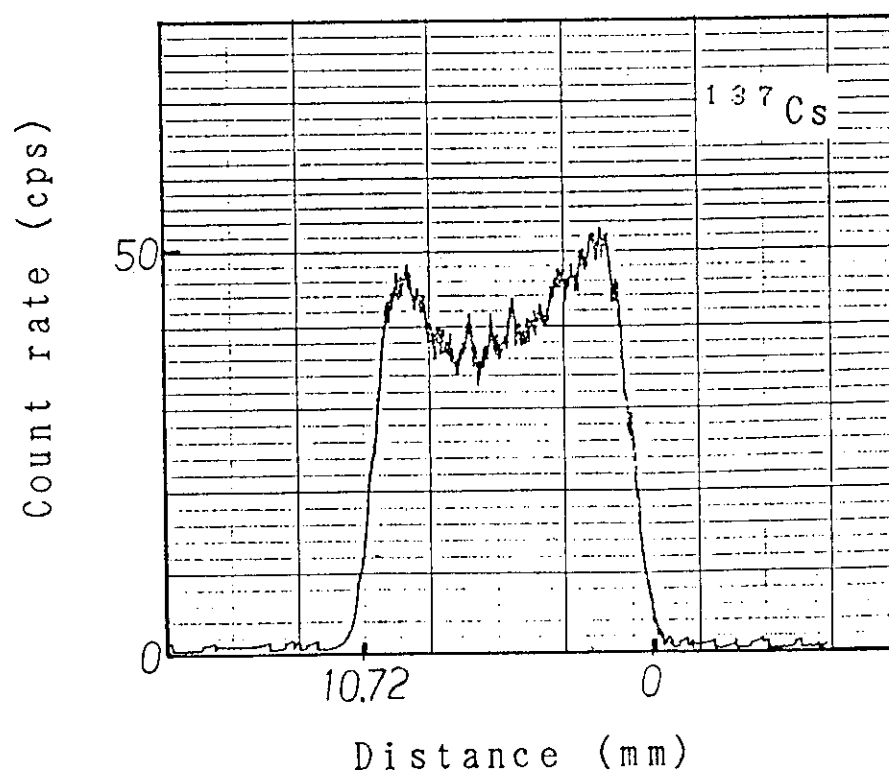
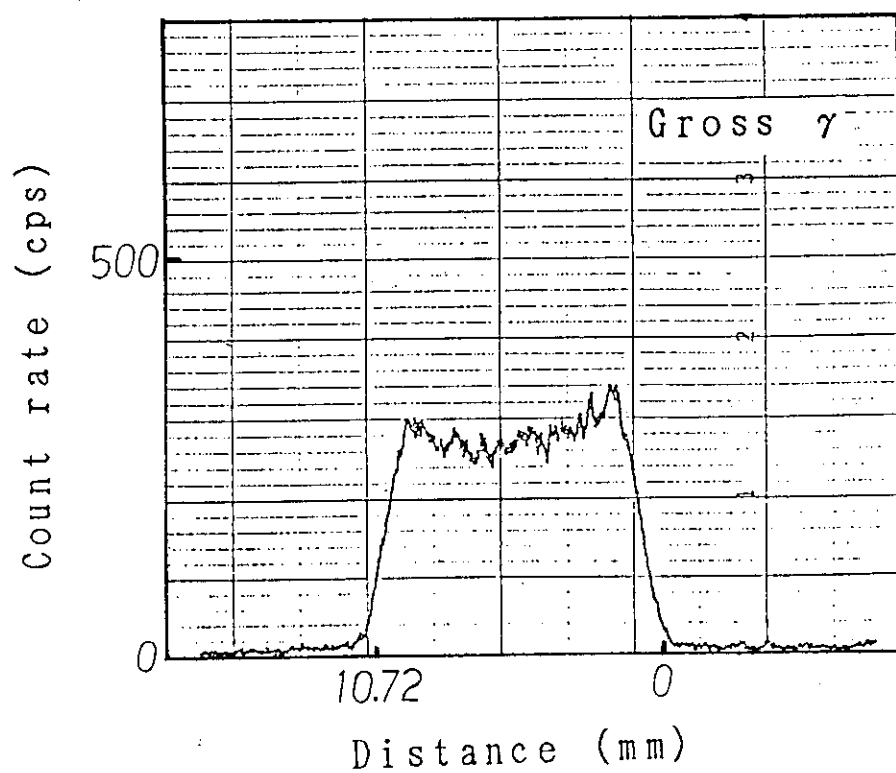


Fig. 16 Result of micro  $\gamma$ -ray scanning for the sample taken from NJB12 rod

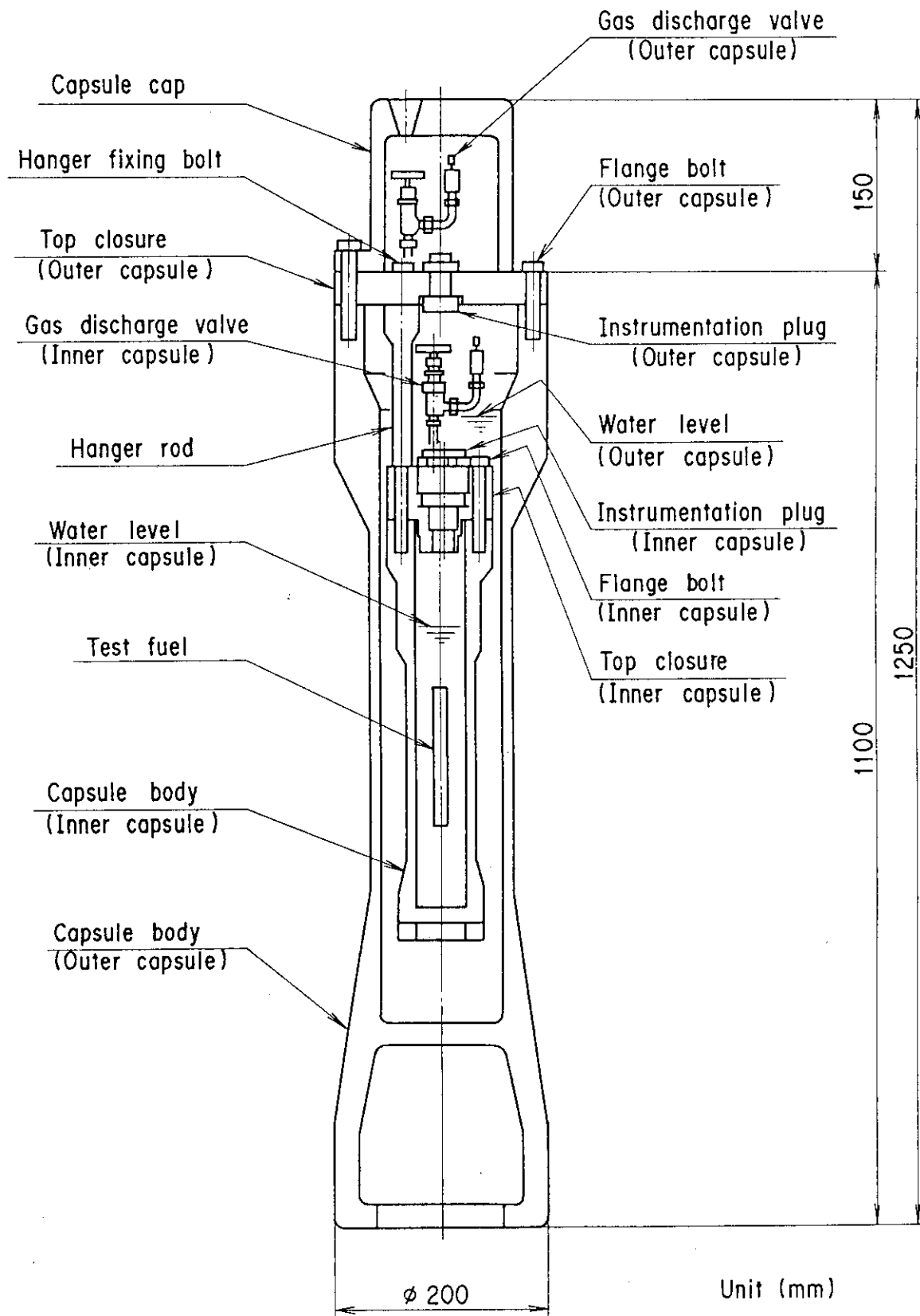


Fig. 17 Schematic configuration of experimental capsule

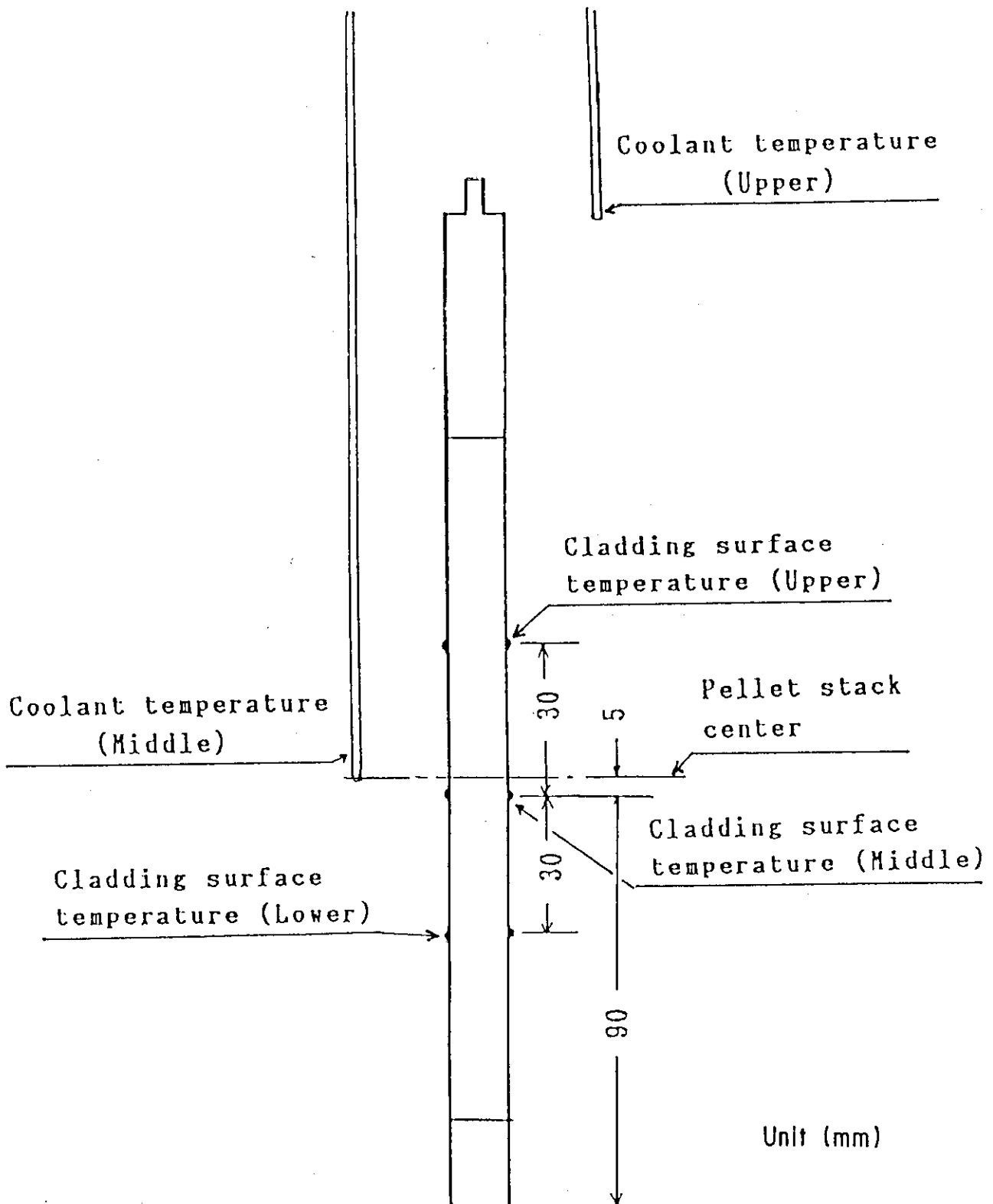


Fig. 18 Instrumentation for Test JM-1

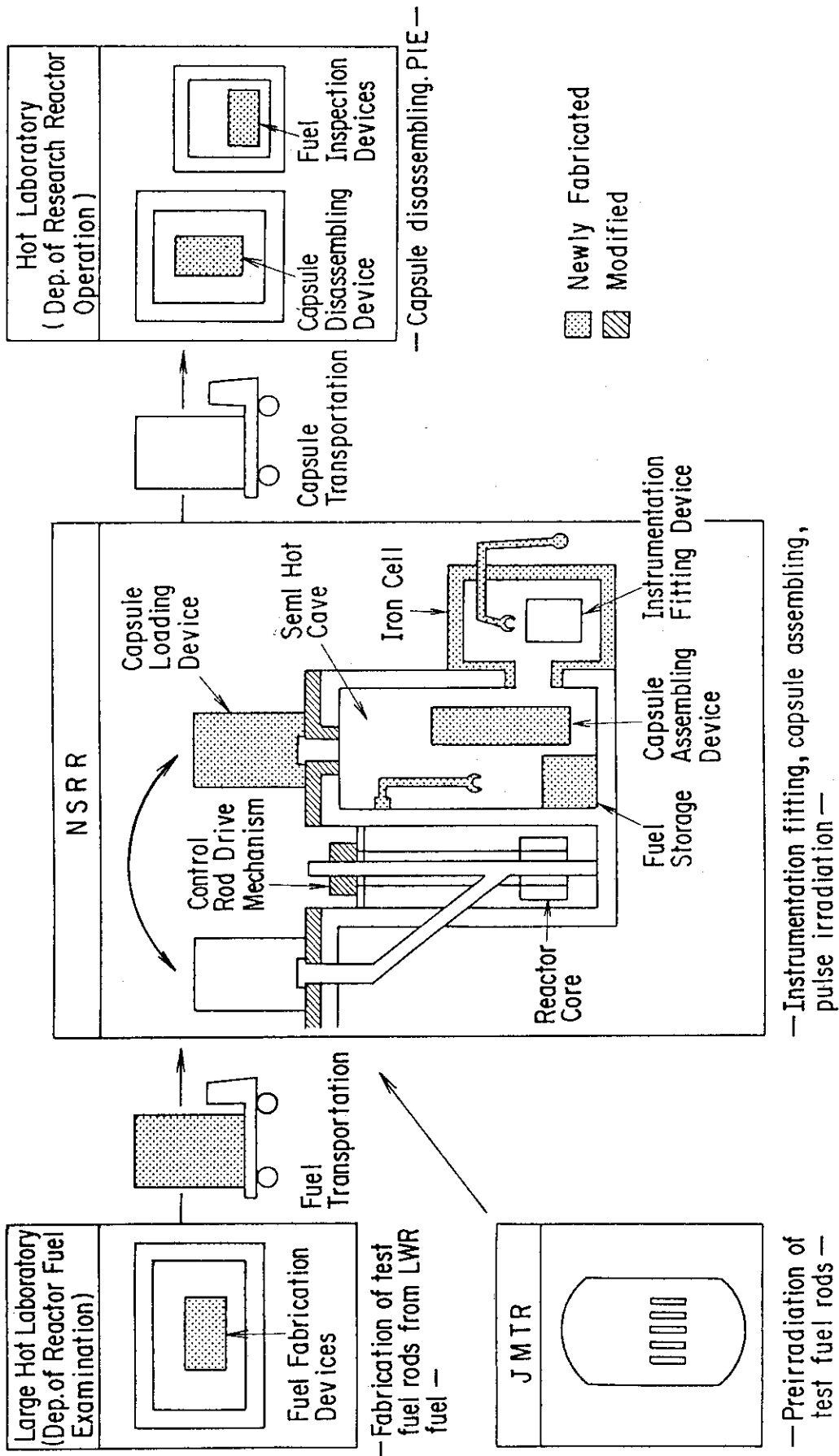
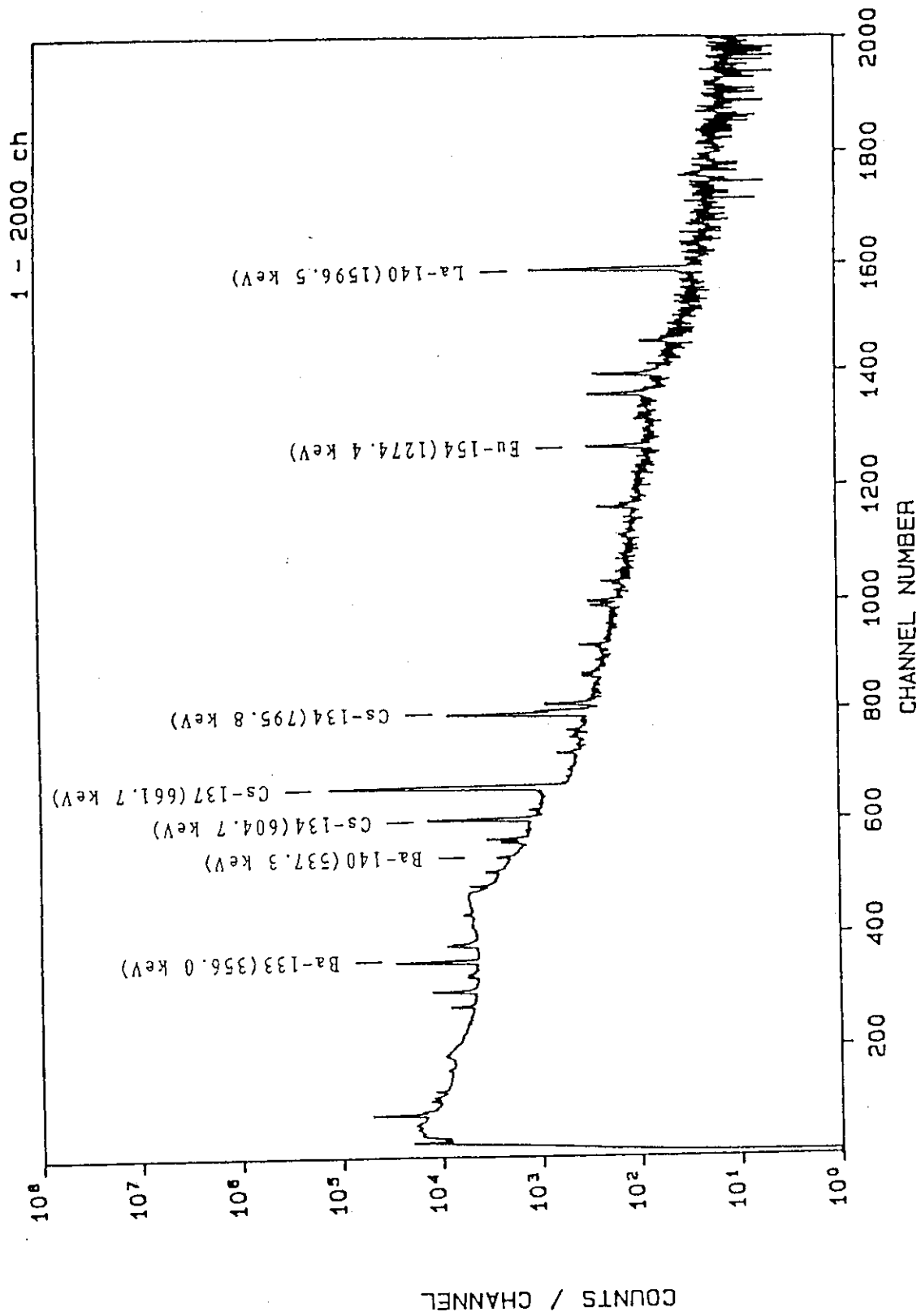


Fig. 19 Outline of general procedure for the pre-irradiated fuel test



Fig. 20  $\gamma$ -ray spectrum measurement for the processed solution

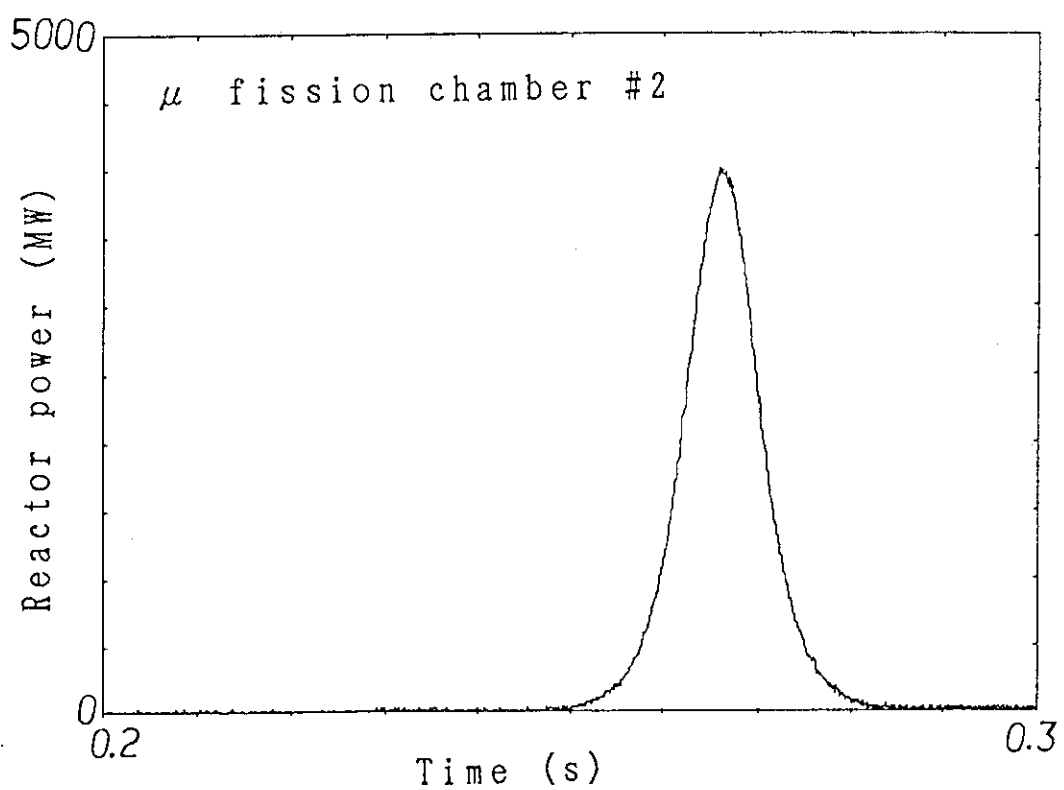
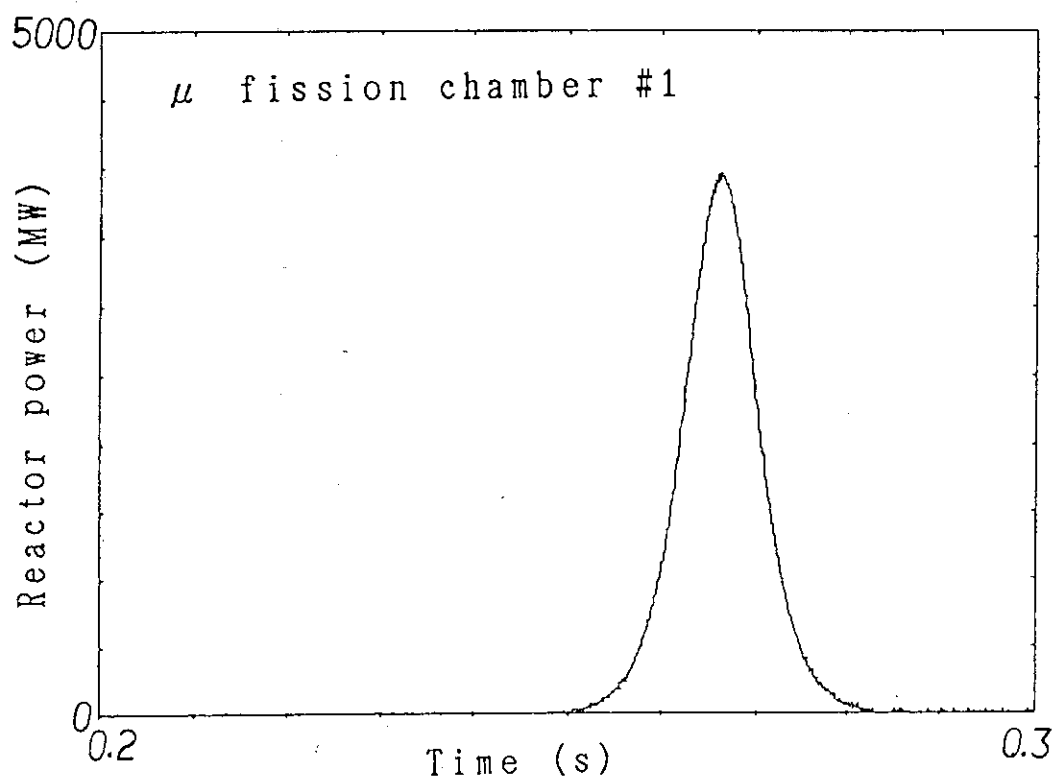


Fig. 21 Reactor power measured by micro fission chamber in Test JM-1

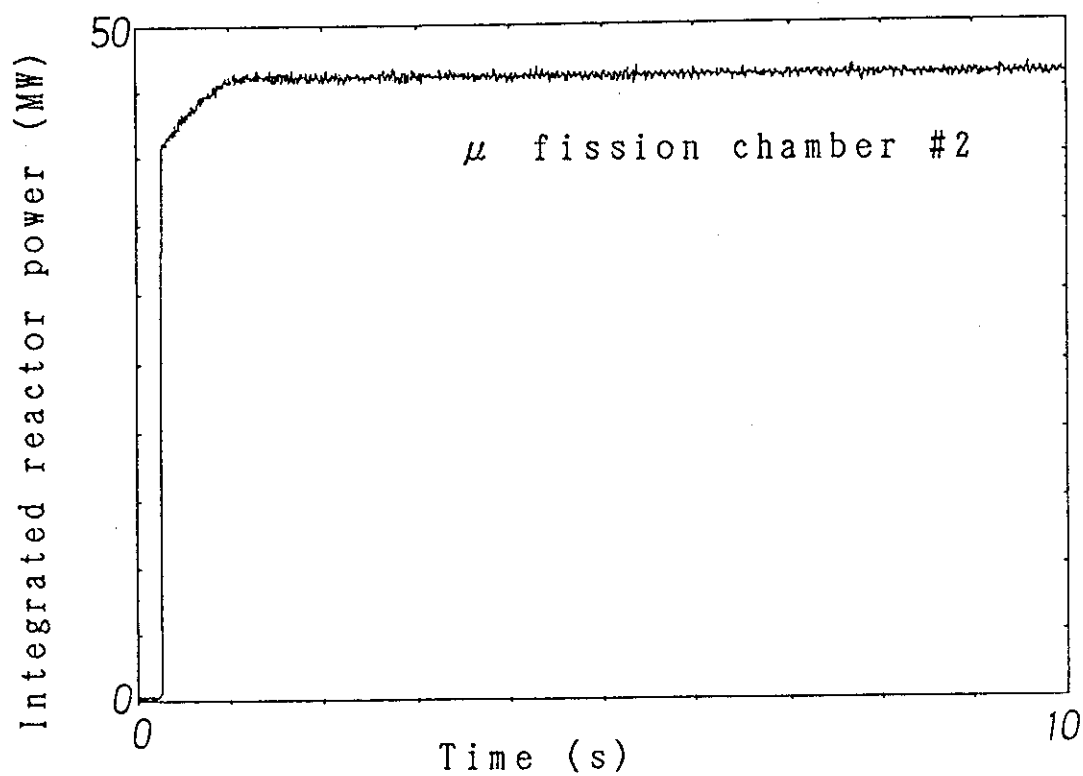
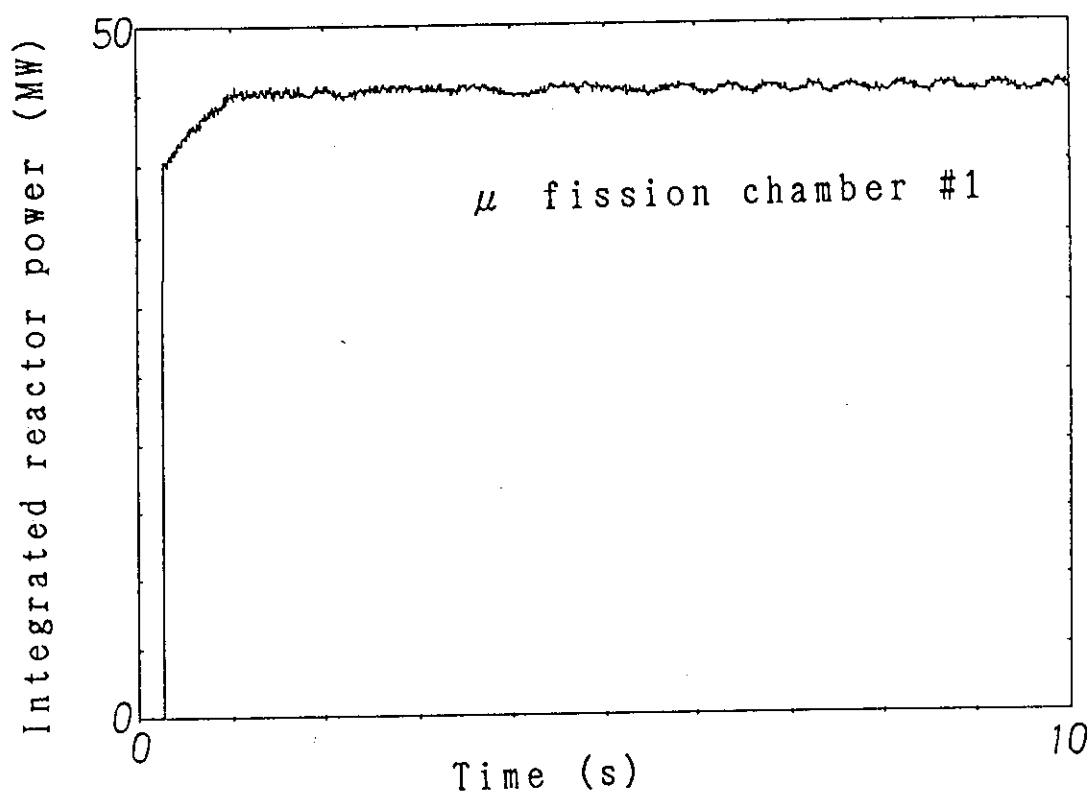


Fig. 22 Integrated reactor power measured by micro fission chamber in Test JM-1

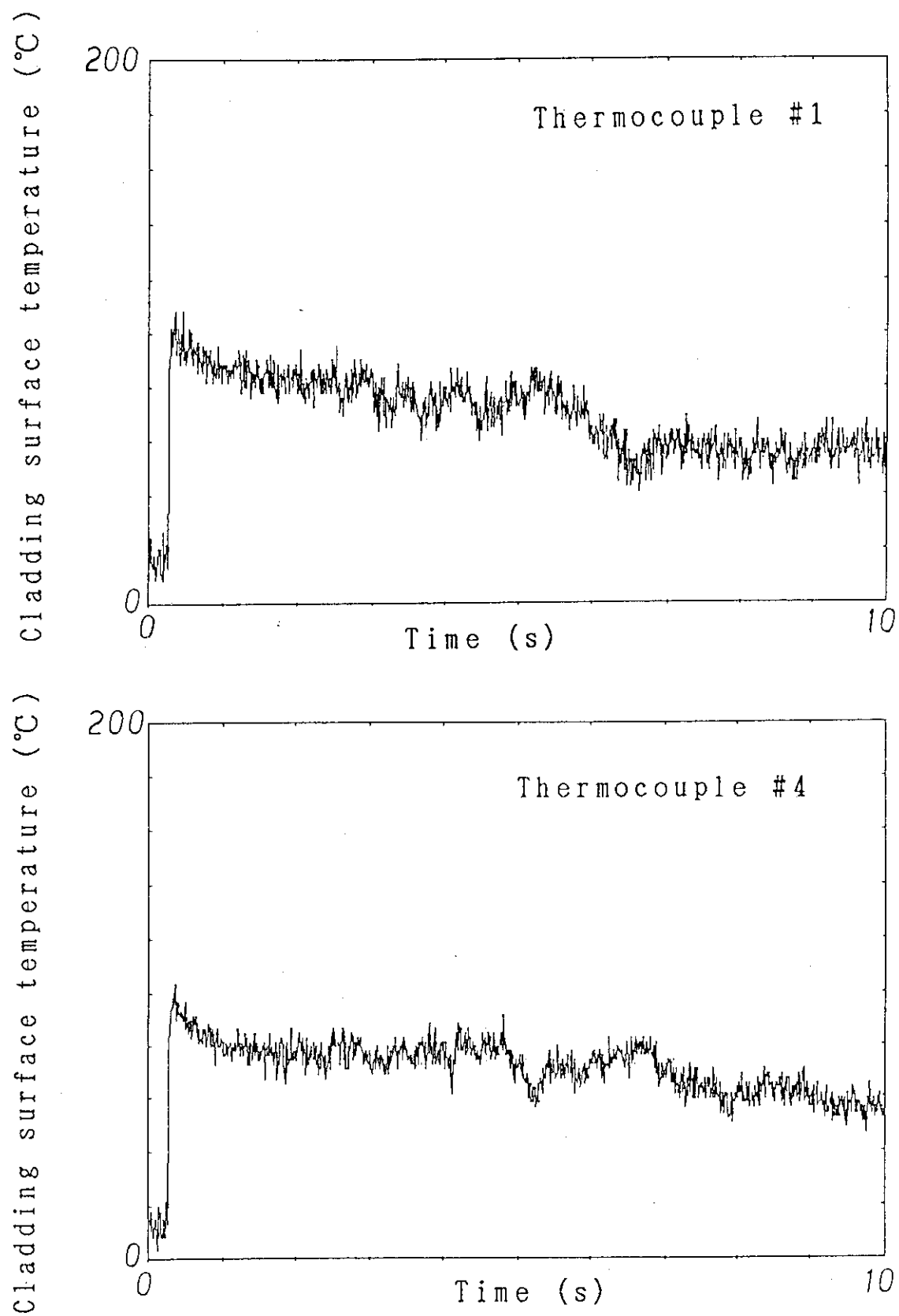


Fig. 23 Transient histories of the cladding surface temperature measured in Test JM-1 (lower location)

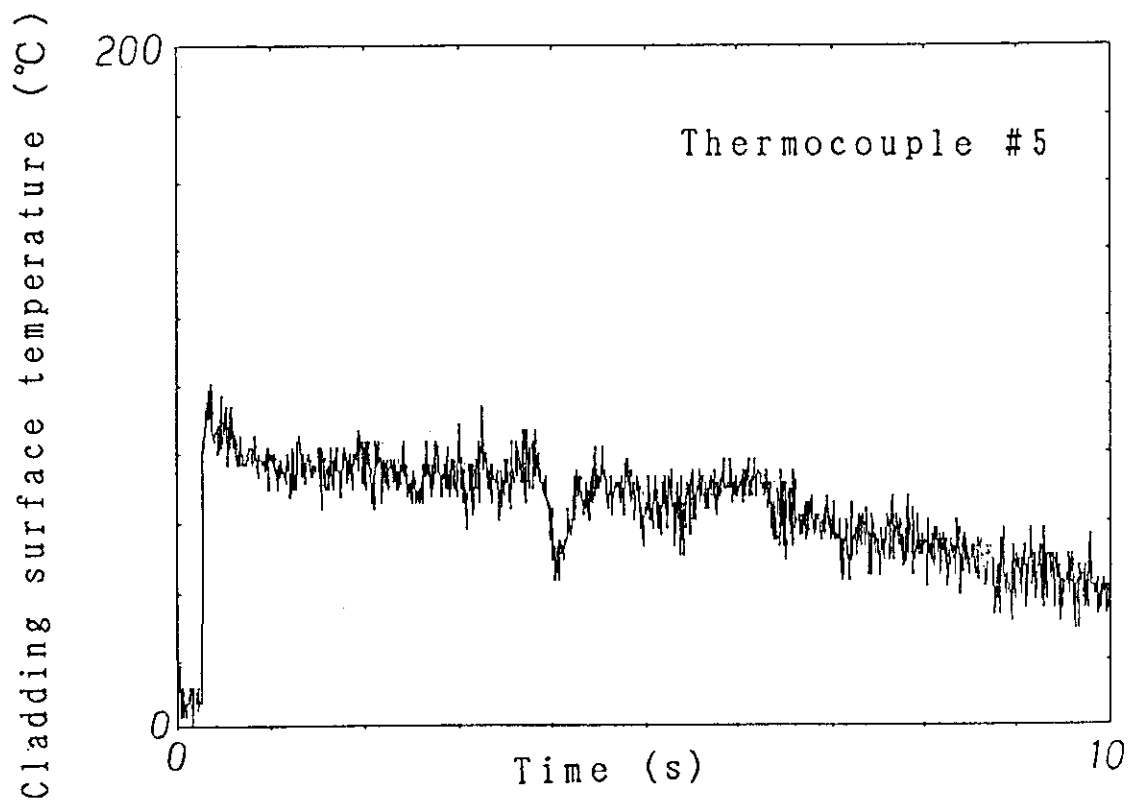
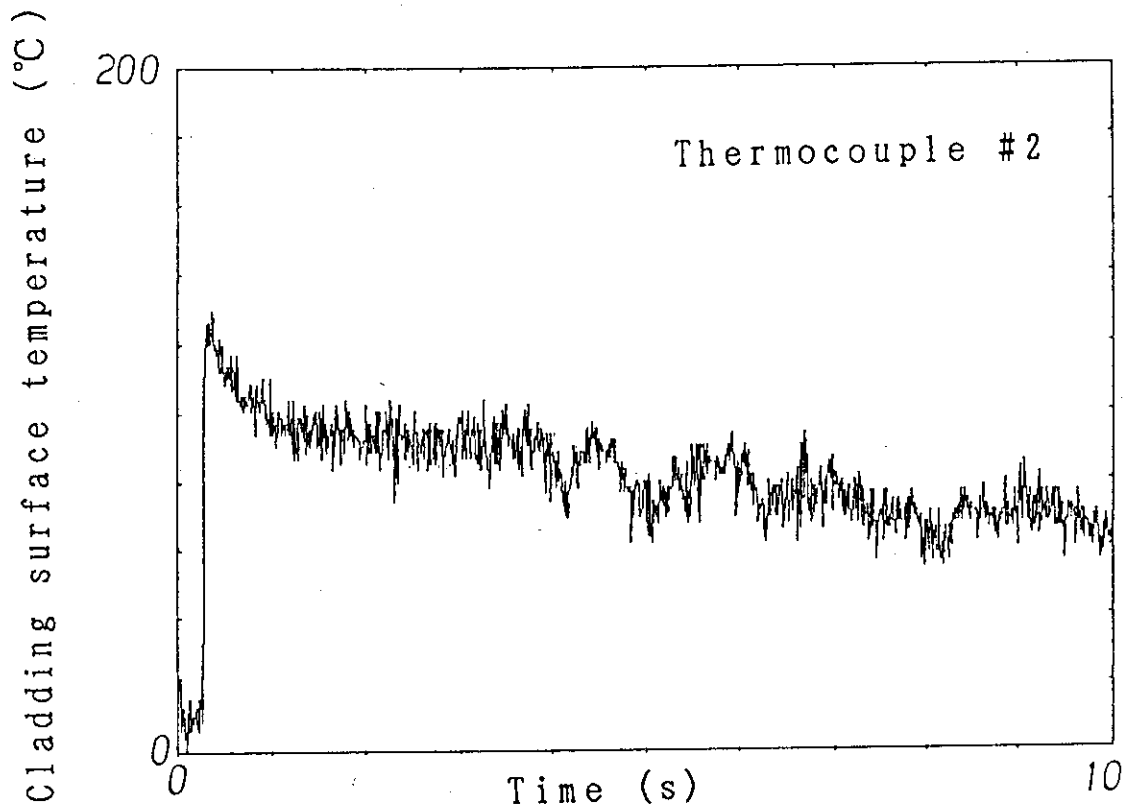


Fig. 24 Transient histories of the cladding surface temperature measured in Test JM-1 (center location)

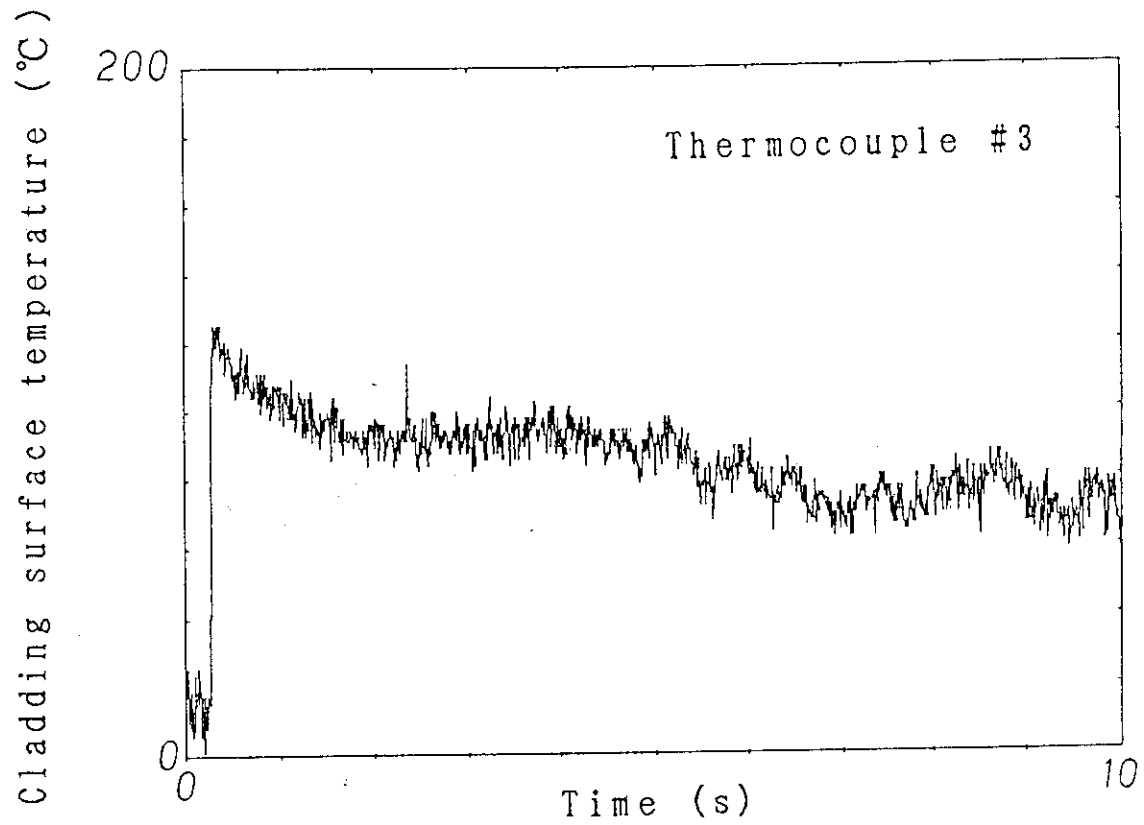


Fig. 25 Transient history of the cladding surface temperature measured in Test JM-1 (upper location)

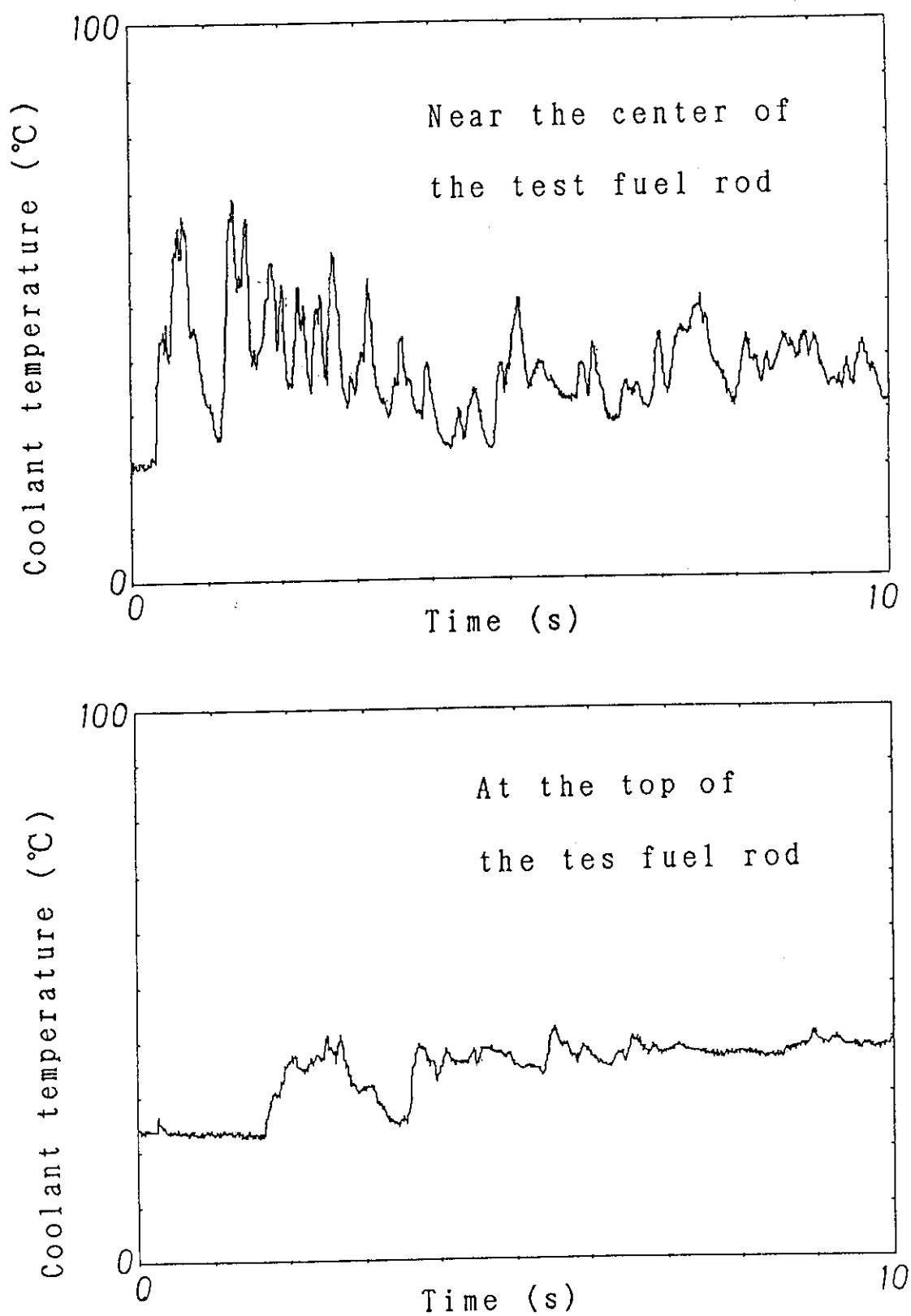


Fig. 26 Transient histories of the coolant temperature measured in Test JM-1

# Data Analysis --Laser Bow vs. Distance Plot

Date Of Data Collection: 4 Aug 1989 14:35:36

Rod NJB07

Hot Lab Number H124

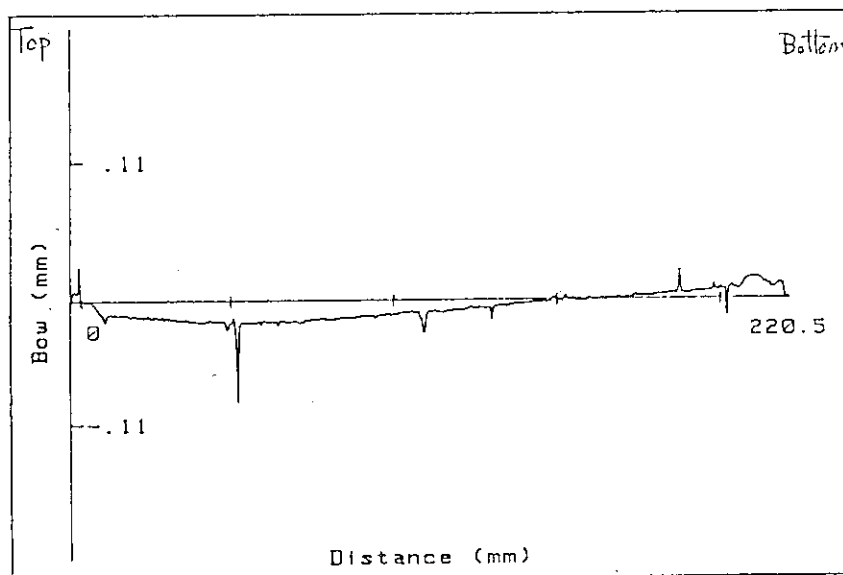
Rod Type P-JMTR

Angle 0 Deg

Max Bow .03 mm  
At 3 mm

Min Bow -.08 mm  
At 51.5 mm

Length 220.24 mm



# Data Analysis --Laser Bow vs. Distance Plot

Date Of Data Collection: 4 Aug 1989 14:35:36

Rod NJB07

Hot Lab Number H124

Rod Type P-JMTR

Angle 90 Deg

Max Bow .03 mm  
At 3 mm

Min Bow -.03 mm  
At 87.5 mm

Length 220.24 mm

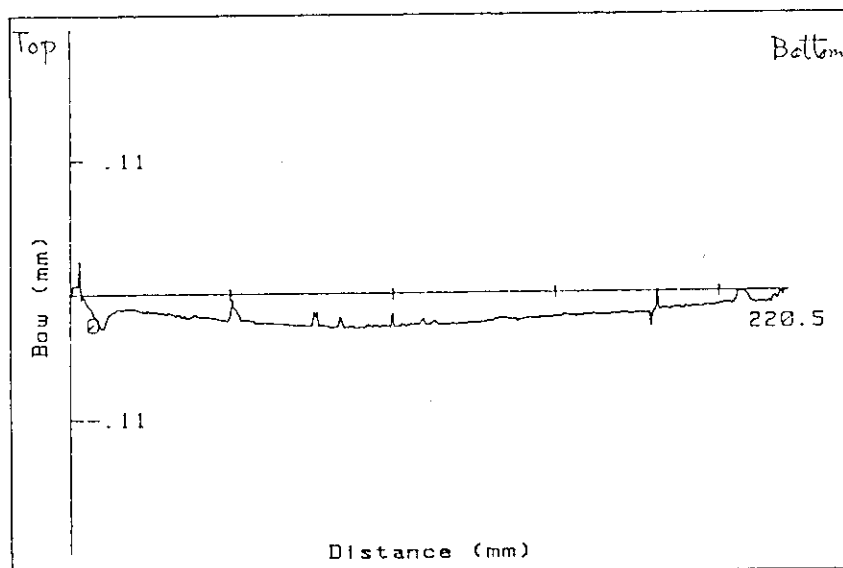


Fig. 27 Result of bending measurement for NJB07 rod after the pulse irradiation



## Data Analysis --Laser OD vs. Distance Plot

Date Of Data Collection: 4 Aug 1989 14:35:36

Rod NJB07

Hot Lab Number H124

Rod Type P-JMTR Angle 0 Deg

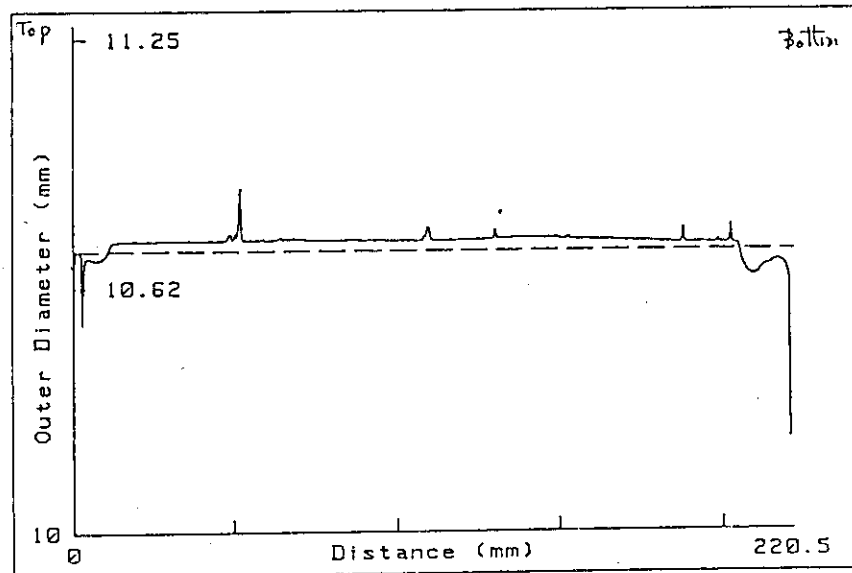
Max OD 10.88 mm

At 51.5 mm

Min OD 10.53 mm

At 3 mm

Length 220.24 mm



## Data Analysis --Laser OD vs. Distance Plot

Date Of Data Collection: 4 Aug 1989 14:35:36

Rod NJB07

Hot Lab Number H124

Rod Type P-JMTR Angle 90 Deg

Max OD 10.79 mm

At 180.5 mm

Min OD 10.51 mm

At 3 mm

Length 220.24 mm

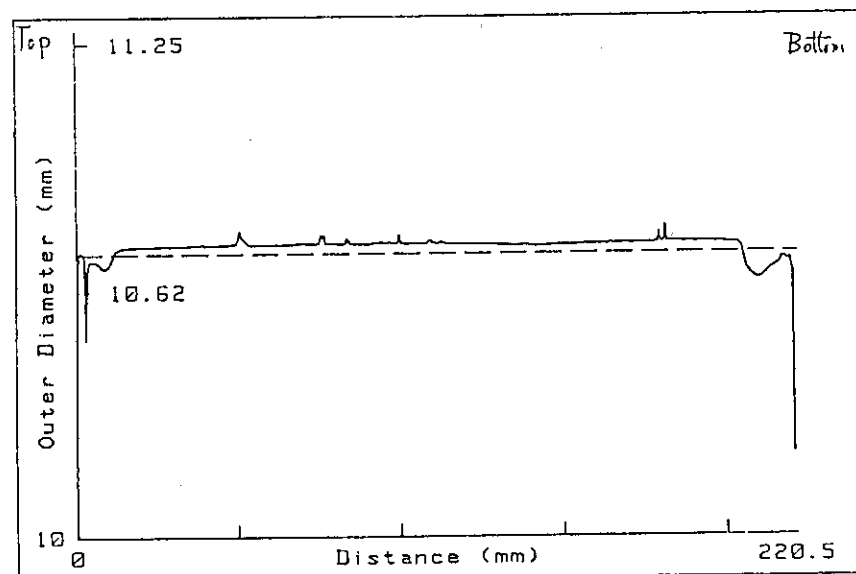


Fig. 28 Result of axial profile measurement for NJB07 rod after the pulse irradiation

1989.8.4

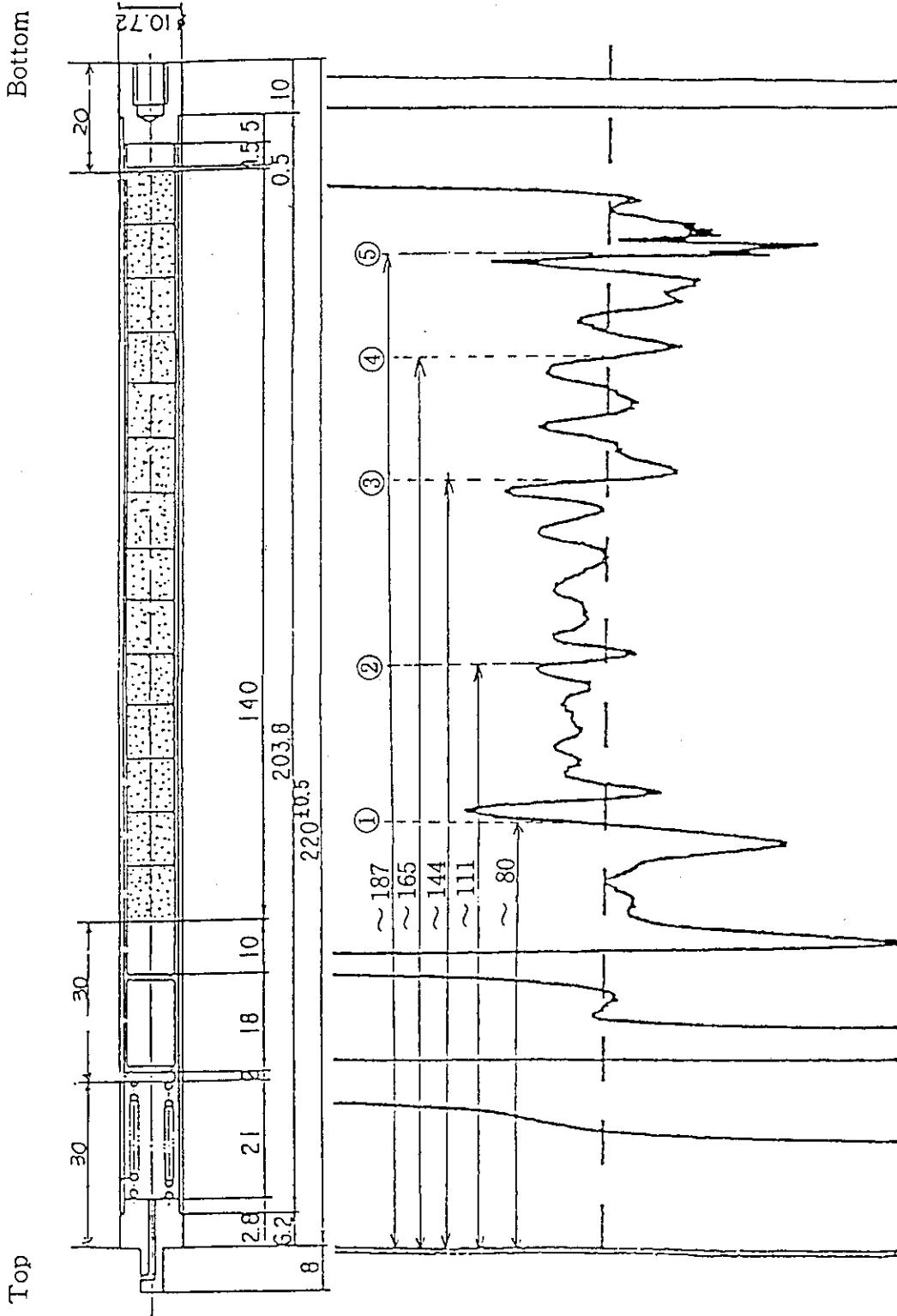


Fig. 29 Result of the eddy current measurement for NJB07 rod after the pulse irradiation

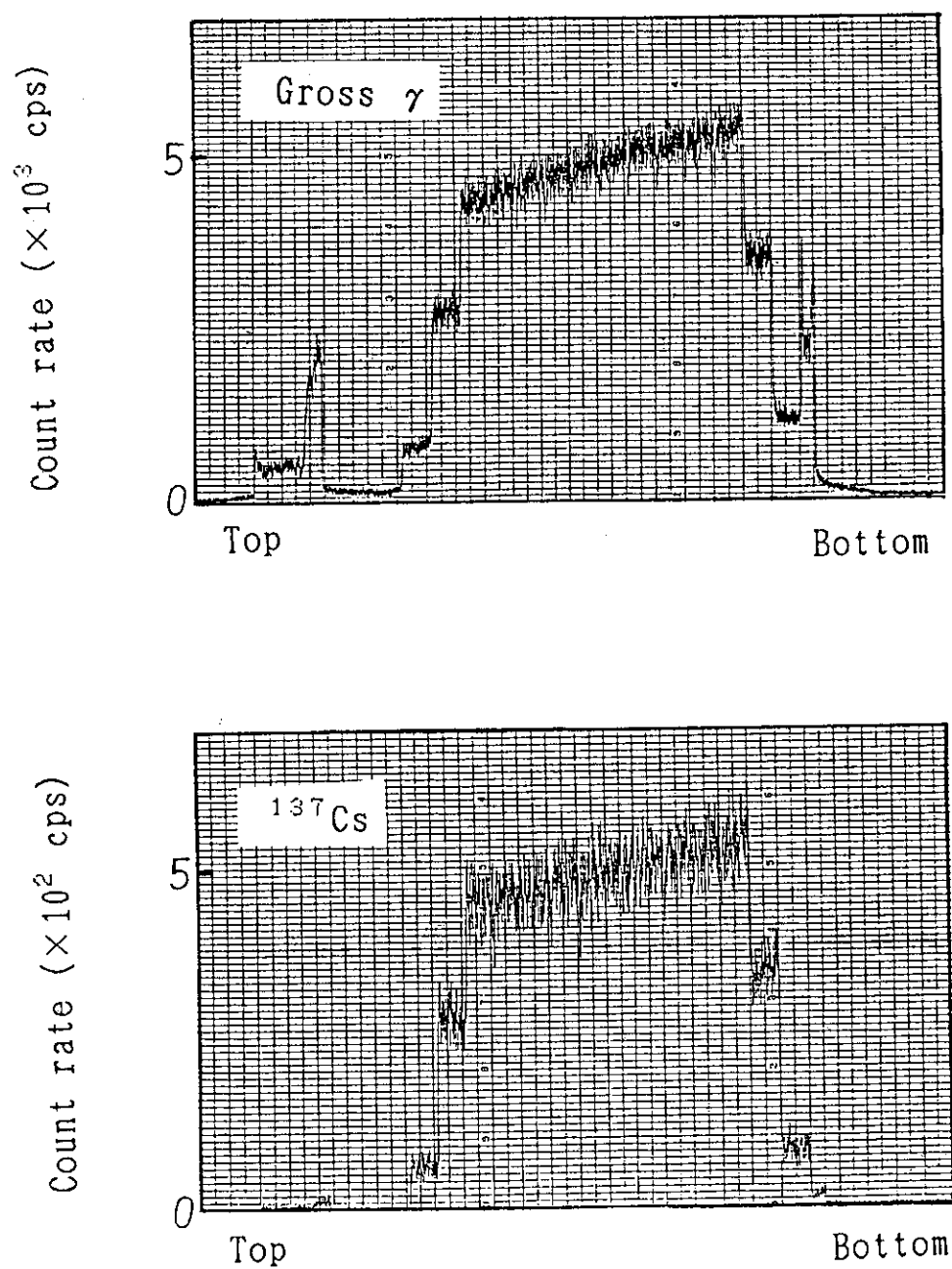


Fig. 30 Result of  $\gamma$ -ray scanings for NJB07 rod after the pulse irradiation

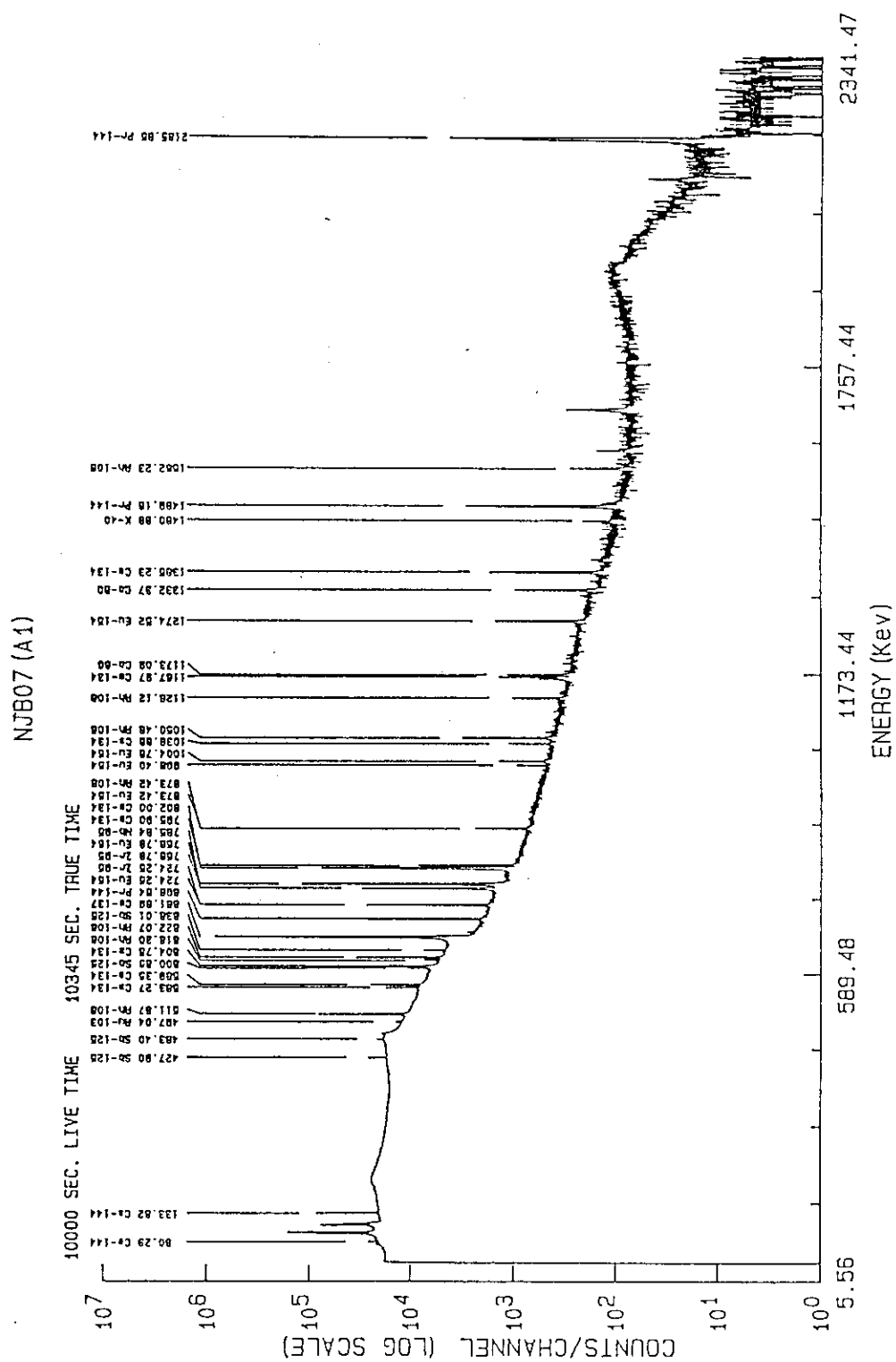


Fig. 31 Result of  $\gamma$ -ray spectrum measurement for NJB07 rod after the pulse irradiation

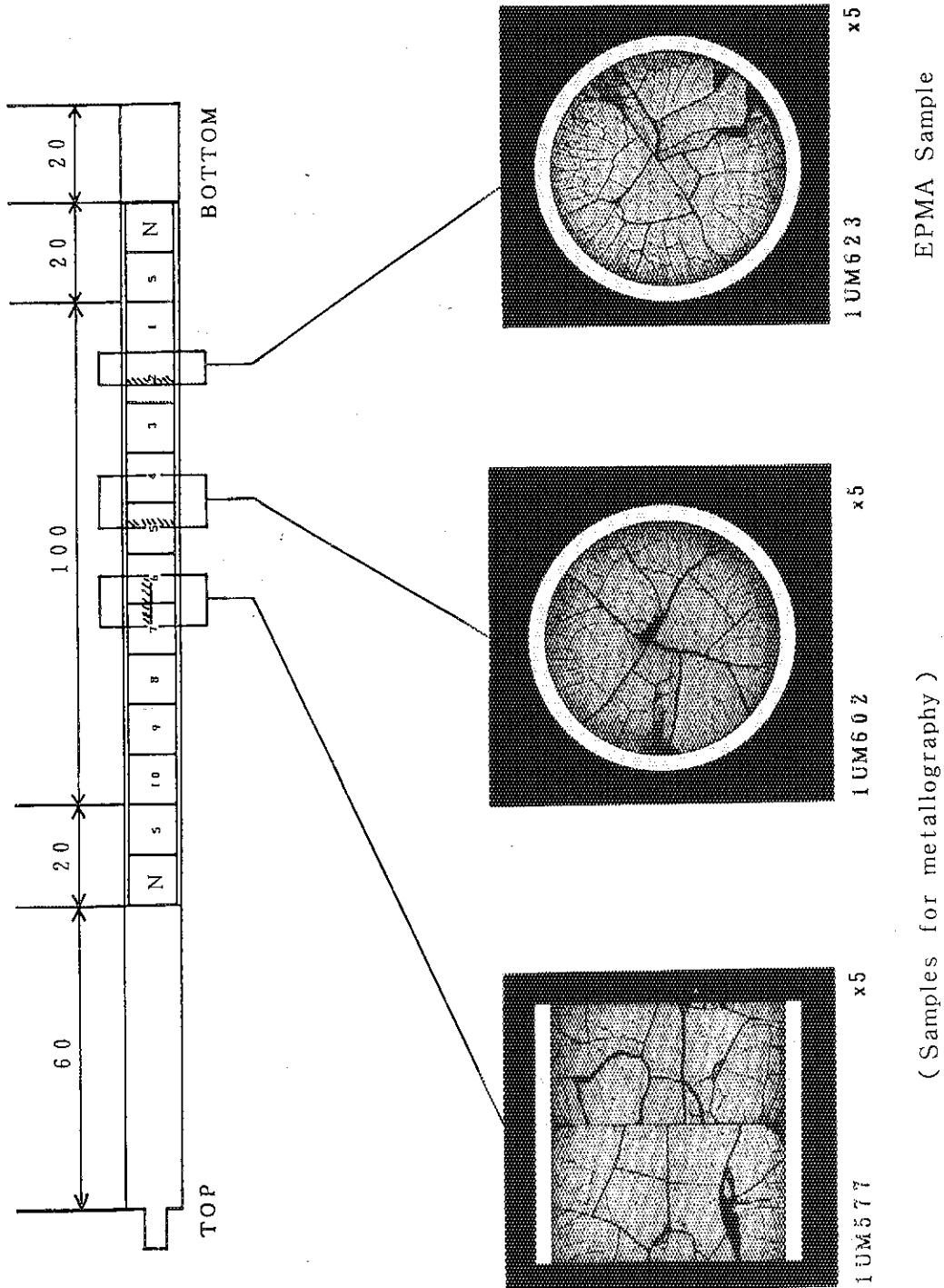


Fig. 32 Sampling positions for metallography after the pulse irradiation

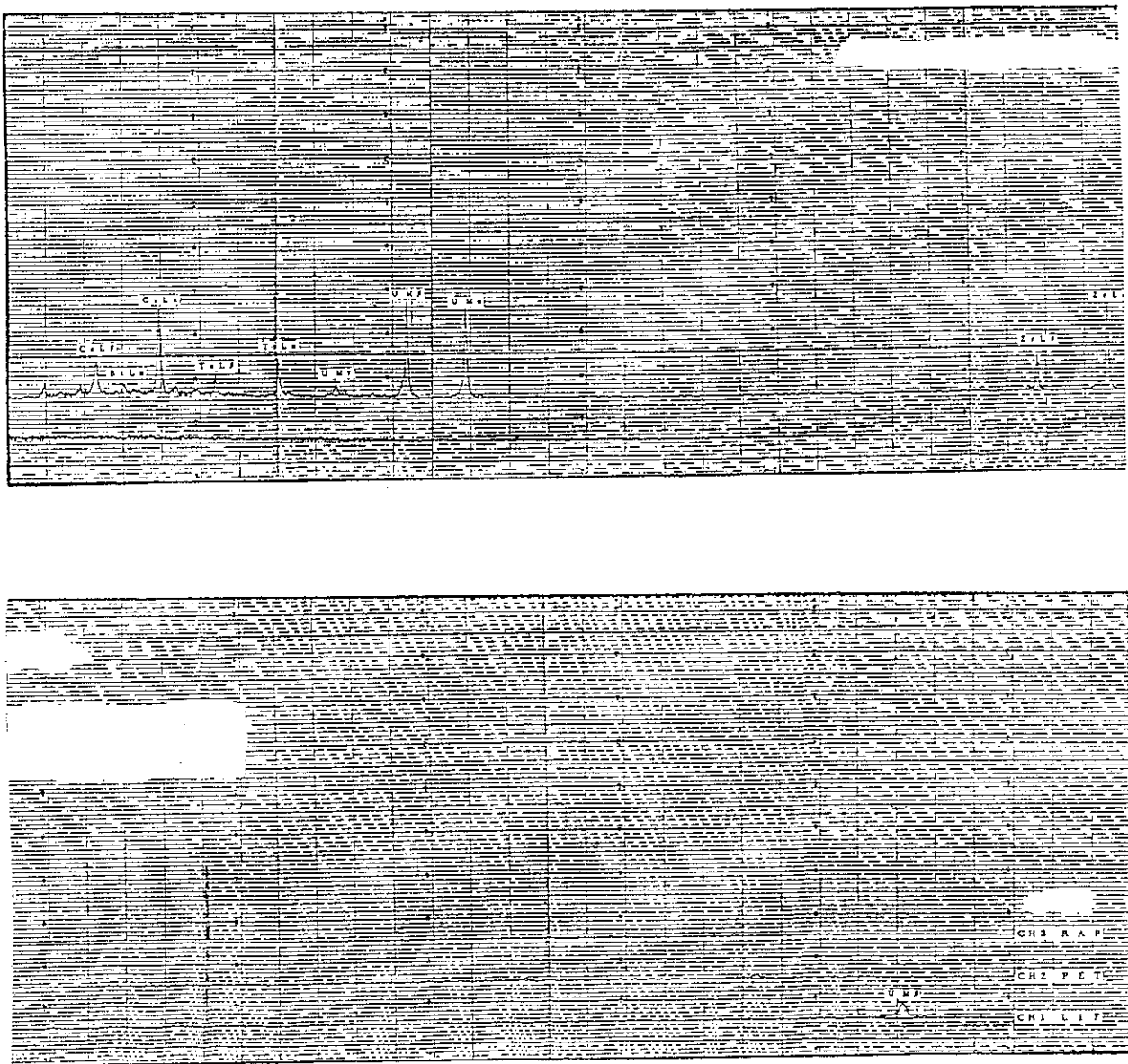


Fig. 33 Point analysis of the cladding inner surface by energy dispersion method after the pulse irradiation

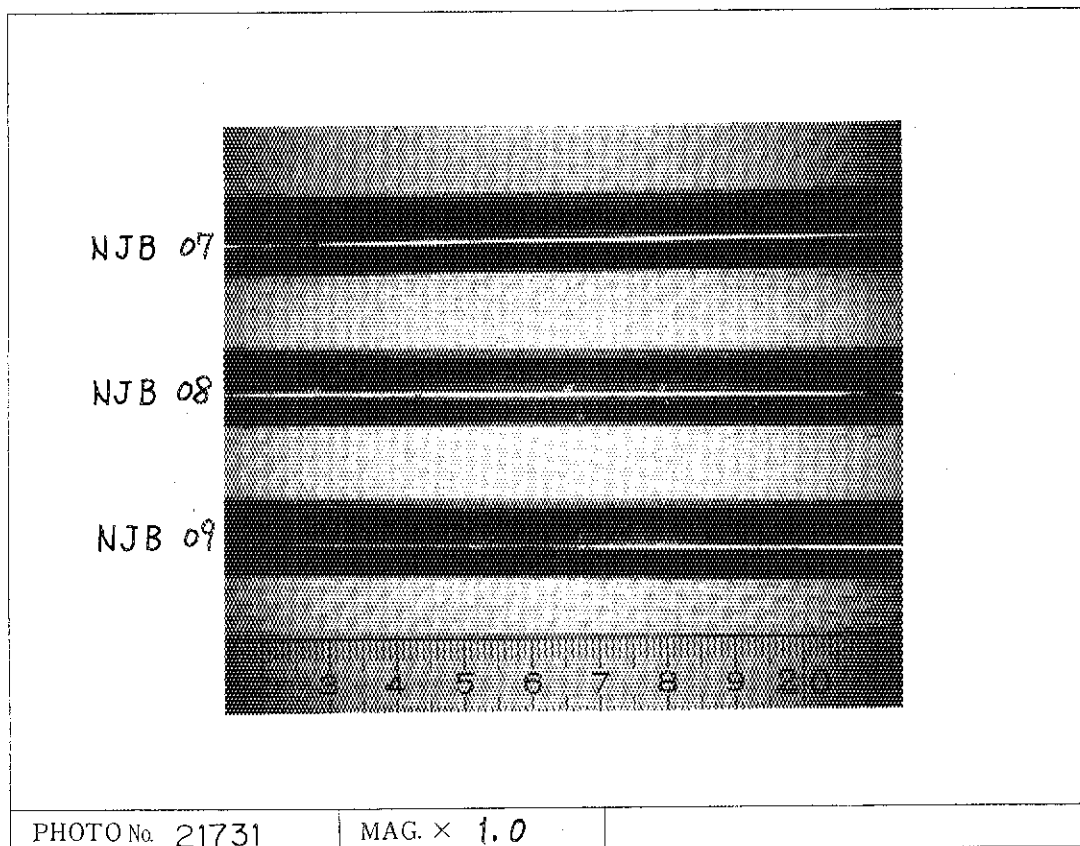
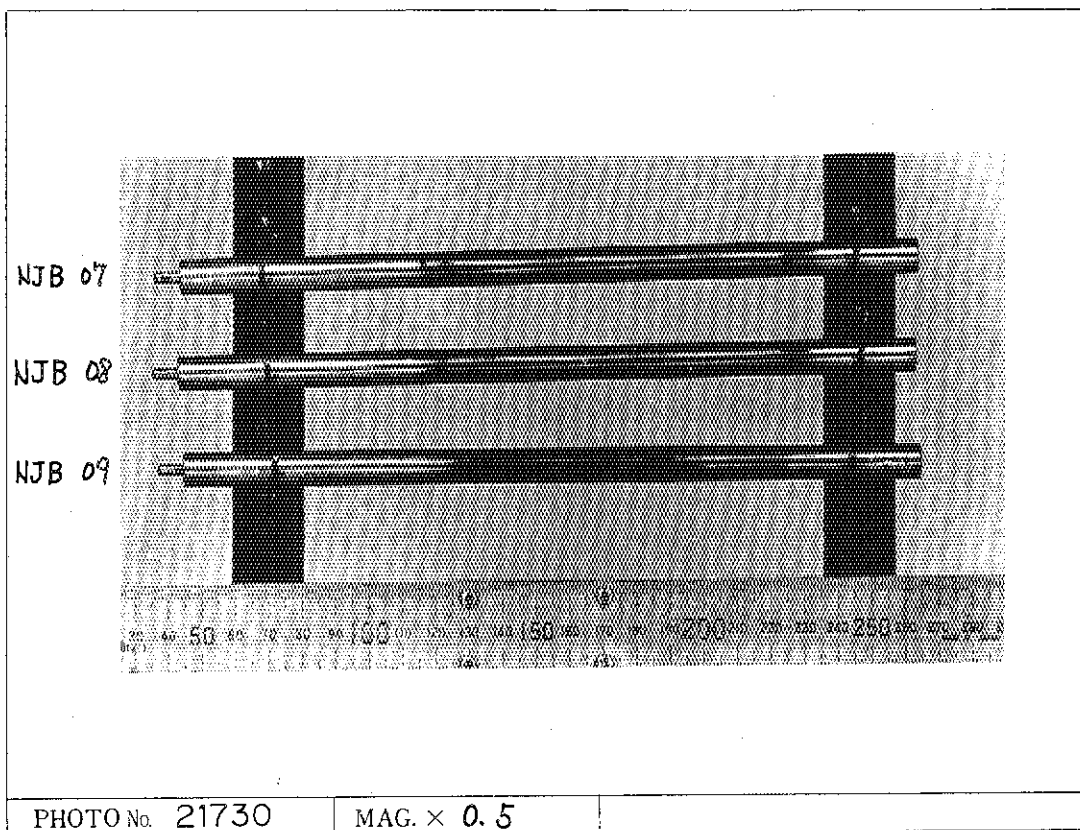


Photo. 1 Appearance of NJB07 rod after the completion of the pre-irradiation

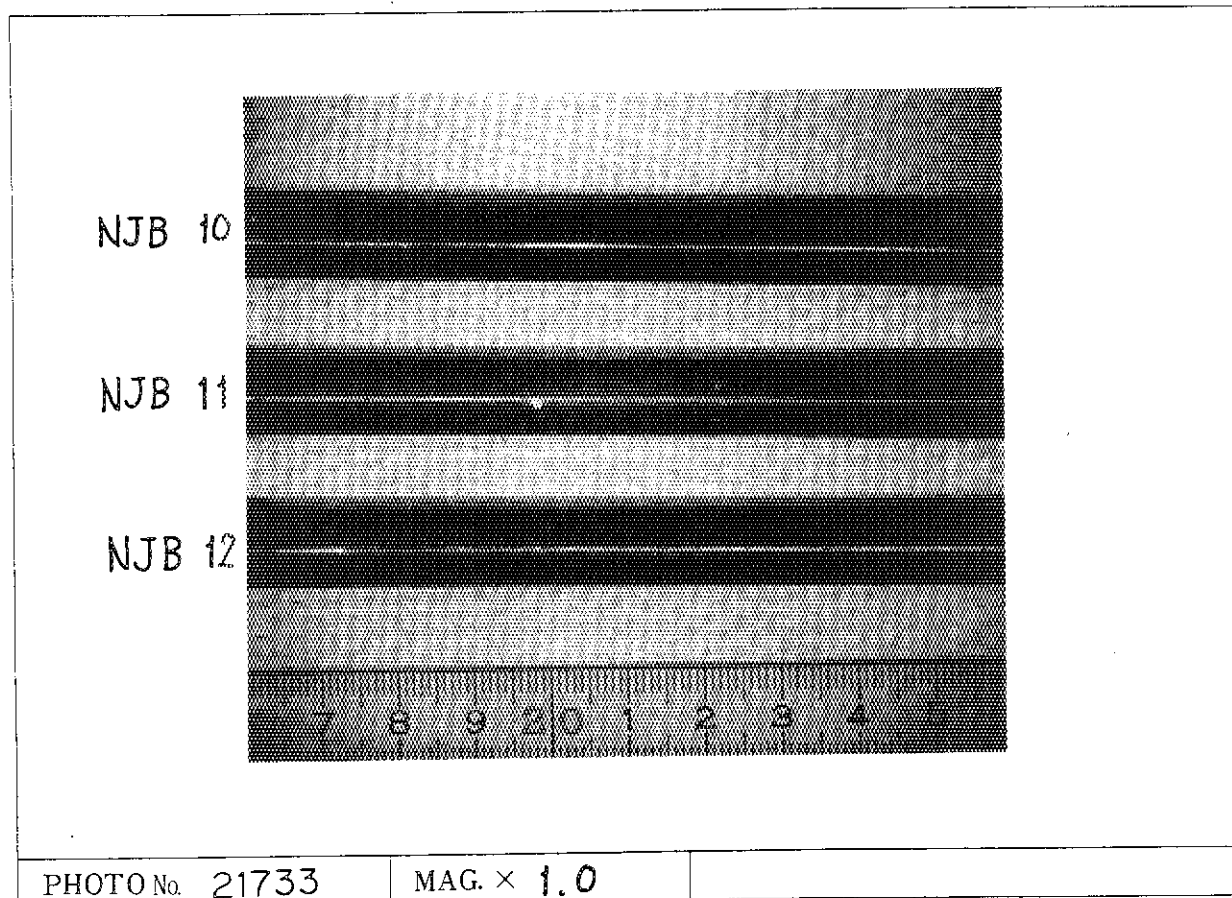
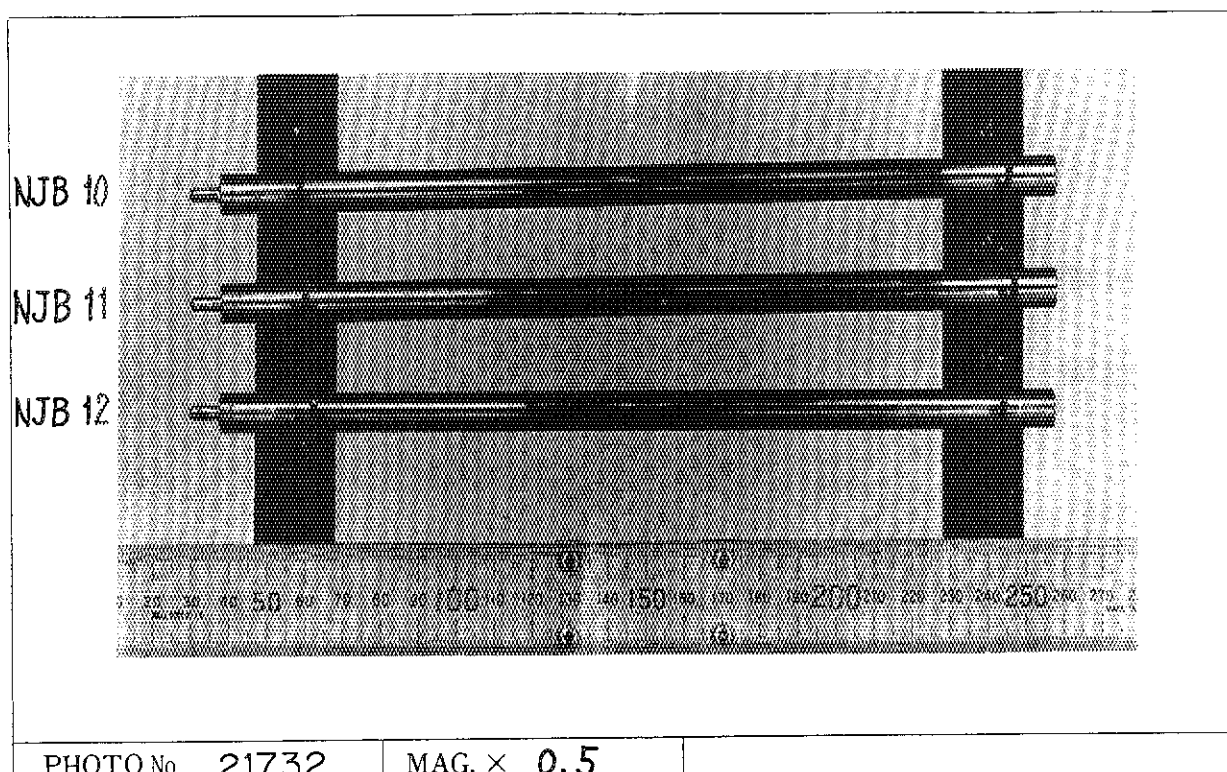


Photo. 2 Appearance of NJB12 rod after the completion of the pre-irradiation



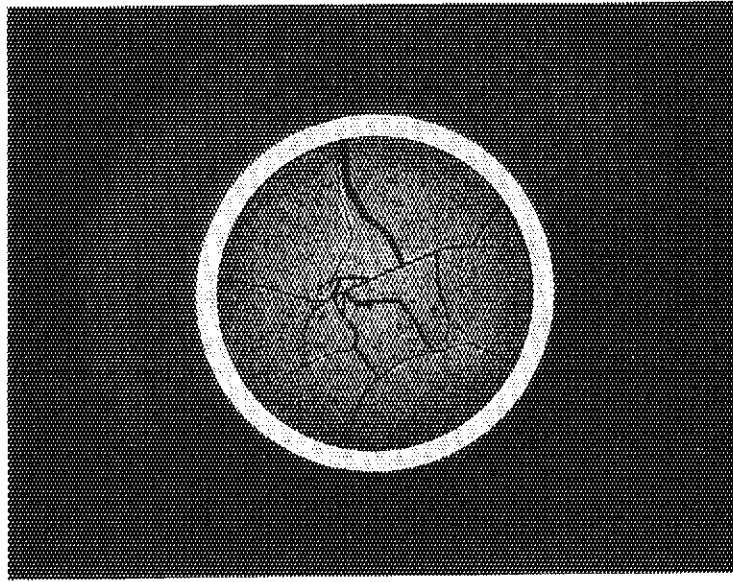


PHOTO No. 21347	MAG. $\times$ 5	L max etched
-----------------	-----------------	--------------

Photo. 3 Macroscopic photograph of the cross-sectional sample taken from NJB12 rod

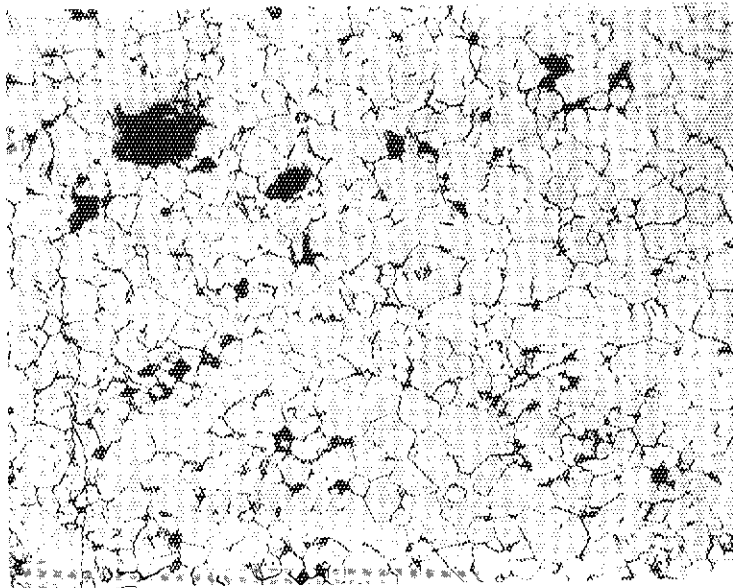


PHOTO No. 21348	MAG. $\times$ 400	L max etched Center
-----------------	-------------------	---------------------

Photo. 4 Microscopic photograph of the cross-sectional sample taken from NJB12 rod (central position)

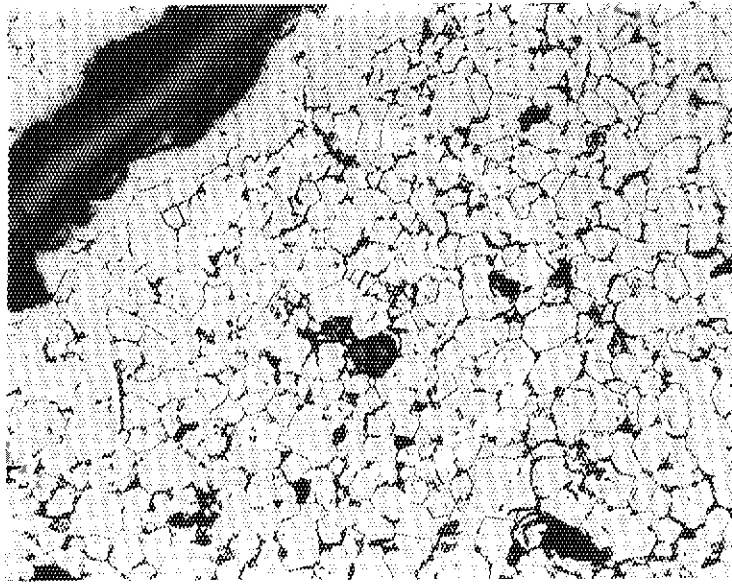


PHOTO No. 21349	MAG. $\times 400$	L max	etched	Middle
-----------------	-------------------	-------	--------	--------

Photo. 5 Microscopic photograph of the cross-sectional sample taken from NJB12 rod (middle position)

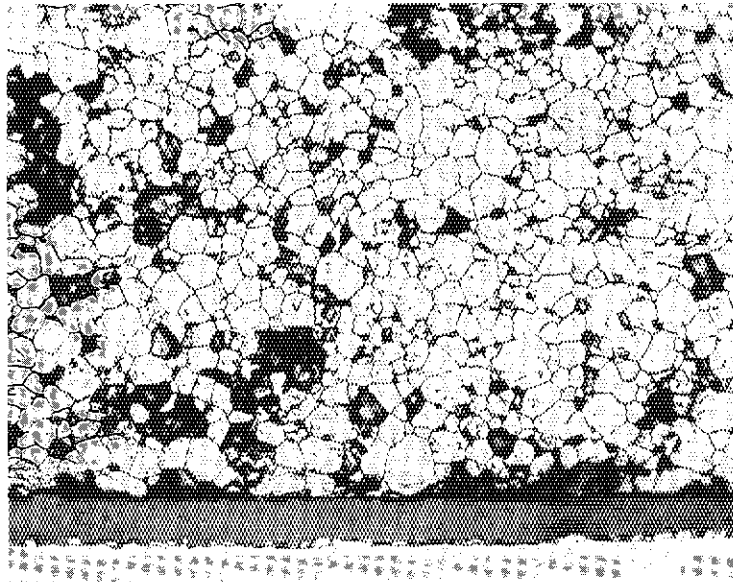


PHOTO No. 21350	MAG. $\times 400$	L max	etched	Periph.
-----------------	-------------------	-------	--------	---------

Photo. 6 Microscopic photograph of the cross-sectional sample taken from NJB12 rod (peripheral position)

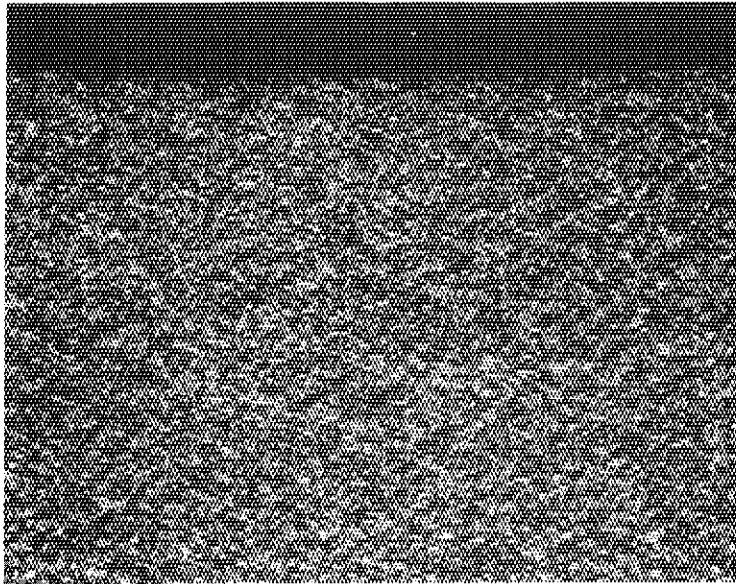


PHOTO No. 21353

MAG.  $\times 200$ 

L max etched

Inner

Photo. 7 Microscopic photograph of the inside of the cladding tube which belongs to the cross-sectional sample taken from NJB12

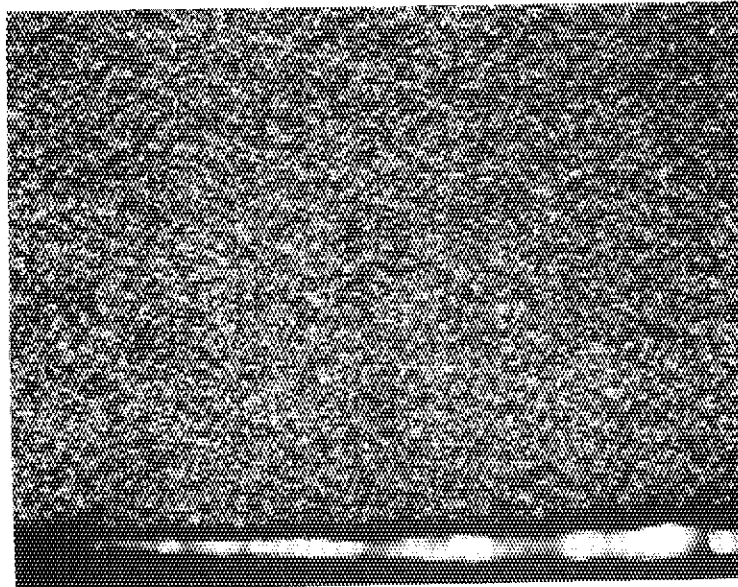


PHOTO No. 21354

MAG.  $\times 200$ 

L max etched

Outer

Photo. 8 Microscopic photograph of the outside of the cladding tube which belongs to the cross-sectional sample taken from NJB12

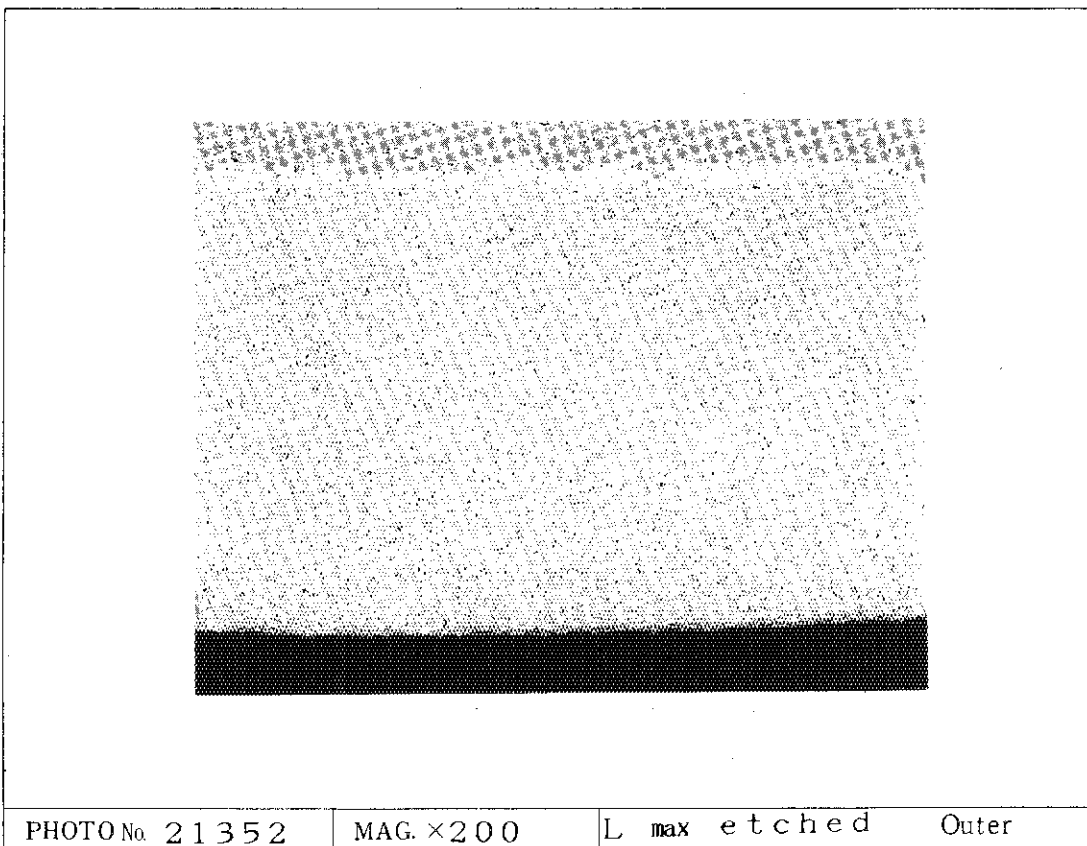
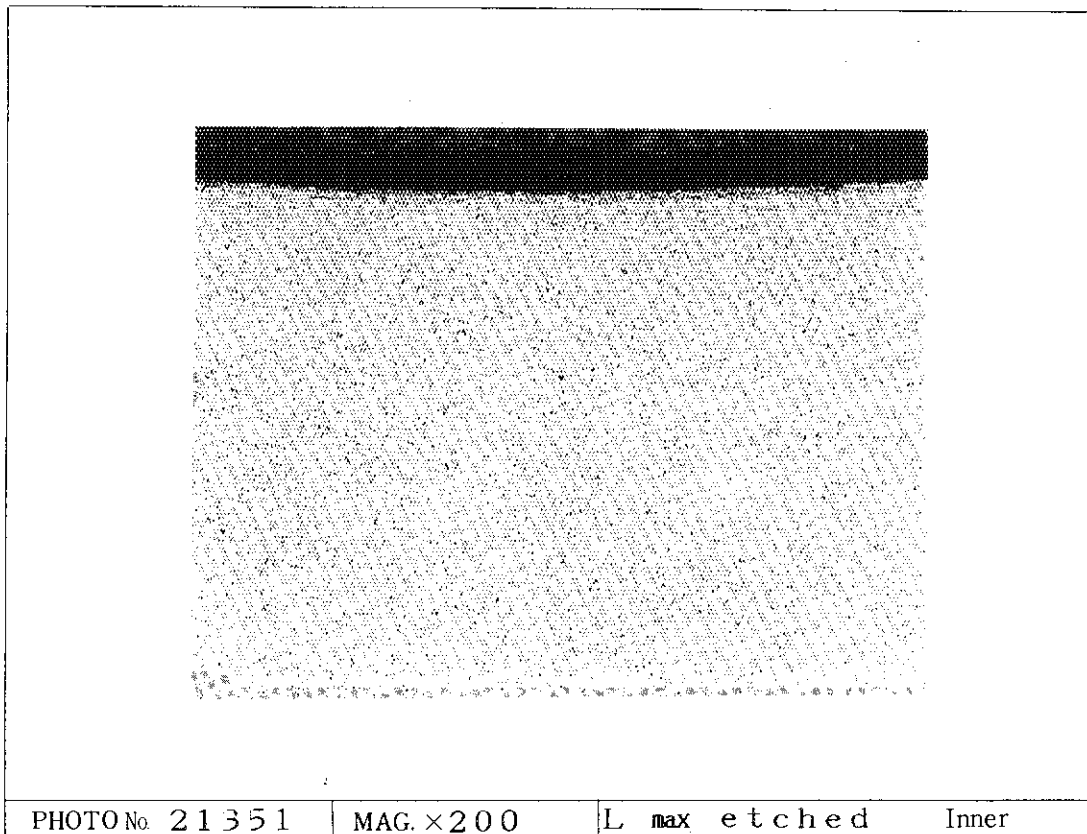


Photo. 9 Precipitation of hydride in the cladding tube of the cross-sectional sample taken from NJB12 rod

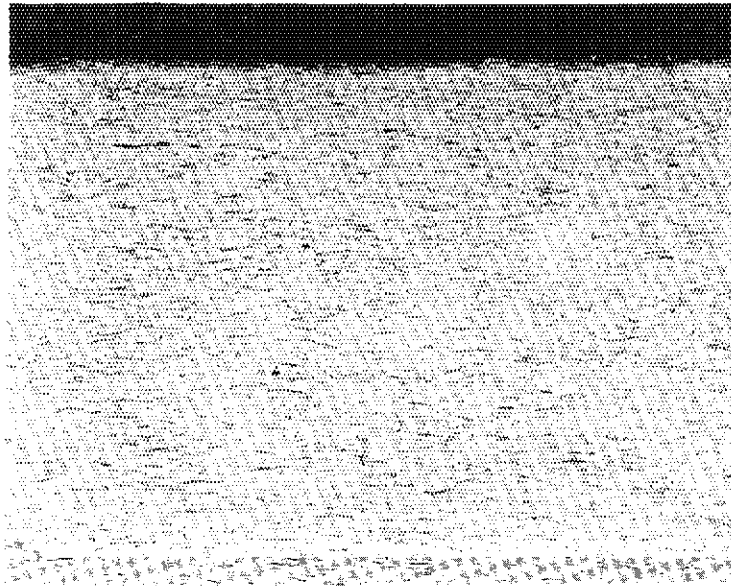


PHOTO No. 21385

MAG.  $\times 200$

L min etched

Inner

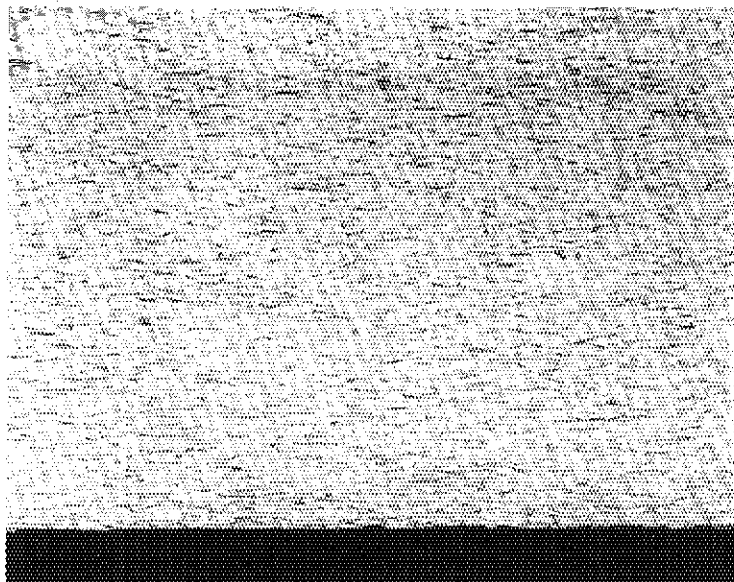


PHOTO No. 21386

MAG.  $\times 200$

L min etched

Outer

Photo. 10 Precipitation of hydride in the cladding tube of the longitudinal sample taken from NJB12 rod

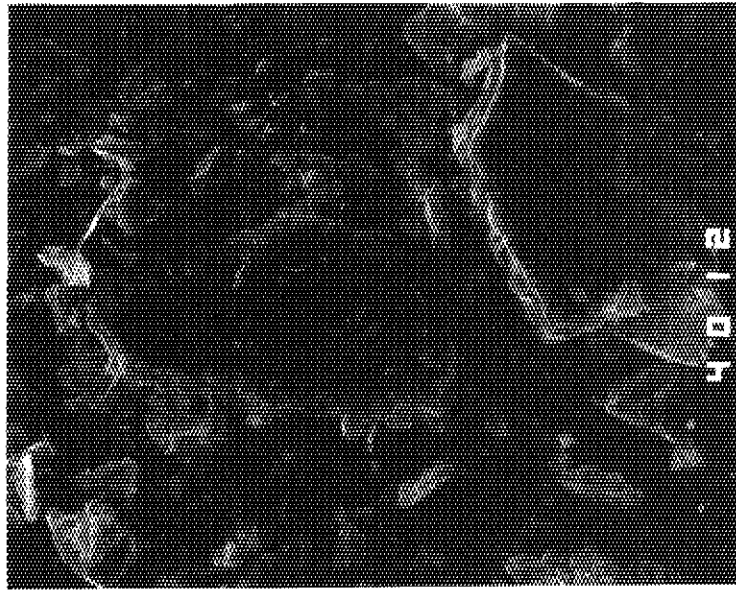


PHOTO No. 21397	MAG. × 3000	SEI
-----------------	-------------	-----

Photo. 11 Secondary electron image of the cladding inner surface measured after the completion of the pre-irradiation

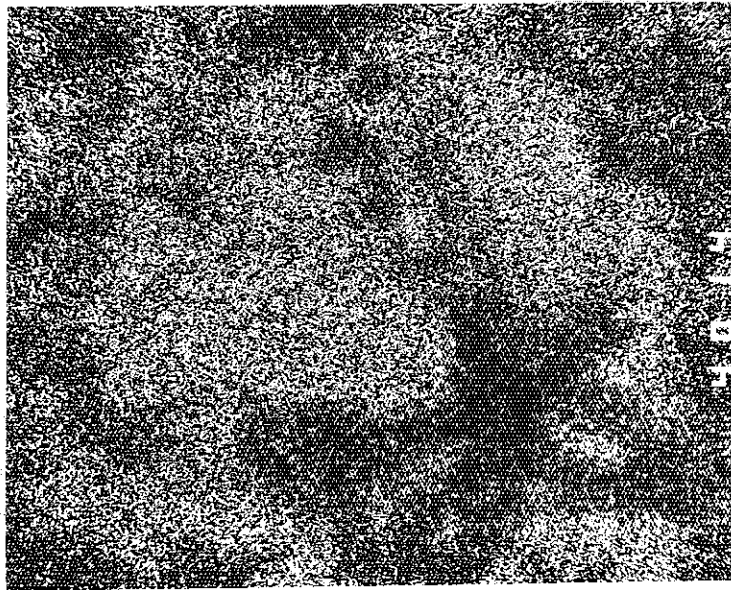


PHOTO No. 21398	MAG. × 3000	U-Mα
-----------------	-------------	------

Photo. 12 Surface analysis of the cladding inner surface by wavelength dispersion method (uranium)

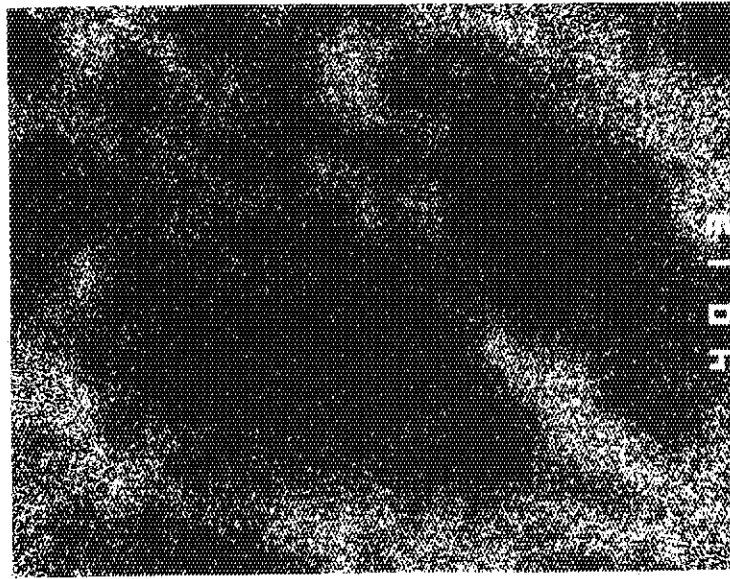


PHOTO No. 21399

MAG. × 3000

Zr-L $\alpha$ 

Photo. 13 Surface analysis of the cladding inner surface by wavelength dispersion method (zirconium)

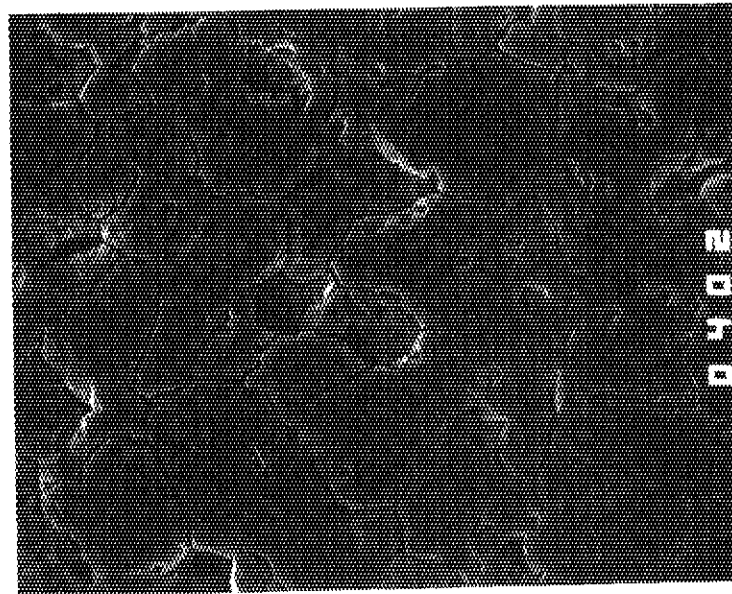


PHOTO No. 21432

MAG. × 1000

Periphery

SEI

Photo. 14 Secondary electron image of the fuel sample (peripheral position)



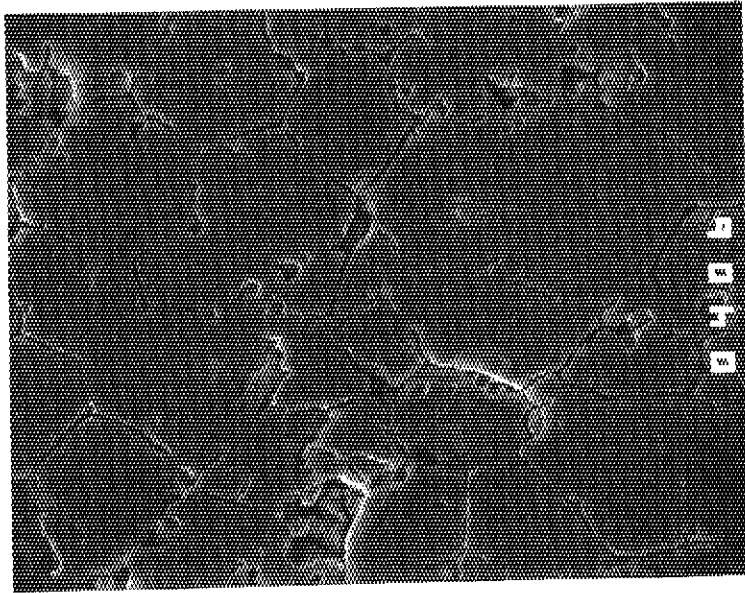


PHOTO No. 21437	MAG. × 1000	Middle	SE I
-----------------	-------------	--------	------

Photo. 15 Secondary electron image of the fuel sample  
(middle position)

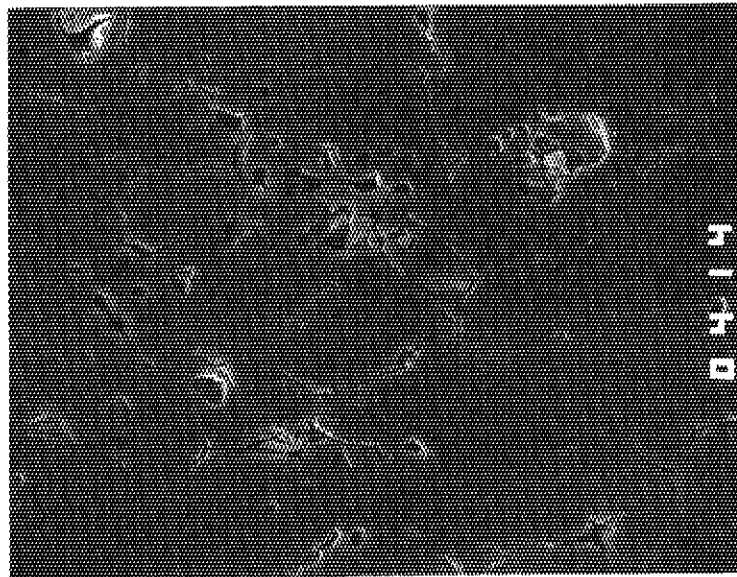


PHOTO No. 21445	MAG. × 1000	Center	SE I
-----------------	-------------	--------	------

Photo. 16 Secondary electron image of the fuel sample  
(central position)



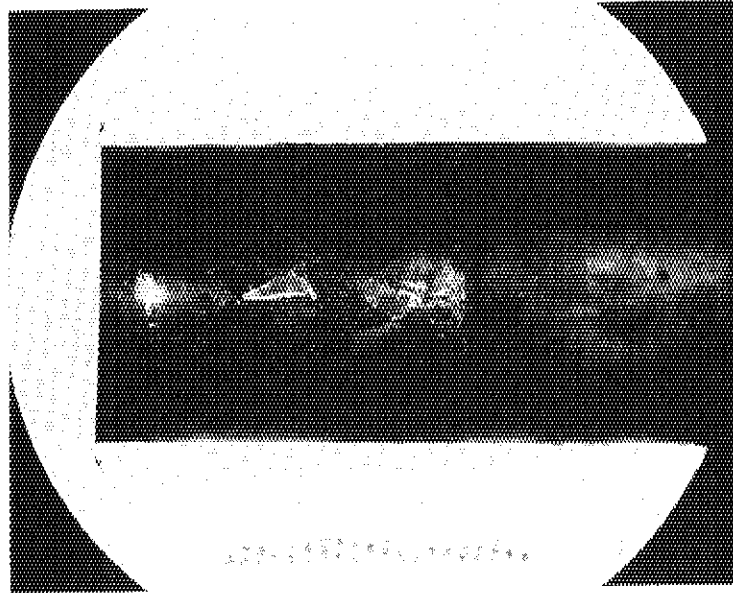


PHOTO No. 21392

MAG.  $\times$  5

1-2

Photo. 17 Appearance of the cladding inner surface of the sample for X-ray microprobe analysis

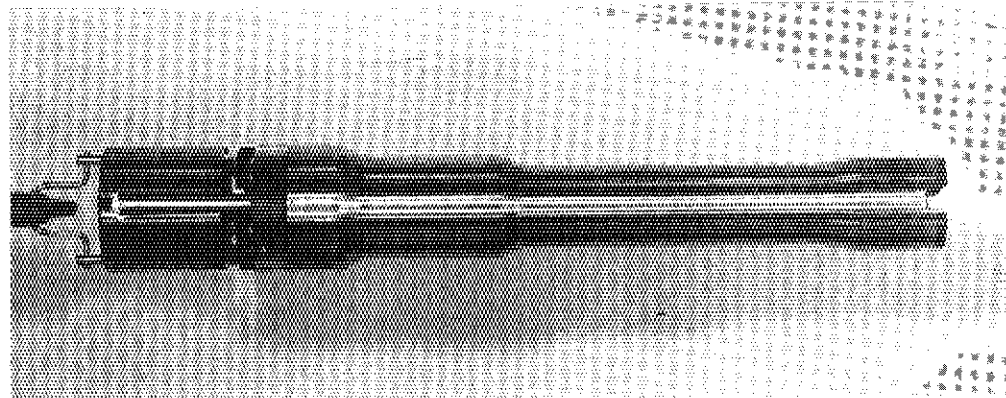
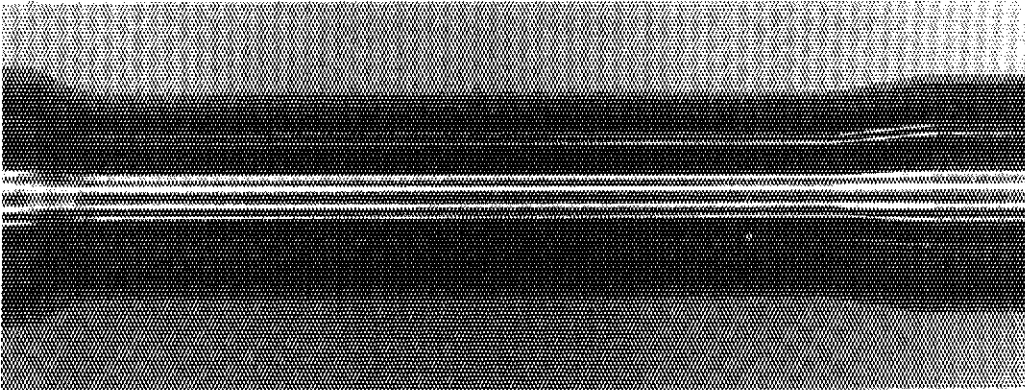
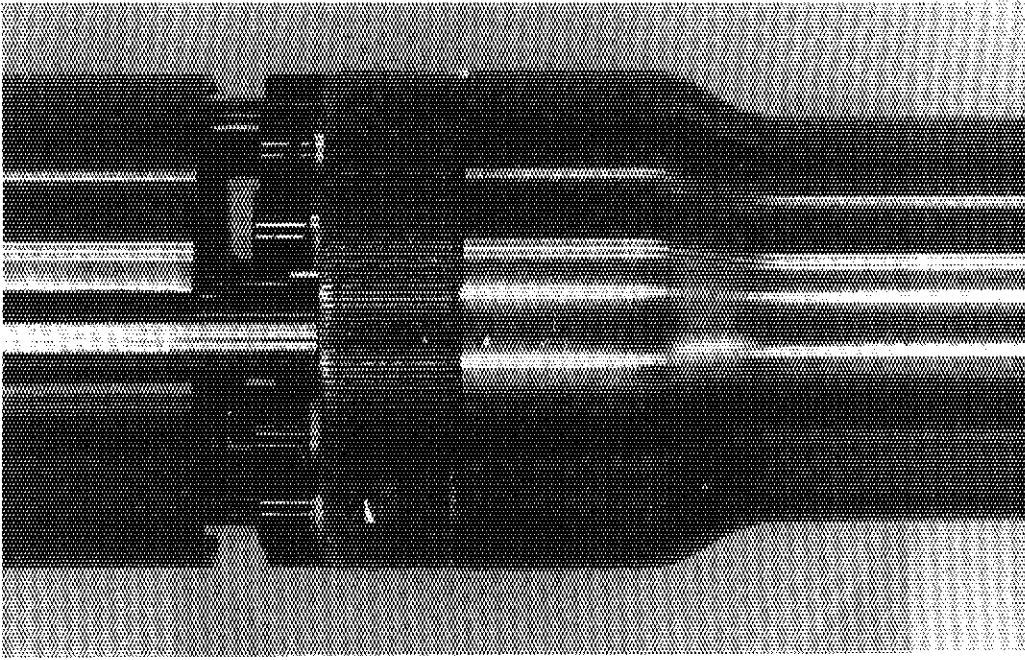
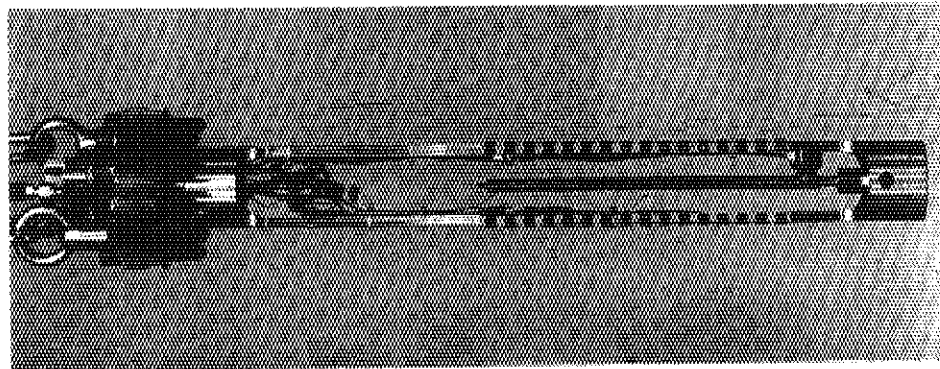
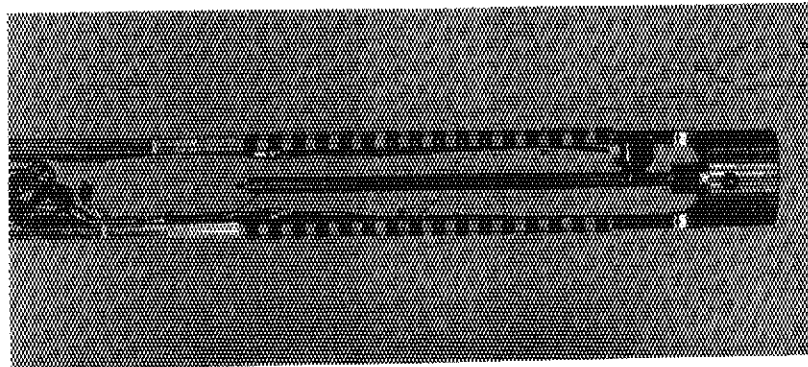


Photo. 18 Appearance of the inner capsule after the pulse irradiation

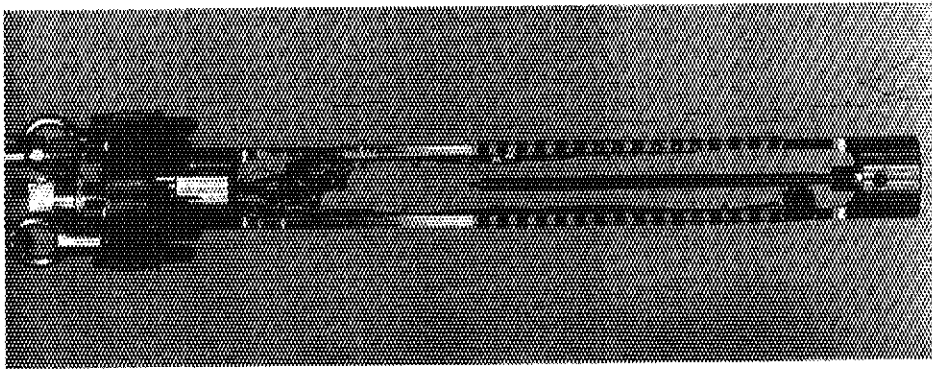


1C 1CL0116

0°

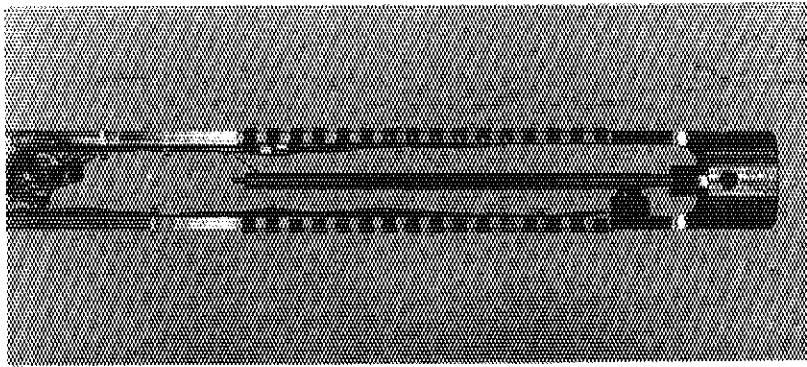


1C 1CL0117



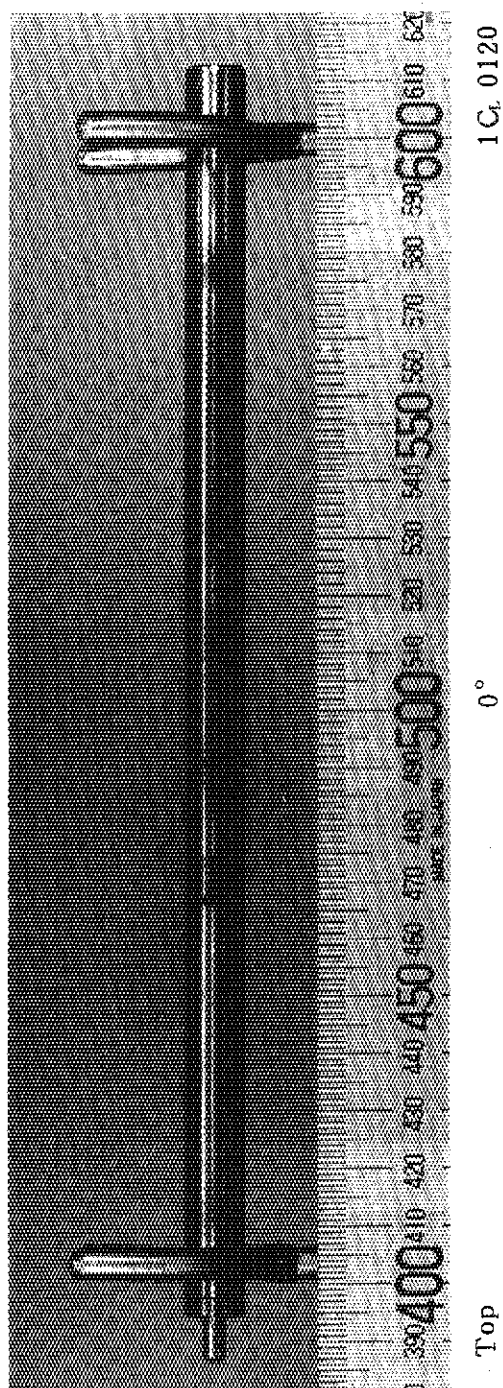
1C 1CL0118

180°



1C 1CL0119

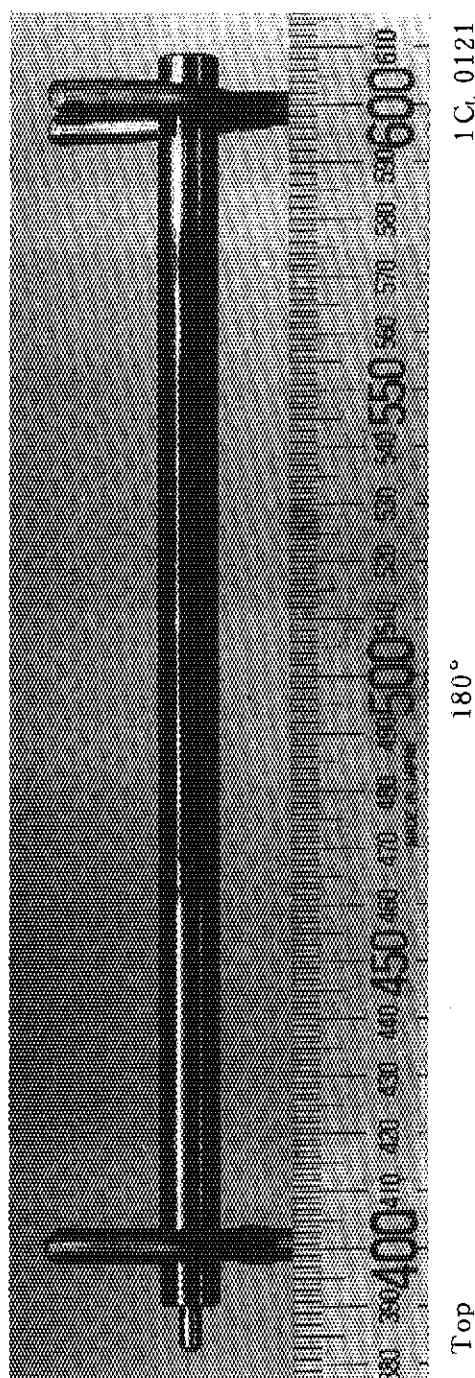
Photo. 19 Appearance of the test fuel rod supported by the holder after the pulse irradiation



1C4 0120

0°

Top



1C4 0121

180°

Top

Photo. 20 Appearance of the test fuel rod after the pulse irradiation

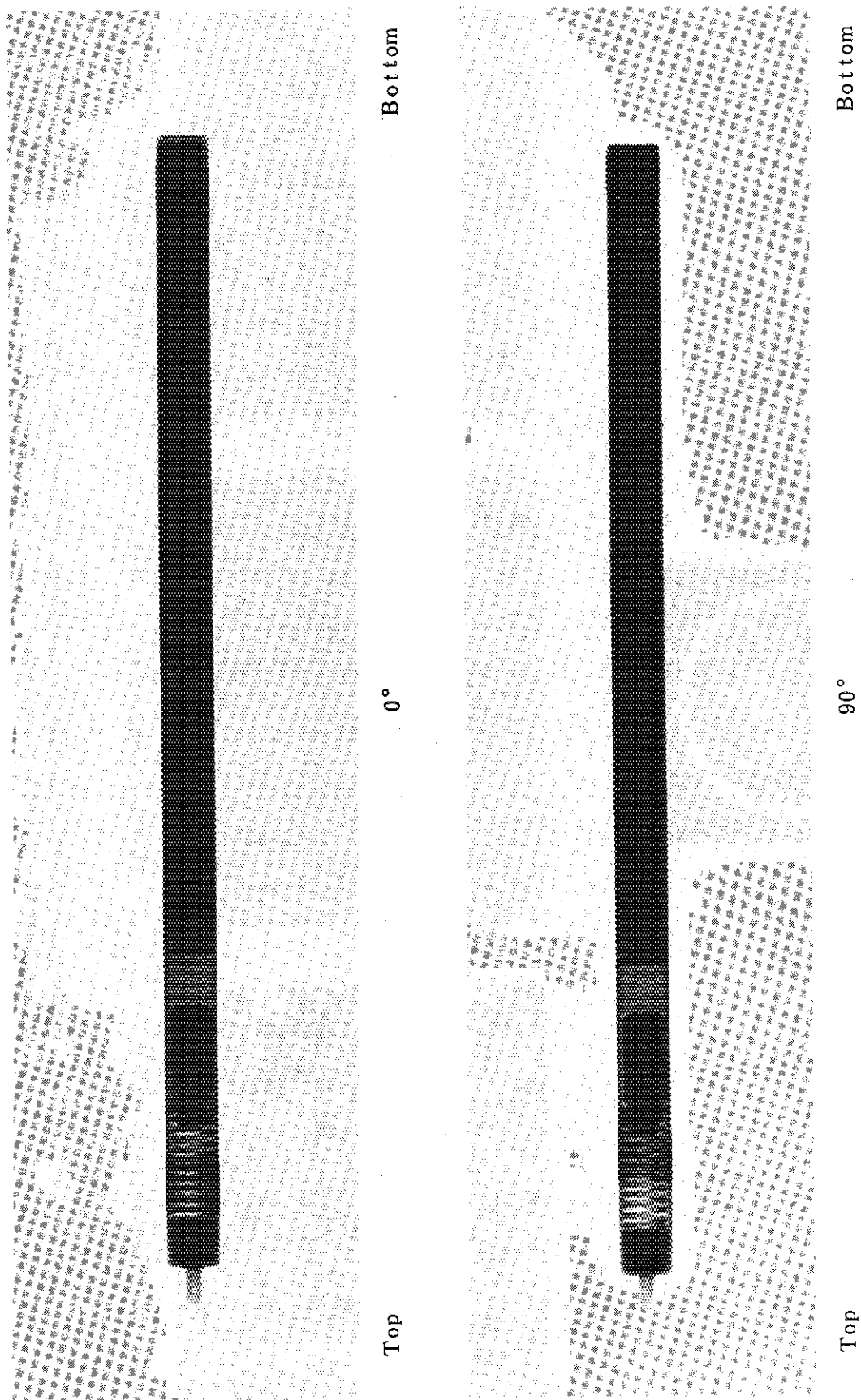
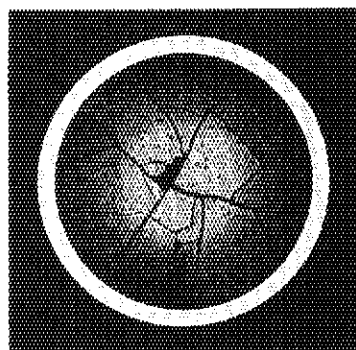
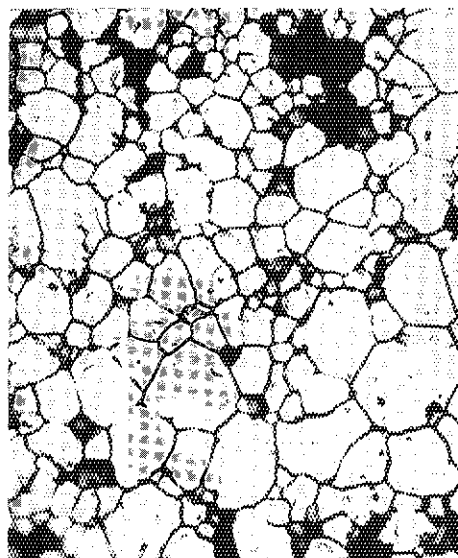


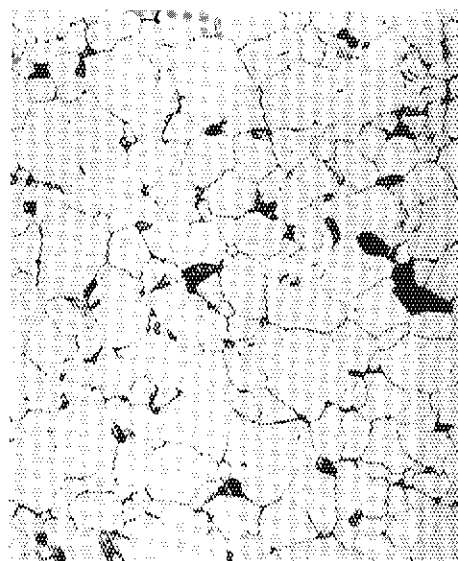
Photo. 21 X-ray radiograph of the test fuel rod after the pulse irradiation



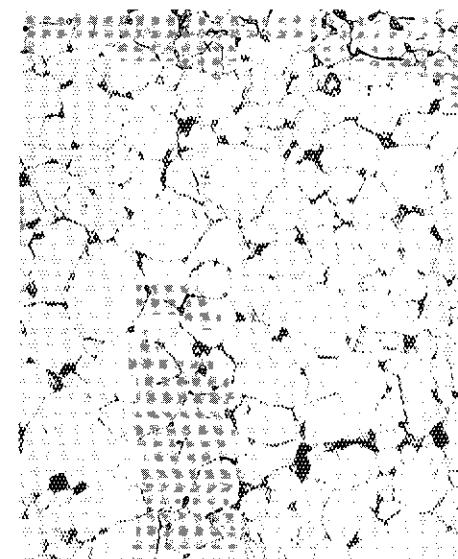
1UM603 × 5



1UM616 ( Periphery ) × 1000

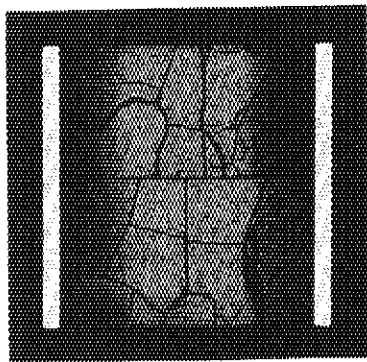


1UM617 ( Middle ) × 1000

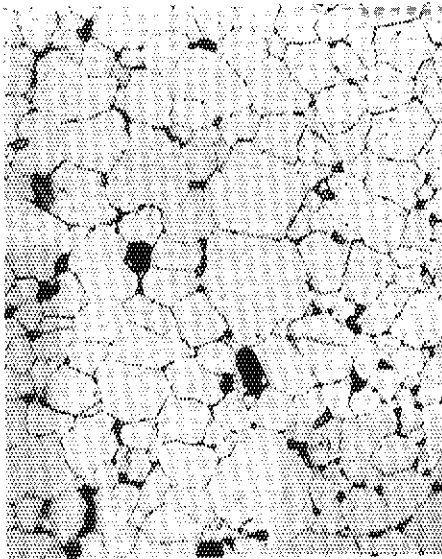


1UM618 ( Center ) × 1000

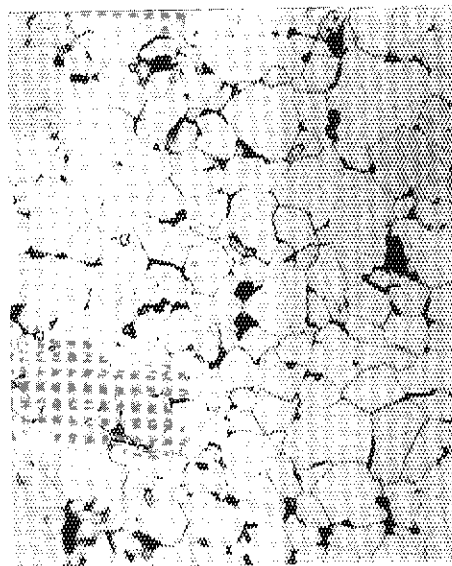
Photo. 22 Macroscopic and microscopic photographs of the fuel after etching for the sample of radial section



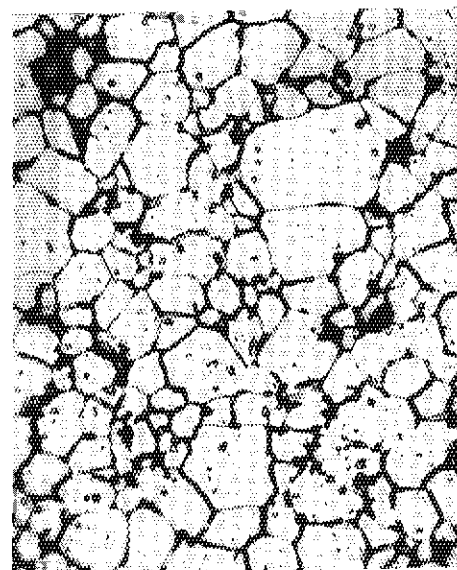
1UM578 × 5



1UM593 ( Center ) × 1000



1UM592 ( Middle ) × 1000



1UM591 ( Periphery ) × 1000

Photo. 23 Macroscopic and microscopic photographs of the fuel after etching  
for the sample of longitudinal section



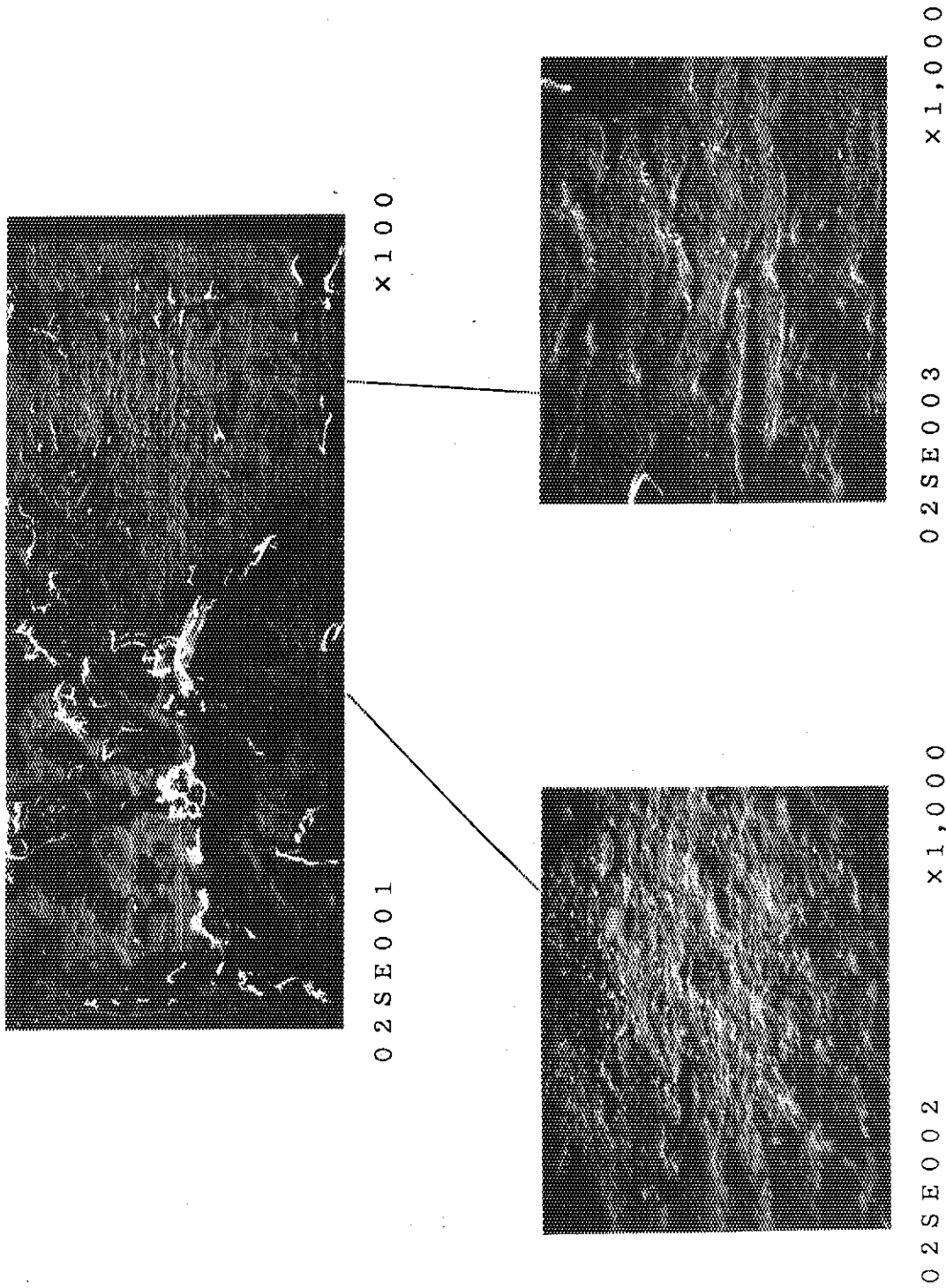
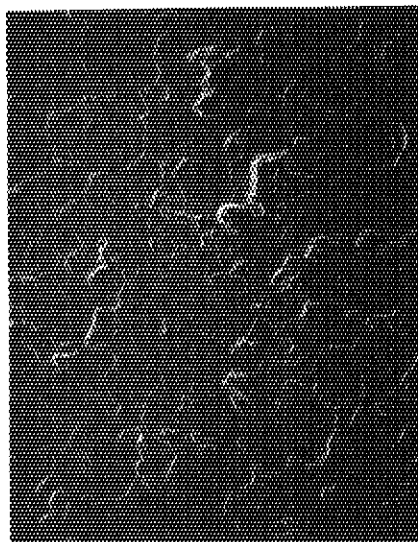
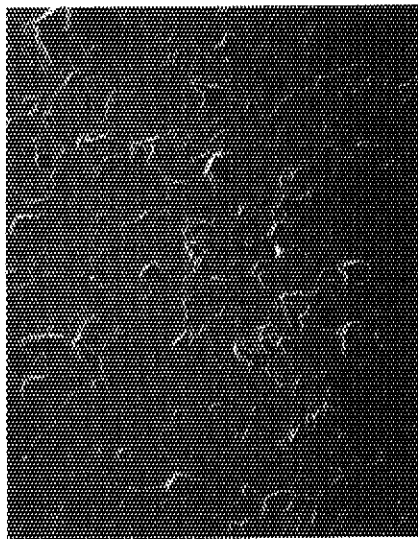


Photo. 24 Secondary electron image of the cladding inner surface after the pulse irradiation

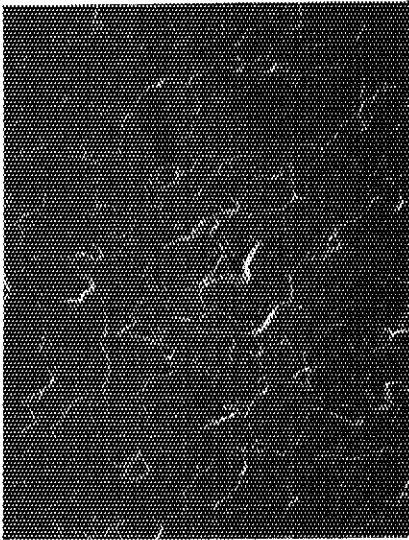




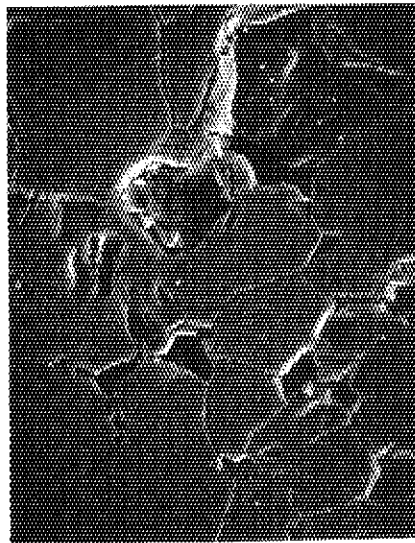
02SE006 (Periphery)  $\times 1000$



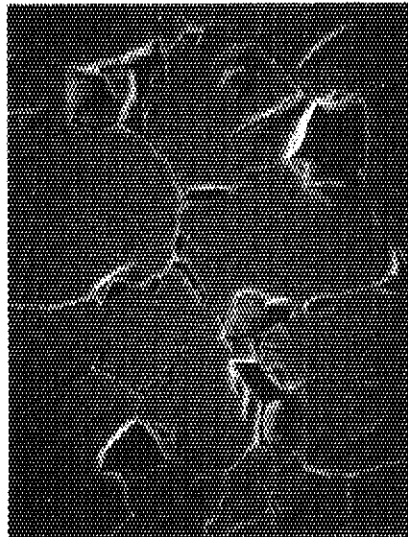
02SE007 (Middle)  $\times 1000$



02SE008 (Center)  $\times 1000$



02SE009 (Periphery)  $\times 3000$



02SE010 (Middle)  $\times 3000$



02SE011 (Center)  $\times 3000$

Photo. 25 Secondary electron image of the fuel surface after the pulse irradiation